c.3.

008182

DEPARTMENT OF
MINERALS AND ENERGY

BUREAU OF MINERAL RESOURCES, GEOLOGY AND GEOPHYSICS

Record 1974/145

PETROGRAPHIC AND GEOCHEMICAL STUDY OF THE RINGWOOD EVAPORITE DEPOSIT

by

A.J. Stewart

Record 1974/145

PETROGRAPHIC AND GEOCHEMICAL STUDY OF THE RINGWOOD EVAPORITE DEPOSIT

by

A.J. Stewart

CONTENTS

FIGURES

SUMMARY

The Ringwood evaporite deposit is situated 100 km east of Alice Springs, in the Northern Territory. The evaporite rocks crop out in the core of a plunging anticline in the Upper Precambrian Bitter Springs Formation of the Amadeus Basin. The evaporites comprise gypsum at the surface, and gypsum, anhydrite, and dolomite at depth; they are capped by massive algal limestone and limestone breccia. The evaporite outcrop was air-drilled by BMR in 1968 in order to examine the evaporite rocks, and to determine whether any deposits of sulphur or potash existed. The total depth reached was 852 feet (260 m); 675'5" (206 m) was continuously cored, and 626'6" (191 m; 92%) recovered. Duplicate samples of the cuttings were taken every 5 feet (1.52 m).

Petrographic examination of the evaporites found the following sixteen minerals: gypsum, dolomite, chalcedonic silica, quartz, chlorite, anhydrite, pyrite, rutile, organic matter, celestite, microcline, tourmaline, sphene, plagioclase, and ilmenite; sulphur and potassium-bearing evaporite minerals are absent. The first six minerals listed account for 99% of the rocks. Gypsum is everywhere recrystallized to large anhedral grains which are commonly poikilitic around inclusions of dolomite, anhydrite, and celestite. Dolomite is very finely crystalline and anhedral, and is regarded as primary or early diagenetic in origin. Chalcedonic silica forms laminae and irregular streaks associated with dolomite, and is nearly isotropic; quartz occurs as cherty aggregates and also as isolated euhedra. Chlorite forms small colourless porphyroblasts associated with dolomite; analysis by electron microanalyser showed that it is high in magnesium and aluminium. Anhydrite is generally recrystallized to a bladed form with a preferred dimensional orientation, but some evaporite laminae consist of minute laths of anhydrite and finely crystalline granular dolomite. Veins of clear blue anhydrite are present in the lower part of the evaporite deposit.

The evaporite rocks comprise five main types: dolomite-gypsum breccia, bituminous dolomite, friable dolutite, anhydrite, and veins of satin-spar sypsum. All five rock-types form an interbedded assemblage in the lower part of the core, below 436 feet (133 m); above this depth, bituminous dolomite is absent (except for a single bed at 220 feet (67 m)), and the characteristic rock-type is the dolomite-gypsum breccia.

The bituminous dolomite is laminated grey-brown to black, tough, fine-grained, and contains abundant pyrite, organic matter, and chalcedonic silica. It is everywhere

brecciated, and the clasts are cemented by coarse anhydrite or gypsum. The dolomite-gypsum breccia consists of angular fragments of pale grey, fine-grained gypsiferous dolomite with a silty component of quartz, chlorite, and rare microcline in a matrix of coarse-grained granular gypsum. The dolutite is pale to dark grey, fine-grained, soft and friable, and consists of clay to silt-sized grains of dolomite, plus chalcedonic silica, pyrite, and chlorite; the rock forms isolated beds up to 1 m thick. Anhydrite rock is grey to greyish-blue, medium-grained, lineated, and forms contorted laminae and lenses and a few larger masses associated with the dolomite-gypsum breccia; it is only found below 465 feet (141.71 m). Acicular gypsum forms cross-cutting veins of satin-spar, with the needles oriented at a high angle to the walls of the veins.

Geochemical investigations of the Ringwood evaporites included full chemical analyses of 12 samples, partial analyses of 25 samples, and analysis for minor elements of the entire set of cuttings (166 samples). The fully analysed samples included three bulk samples, one from the entire set of cuttings and one each from the cuttings from the lower and upper parts of the hole, and three composite samples of the dolomite-gypsum breccia, bituminous dolomite, and dolutite. As expected, magnesium and carbonate are more abundant in the lower part of the core, and calcium, sulphate, and water in the upper part. Total rock norms were calculated from the full analyses; the average normative composition of the Ringwood evaporite deposit (from analyses of the entire cuttings set) is: 53 percent gypsum, 25 percent dolomite, 9 percent quartz (plus chalcedonic silica), 7 percent chlorite, 5 percent anhydrite, 1 percent other minerals. Comparison of the three analysed rock-types reveals that normative gypsum and anhydrite are most abundant in the dolomite-gypsum breccia, whereas normative dolomite is most abundant in bituminous dolomite and dolutite. In addition, normative quartz (plus chalcedonic silica), chlorite, pyrite, rutile, apatite, and halite are also concentrated in dolutite, suggesting that this rock contains an appreciable detrital content, probably originating as wind-blown dust.

In the partial analyses, the 25 samples were taken randomly from the entire set of cuttings, and were analysed for calcium, magnesium, sulphate, carbonate, and water. Partial rock norms were calculated from these, and the normative gypsum : normative anhydrite ratio determined for each sample; when plotted against depth, the ratio shows a roughly exponential increase upwards, indicating that the gypsum formed by hydration of anhydrite by meteoric water.

The entire cuttings set was analysed for minor elements, and the average results are: 0.13 percent potassium, 0.07 percent fluorine, 0.05 percent strontium, and 0.0065 percent manganese. Potassium, fluorine, and manganese are concentrated in dolomite beds; strontium is concentrated in gypsum beds. The maximum content of potassium found was 0.6 percent at a depth of 280 to 285 feet (85.34 to 86.87 m).

Fourteen core samples were analysed for boron; the maximum content found was 0.02%. Two core samples of bituminous dolomite were analysed for base metals; no enrichment is apparent.

Of the four main hypotheses of ancient evaporite origin - evaporation of seawater in (1) a sabkha, (2) an epeiric sea, (3) a desiccating deep ocean basin, and (4) a barred basin - only the last is consistent with the observed features of the Ringwood deposit. The diagnostic features of a sabkha, such as red-beds, algal-mat stromatolites, desiccation cracks and flat-pebble conglomerate, nodular anhydrite, and laminae of aeolian silt are absent from the Ringwood rocks, and the oxidizing environment of the epeiric sea is contra-indicated by the abundance of pyrite, organic matter, and grey to black colours of the Ringwood rocks. The known occurrences of evaporites in the Bitter Springs Formation do not show the concentric distribution of the desiccating deep basin model, and associated deep-water clastic rocks are absent. The Ringwood rocks meet all the criteria for the classical barred basin, including a basal pyritic bituminous dolomite, interbedded with and overlain by white to grey gypsum and anhydrite, followed by limestone breccia and massive stromatolitic limestone indicative of an algal reef. The geological history of the deposit can be summarized as follows:

1. Formation of lagoon inside off-shore algal reef, stagnation and evaporation of seawater inside lagoon.

2. Deposition of primary dolomite, opaline silica, organic matter, and pyrite.

3. Further evaporation, deposition of primary anhydrite.

4. Intermittent deposition of dolutite during times of influx of wind-borne dust or alluvial silt.

5. Gradual and irregular dilution of lagoon water, partial return to conditions of stage 2, increasing deposition of dolomite.

6. Return to normal marine conditions by collapse of reef or subsidence of entire area.

7. Burial of evaporite below remainder of Amadeus Basin sequence.

8. Diagenesis, recrystallization, and burial metamorphism of evaporites, including growth of chlorite and conversion of any pre-existing gypsum to anhydrite.

9. Folding and brecciation of evaporites, mobilization and recrystallization of anhydrite.

10. Erosion to present day, eventually allowing penetration of evaporite by meteoric water resulting in hydration of anhydrite to gypsum, precipitation of celestite, and filling of joints with satin-spar.

INTRODUCTION

General

BMR Alice Springs No. 3 was an exploratory hole drilled in 1968 into evaporite rocks in the core of the Ringwood Dome, which lies 100 km east of Alice Springs in the Northern Territory of Australia, at latitude 23°53'S, longitude 134°53'E (Fig. 1). The Dome was discovered by A.T. Wells (BMR) in 1964 (Wells et al., 1967). The evaporites in the Dome are part of the Upper Precambrian (Adelaidean*) Bitter Springs Formation of the Amadeus Basin sequence. The hole was the first in a drilling program whose aims were to explore the nature of the numerous evaporite occurrences in the Bitter Springs Formation, and to ascertain whether any associated deposits of potash or sulphur existed. Three more holes west of Alice Springs were drilled in 1970, at Goyder Pass, in the Gardiner Range, and north of Curtin Springs (Wells & Kennewell, 1972). The Ringwood hole was drilled by a drill party from the Petroleum Technology Section of the Bureau of Mineral Resources, using a Mayhew-1000 rig. Rotary air-drilling, coring, and reaming were used exclusively. The hole reached a total depth of 852 feet (259.69 m)**, of which 675'5" (205.87 m) was continuously cored, and 626'6" (190.96 m) recovered (Fig. 2). No fluids, sulphur, or potash were encountered, and the hole was plugged and abandoned. Details of the well history and drilling data are set out in the completion report (Stewart, 1969).

From field examination of the core and cuttings the upper 436 feet (132.87 m) of the core*** (Fig. 2) was described as consisting of gypsum with abundant fragments of 'anhydrite', plus interbeds of grey 'calcareous claystone' (Stewart, 1969); the lower 416 feet (126.8 m) was described as dark, brecciated, 'dolomitic siltstone' plus lesser amounts of the three rock-types found in the upper part of the core. Petrographic and X-ray diffraction examination has shown that the fragments of 'anhydrite' in the upper part of the core and the 'dolomitic siltstone' in the lower part are both composed of dolomite, and that the 'calcareous claystone' is a friable dolutite. Anhydrite is present throughout the core, but is visible in hand specimen only below 465 feet (141.71 m). The changes and corrections to the completion report necessitated by the results of the present study are set out in Stewart (1974).

* The period of time between about 1400 m.y. and the beginning of the Cambrian (Dunn et al., 1966)

** The Ringwood Dome was drilled before Australia adopted the metric system. Datum for all measurements is ground surface at the top of the well

*** Throughout this report, 'upper part of the core' and 'lower part of the core' refer to the parts of the core above and below this depth.

Geological Setting

The stratigraphy of the Bitter Springs Formation in the north-eastern part of the Amadeus Basin is described in Wells et al. (1967) and Wells et al. (1970), and the geology around the Ringwood Dome is described in the completion report (Stewart, 1969). The dome itself consists of a core of evaporite rocks and an outward-dipping envelope of carbonate and clastic rocks; the rocks of both core and envelope are part of the Gillen Member, which is the lower of the two members constituting the Bitter Springs Formation in this area. The evaporite core of the dome has a hook-shaped outcrop (Fig. 3), which measures 1600 m east-west and 550 m north-south. Much of the evaporite is concealed beneath a capping of carbonate rocks of the envelope of the dome (Fig. 4). The capping consists of friable thin-bedded contorted limestone overlain by thick massive algal limestone with abundant bulbous stromatolites facing in various directions, including some downward. These beds continue down dip to form the northern and western flanks of the dome, but here they are separated from the under-lying evaporite by masses of friable algal limestone and friable limestone breccia. The friable limestones lens out beneath the sediments of the southern flank of the dome; these consist of interbedded tough limestone, micaceous siltstone, dolomite, and sandstone.

The structure of the Ringwood Dome is incompletely known, as the eastern part is concealed by alluvium, and no plunge is discernible there. The evaporite rocks almost certainly continue west in the subsurface beyond the present area of outcrop.

PETROGRAPHIC DESCRIPTION OF EVAPORITES

INTRODUCTION

Thirty-nine standard thin sections were cut from the Ringwood core; their positions are plotted in Figure 2. All but two were ground under kerosene instead of water, in order to prevent dissolution of any water-soluble minerals; however, this procedure did not prevent the dehydration of gypsum to bassanite ($CaSO_4 \cdot \frac{1}{2}H_2O$; Plaster of Paris) at hot points in the sample slices, and bassanite, commonly in optical continuity with the gypsum, occurs at the contact of gypsum and dolomite in nearly every thin section. The identification as bassanite was confirmed by X-ray diffraction. The two thin sections ground under water contain no bassanite.

12

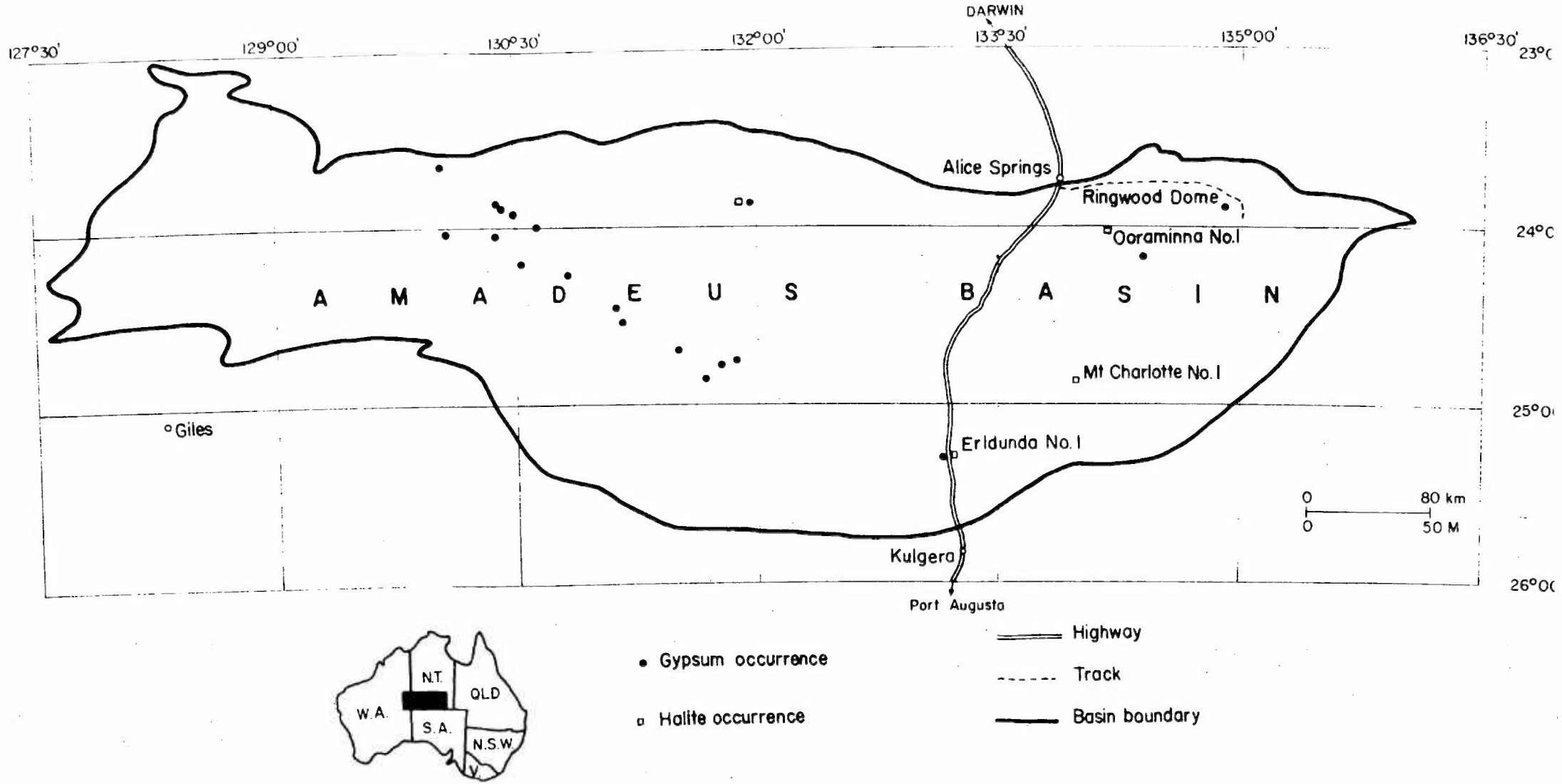

Fig. 1. Locality map of Amadeus Basin, showing location of Ringwood Dome and positions of known gypsum and halite occurrences in Bitter Springs Formation.

AUS :

(3)

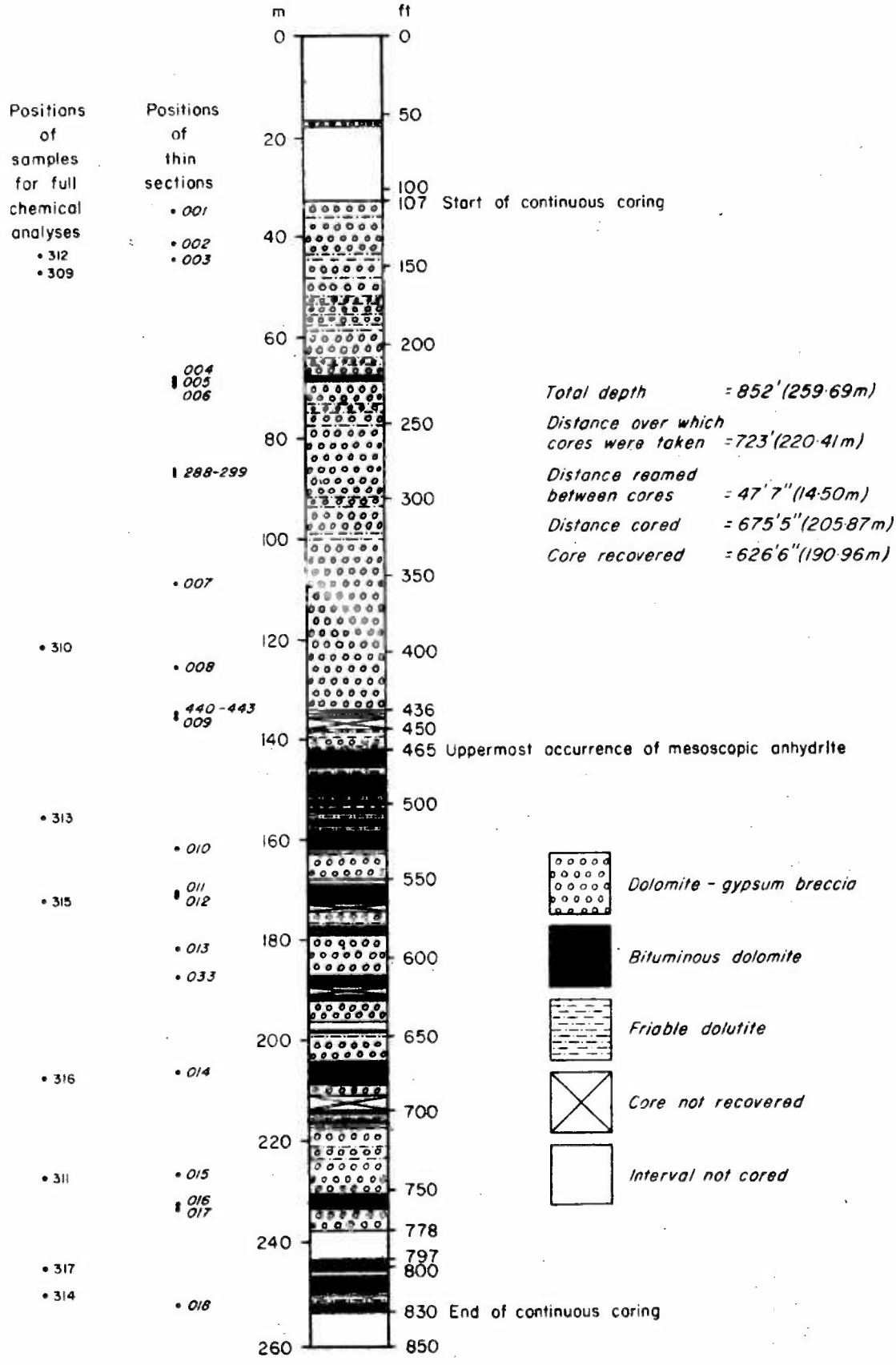

Fig. 2

Generalized lithologic log of BMR Alice Springs No.3 showing main rock types, coring data, and positions of thin-sectioned samples and samples used for full chemical analyses. All sample numbers preceded by 71110.

Record 1974/145

F 53/A 14/187

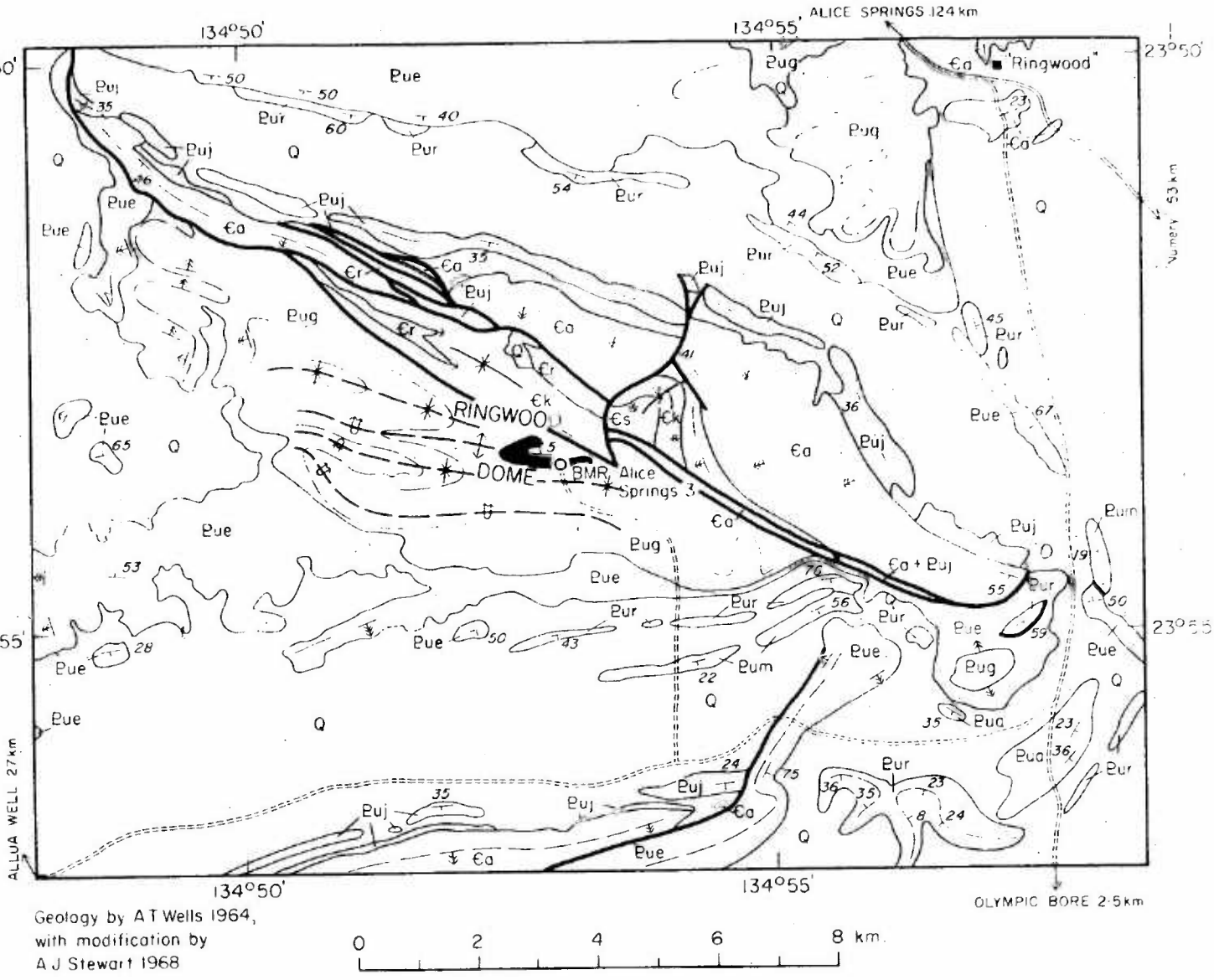

QUATERNARY

Q	Sand and alluvium	

CAMBIAN — Pertaoorrta Group

Shannon Formation	€s	Siltstone, shale, limestone, dolomite
Giles Creek Dolomite	€k	Dolomite, limestone, siltstone, shale
Todd River Dolomite	€r	Pink dolomite
Arumbera Sandstone	€a	Red-brown sandstone, siltstone

UPPER PROTEROZOIC

Pertatataka Formation Julie Member	Puj	Dolomite, limestone, sandstone
Limbla Member	Pum	Sandstone, calcarenite
Ringwood Member	Pur	Dolomite, calcarenite
Areyonga Formation	Pua	Sandstone, arkose, conglomerate, dolomite
Bitter Springs Formation Loves Creek Member	Pue	Algal dolomite, red siltstone
Gillen Member	Pug	Dolomite, green siltstone, sandstone, gypsum (shown in black), limestone

- Geological boundary
- Anticline
- Syncline
- Overturned anticline
- Overturned syncline
- Fault
- Strike and dip of strata
- Overturned strata
- Dip 15°
- Dip 15°–45°
- Dip 45°
- Trend line

(Dip 15°, Dip 15°–45°, Dip 45°, Trend line: airphoto interpretation)

- Road
- Vehicle track
- "Ringwood" Homestead

Fig. 3 Geological map of Ringwood Dome and surrounding area. Gypsum core of dome shown in solid black.

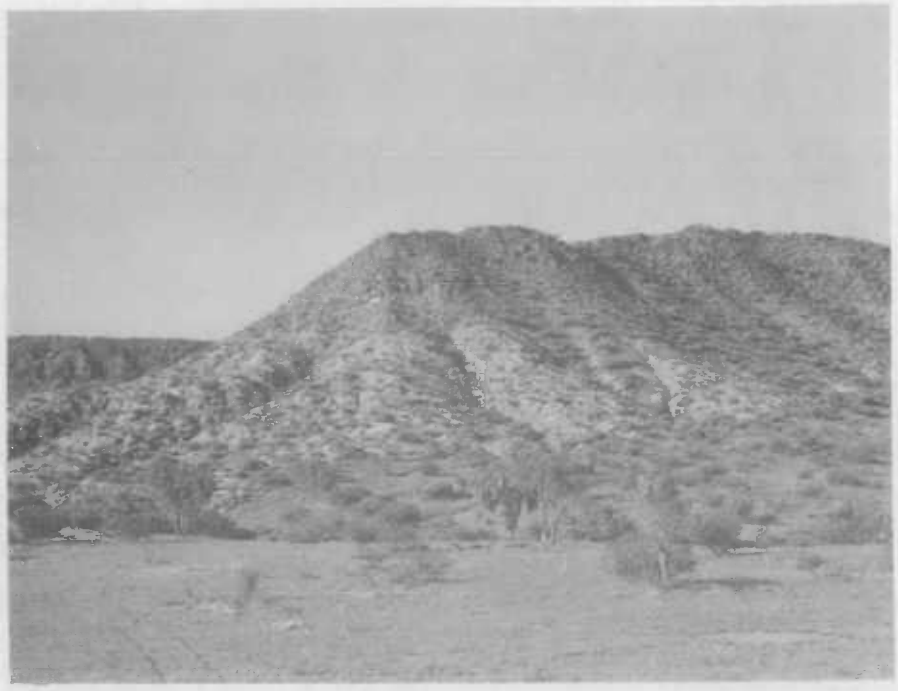

Fig. 4. View from southwest of central part of Ringwood Dome. The lower, deeply dissected part of the hill consists of white earthy weathered gypsum encrusting the underlying bedded gypsum; the upper part of the hill consists of limestone.

The petrographic examination of the Ringwood core has confirmed its bipartite nature noted earlier (Stewart, 1969). The lower part of the core, below 436 feet (132.87 m), consists of five interbedded rock-types, which are, in order of decreasing abundance:

1. Bituminous dolomite
2. Gypsiferous dolomite-gypsum breccia
3. Friable dolutite
4. Anhydrite
5. Acicular gypsum.

The upper part of the core lacks the bituminous dolomite characteristic of the lower part (except for a single bed between 220'10" and 223'11" (67.31 m to 68.25 m)), and its characteristic rock-type is the dolomite-gypsum breccia; in addition, anhydrite in the upper part of the core is visible only in thin section.

As predicted earlier (Stewart, 1969), some of the lithological terms listed above differ from those in the completion report; the changes are:

Term used in completion report	Revised term
Laminated anhydrite	Gypsiferous dolomite
'Dolomitic siltstone'	Bituminous dolomite
Claystone	Friable dolutite

Other changes to the completion report necessitated by the present study are listed in Stewart (1974).

MINERAL DESCRIPTIONS

Sixteen minerals have been identified in the thin sections of the Ringwood core, and, in approximate order of decreasing abundance, they are:

1. Gypsum
2. Dolomite
3. Chalcedonic silica
4. Quartz
5. Chlorite
6. Anhydrite
7. Pyrite
8. Rutile
9. Organic matter
10. Celestite
11. Microcline
12. Muscovite
13. Tourmaline
14. Sphene
15. Plagioclase
16. Ilmenite

The first six minerals make up 99 percent of the core; the others are present only in accessory amounts, except where rare local concentrations occur (e.g., microcline).

Gypsum

Gypsum is the most abundant mineral in the Ringwood core, and most commonly occurs as large pale yellowish-brown equant anhedral grains (Figs 5, 11, 13). These have a 'shagreen' appearance which under crossed nicols is seen to be caused by fine-scale polysynthetic twinning, which probably resulted from heating of the thin sections during preparation (Rogers & Kerr, 1942). Inclusions of other minerals (dolomite, anhydrite, quartz, pyrite, tourmaline, celestite, and rutile) are common in the gypsum grains, and are in places sufficiently numerous to produce a poikilitic texture (Fig. 15). Another variety of gypsum is a fine-grained mosaic aggregate of stubby polygonal crystals, and these commonly grade into laminae and cross-cutting veins and veinlets of acicular gypsum, or satin-spar (Figs 14, 21). Gypsum also forms small streaky wisps and shreds in gypsiferous dolomite. Another variety, in the upper part of the core, takes the form of large poikilitic crystals through which laminae of dolomite continue uninterrupted (Fig. 14), and has its counterpart in the lower part of the core, where gypsum forms large skeletal single crystals which enclose several angular clasts of bituminous dolomite (Fig. 16). These skeletal crystals generally contain abundant anhydrite inclusions, and, with increasing depth down the core, the amount of skeletal gypsum lessens and becomes restricted to a prismatic selvedge situated between the anhydrite and the dolomite clasts.

Dolomite

Dolomite is the second most common mineral in the Ringwood evaporites, and is most abundant in the lower part of the core. It generally occurs as tiny pale brown equant anhedral grains (Fig. 19), but in places larger euhedral dolomite crystals up to 0.5 mm across are present, generally as inclusions in gypsum (Fig. 13) and at the contact of fine-grained dolomite clasts and gypsum cement. Euhedral dolomite rhombs up to 12 mm across form megacrysts in black anhydrite rock in the interval 611'6" to 612'0" (186.38 m to 186.54 m). None of the dolomite, in whatever form, is twinned.

Chalcedonic Silica

The material denoted as chalcedonic silica in the Ringwood evaporite rocks is somewhat enigmatic. In thin section it occurs as clear, pale pinkish brown shreds,

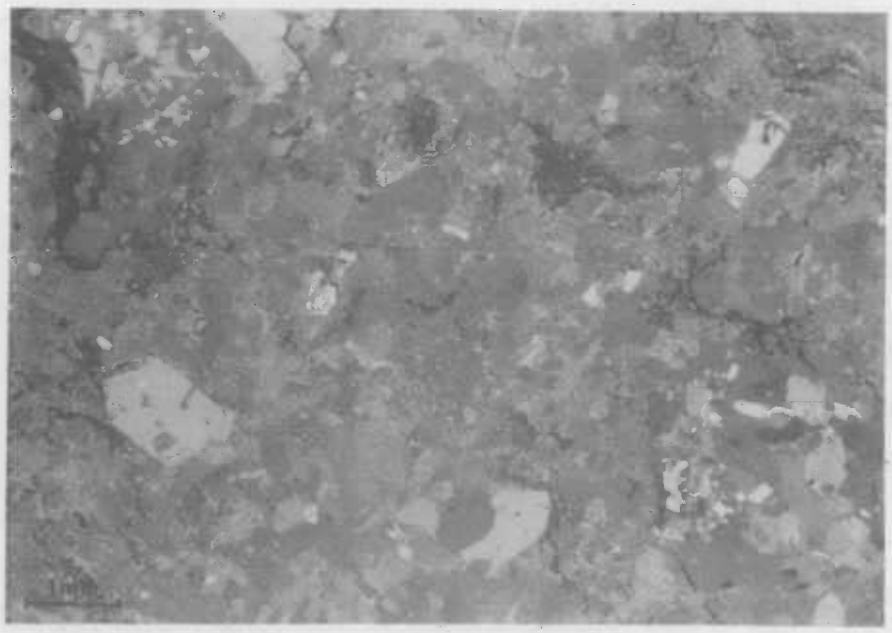

Fig. 5 - Photomicrograph showing cherty aggregates of anhedral quartz (Upper L.H. corner) and larger euhedral quartz crystals (one broken) in granular gypsum. TS 71110004 from 220'8" (67.26 m). Crossed nicols.

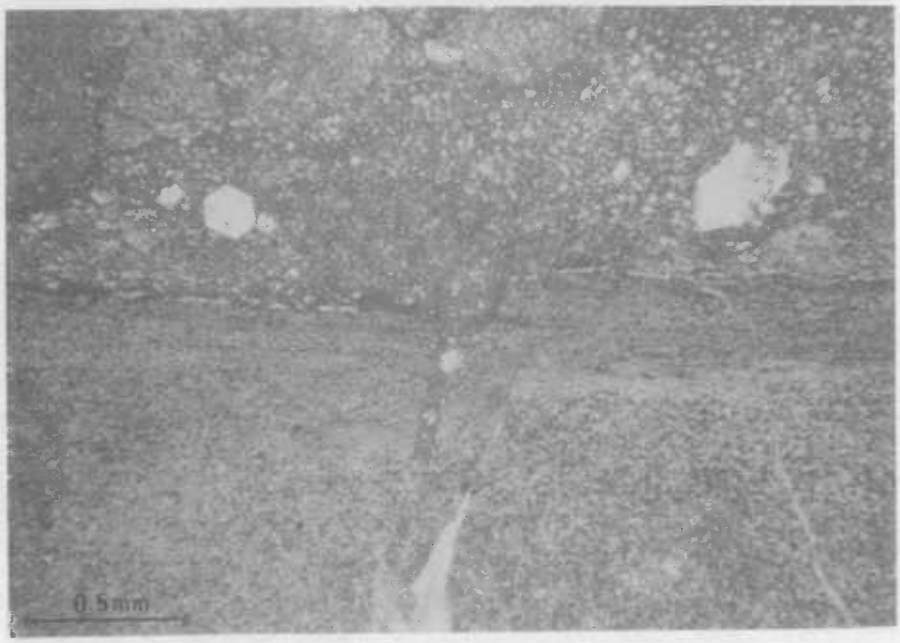

Fig. 6 - Photomicrograph of siliceous bituminous dolomite (bottom of photo) passing up into chalcedonic silica (centre), overlain by recrystallized dolomite with quarta euhedra. TS 71110016 from 760'3" (231.77 m). Plain light.

patches, laminae, and veinlets in the various types of dolomite rock in the core. It is thickest in bituminous dolomite, where it forms discrete laminae (Fig. 6), and along the margins of laminae of acicular gypsum in the dolomite-gypsum breccia (Fig. 21), but it also occurs to a lesser extent along the margins of cross-cutting veins of acicular gypsum, and it is very common as small shreds in friable dolutite. It is commonly crowded with inclusions, chiefly of pyrite, but also including angular grains of quartz, anhedral dolomite, euhedral tourmaline and rutile, and rounded grains of sphene. Small spiny clumps of pale brown needles in the silica are possibly centres of devitrification. Under crossed nicols, the silica is generally nearly isotropic, and shows only faint ghostly diffuse patches of very low birefringence, which are presumably poorly crystallized grains. Elsewhere, the silica is better crystallized, and forms a mosaic aggregate of polygonal quartz with normal birefringence, though still with diffuse grain boundaries and non-uniform extinction. In a few places, the silica forms a well crystallized chert, and the brown colour is generally lost in these parts. Laminae of oolitic cherty silica are present in T.S. 71110012 from 599'11" (170.66 m). X-ray diffraction analysis of hand-picked fragments of chalcedonic silica from friable dolutite at 440 feet (134.09 m) gave a normal quartz pattern. Nowhere does the silica show the fibrous structure typical of chalcedony sensu stricto, but its distinctive appearance and marked difference from the suhedral quartz crystals elsewhere in these rocks make a separate name desirable, and the definition of Deer et al. (1963) of chalcedony (sensu lato) as a group name for cryptocrystalline silica seems to be suitable, modified to chalcedonic silica to take account of the poorly crystallized nature of much of the material.

Quartz

Quartz is present in almost all the thin sections examined, and is particularly abundant in the gypsiferous dolomite. It is most commonly seen as small prismatic euhedra with pyramidal terminations (Fig. 5, 20). Concentric growth zones defined by tiny inclusions of unidentified material are present in some; a few have fluid inclusions with moving bubbles. Larger inclusions of dolomite, gypsum, anhydrite, and (rarely) chalcedonic silica are present in some quartz crystals. The quartz occurs as larger euhedra in gypsum rock (Fig. 5), and also forms cherty aggregates of anhedral to euhedral crystals (Fig. 5). A few euhedral quartz crystals are broken. Angular, silt-sized particles of quartz are commonly present in gypsiferous dolomite (Fig. 21), particularly in the interval 280 to 285 feet (85.34 m to 86.86 m).

Chlorite

Chlorite is found most abundantly in gypsiferous dolomite between 280 and 285 feet (85.34 m to 86.86 m), but has been identified by X-ray diffraction in trace amounts from many other depths. In thin section it occurs as small colourless elongate ragged porphyroblasts up to 0.3 mm long (Fig. 7). Inclusions of dolomite and quartz are common, and in some occurrences occupy a greater volume than the host chlorite.

One crystal of chlorite from a depth of 284 feet (86.56 m) (sample 71110297) was analysed (for use in norm calculations) with an electron probe, model JXA/3A, and the results are set out below:

Oxide	%	Structural Formula		
SiO_2	31.31	Si	2.913)	
			)	4.00
TiO_2	0.00	Al^{iv}	1.087)	
Al_2O_3	21.00	Al^{vi}	1.215)	
			)	
FeO	6.84	Fe	0.531)	
			)	5.94
MgO	29.67	Mg	4.112)	
			)	
CaO	0.79	Ca	0.078)	
Na_2O	0.00	OH	8 (assumed)	
K_2O	0.00		or	
	89.60	$(Mg_{4.1}\ Fe_{.5}\ Al_{1.2}\ Ca_{.1})$		
		$(Si_{2.9}\ Al_{1.1})\ O_{10}\ (OH_8)$		
H_2O (by difference)	10.40			

From: BMR Laboratory Report No. 52, 13 August 1973

Analyst: R.N. England

The calculated structural formula plots in the field of sheridanite in the classification of Hey (1954): the chlorite is a calcian sheridanite.

Anhydrite

Anhydrite is visible in hand-specimen only below 465 feet (141.71 m), but it is present in thin sections from above this depth. The anhydrite forms several varieties, of

Fig. 7 - Photomicrograph showing ragged porphyroblasts of chlorite in gypsiferous dolomite rock. TS 71110295 from 283'1" (86.28 m). Crossed nicols.

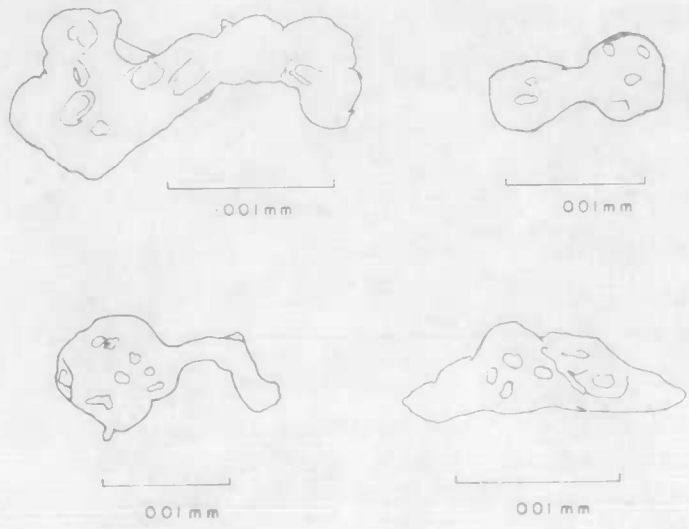

Fig. 8 - Sketches of blebs of bitumen (?) in chalcedonic silica in TS 71110012 from 559'11" (170.66 m).

which the most common is an aggregate of large colourless subhedral to euhedral prisms (Fig. 20), generally with a parallel alignment. This type of anhydrite forms the cement between clasts of bituminous dolomite in the lower part of the core. In the dolomite-gypsum breccia, the anhydrite forms small isolated equant to prismatic anhedral grains included in the gypsum (Fig. 15), and these become larger and more numerous down the core; many of the grains show a common optical orientation. Below 465 feet (141.7 m), anhydrite in the dolomite-gypsum breccia commonly forms monomineralic laminae of medium to large subhedral prismatic crystals, generally with their long axes oriented parallel to the lamination. Other laminae consist of very fine-grained kinked and plicated felted aggregates consisting of anhydrite laths and dolomite granules, with the anhydrite laths oriented parallel to the lamination, and still other laminae consist of medium-grained aggregates of equant subhedral grains of anhydrite. Larger masses of pure coarse anhydrite are present at several places down the core, e.g. between 556 and 558 feet (169.47 m to 170.08 m).

Pyrite

Pyrite is very common in the dolomite rocks, and forms tiny opaque euhedral pyritohedra (Figs 17, 19). From 107'6" to 110'4" (32.77 m to 33.63 m), 251'7" to 253'3" (76.68 m to 77.19 m), and 652'0" to 658'0" (198.75 m to 200.58 m) pyrite occurs as euhedral interpenetrating twinned pyritohedra up to 10 mm across.

Rutile

Rutile occurs mostly as small clear pinkish-brown euhedral prisms, commonly with pyramidal terminations. Some prisms form out-growths on rounded grains of detrital ilmenite, sphene, and rutile.

Organic Matter

The presence of organic matter in the Ringwood evaporite rocks was originally noted at the drill site, when a brown oily slime floated to the surface of the water during washing of the drill cuttings, especially those from the bottom 22 feet (6.71 m) of the hole (Stewart, 1969). In thin section, the substance denoted as 'organic matter' is of two types. In the first, it takes the form of tiny colourless to pale greyish-brown streaks, wisps, and blebs which are found only in laminae of chalcedonic silica in bituminous dolomite. The smaller of these particles

commonly have a skeletal or reticulate shape which arises from the polygonal shape of the quartz crystals between which the particles are situated. Most of the larger blebs have an irregular rounded appearance with numerous concavities and protuberances (Fig. 8), but some are angular with re-entrant angles, and look like negative crystals. All the blebs and particles have a high negative relief, are isotropic, and rather give the impression of being empty of solid material: they may be the imprints left by blebs of bitumen in the silica. The other variety of organic matter occurs as patches and laminae of an unresolvable brown stain, commonly associated with the blebs described above, but it is also common in non-siliceous dolomite rocks, where it forms thin brown laminae, i.e., laminae of brown-stained dolomite.

Celestite

Celestite occurs as groups of colourless anhedral crystals with moderately high relief; in places it forms skeletal crystals (Fig. 9). It is found only in association with gypsum in the upper part of the core, and was not observed below 284'10" (86.81 m).

Microcline

Microcline is abundant between 280 and 285 feet (85.34 m to 86.86 m), and occurs as small, angular grains which show a variety of forms ranging from angular anhedral laths (Fig. 11, a-e) to equant subhedral to euhedral shapes (Fig. 11, f-o); re-entrant angles are fairly common (Fig. 11, d,j,o). Extinction is generally sharp and uniform, but some grains show wavy and patchy extinction, and a few twinned crystals were seen (Fig. 11, k-o), one of which was kinked (Fig. 11, k). Cross-hatched twinning is rare, but was clearly seen in several grains.

Muscovite

Muscovite forms small colourless rather ragged flakes which are commonly slightly bent.

Tourmaline

Tourmaline occurs as distinctive euhedral length-fast needles and prisms up to 0.25 mm long (Fig. 10). The majority are colourless, but a few are greenish-blue or greenish-brown. Many of the crystals have a detrital fragment of coloured tourmaline situated at one end (Fig. 10). Some needles are broken, and the pieces displaced.

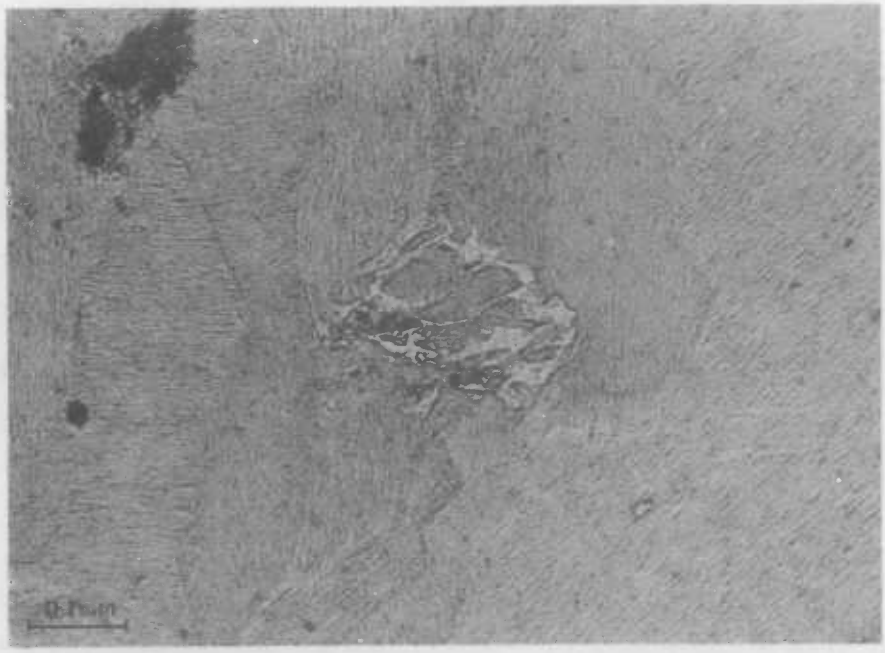

Fig. 9 - Photomicrograph of skeletal celestite crystal in granular gypsum with shagreen appearance. TS 71110295 from 283'1" (86.28 m). Plain light.

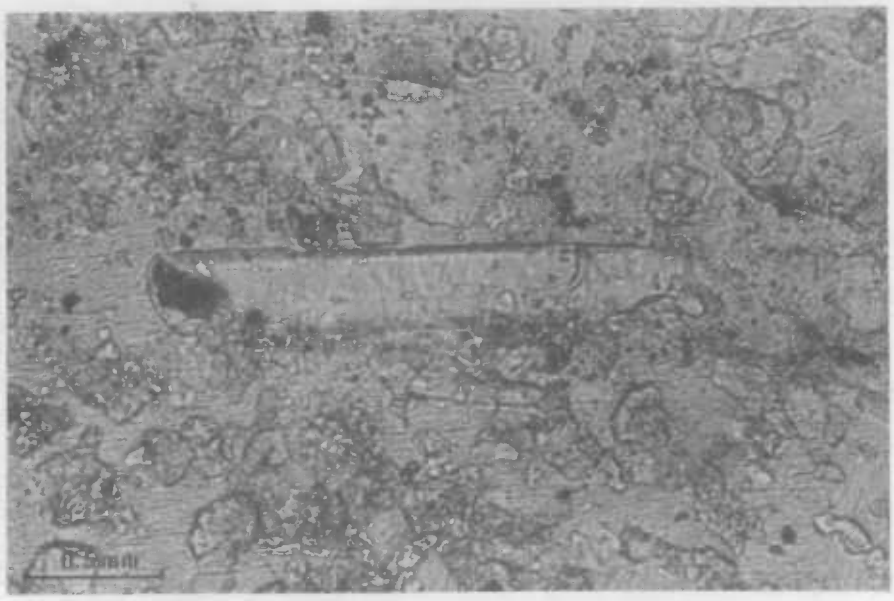

Fig. 10 - Photomicrograph of colourless subhedral tourmaline crystal with coloured detrital fragment at left hand end; in poikilitic gypsum with anhedral dolomite grains and pyrite. TS 71110002 from 136'10" (41.62 m). Plain light.

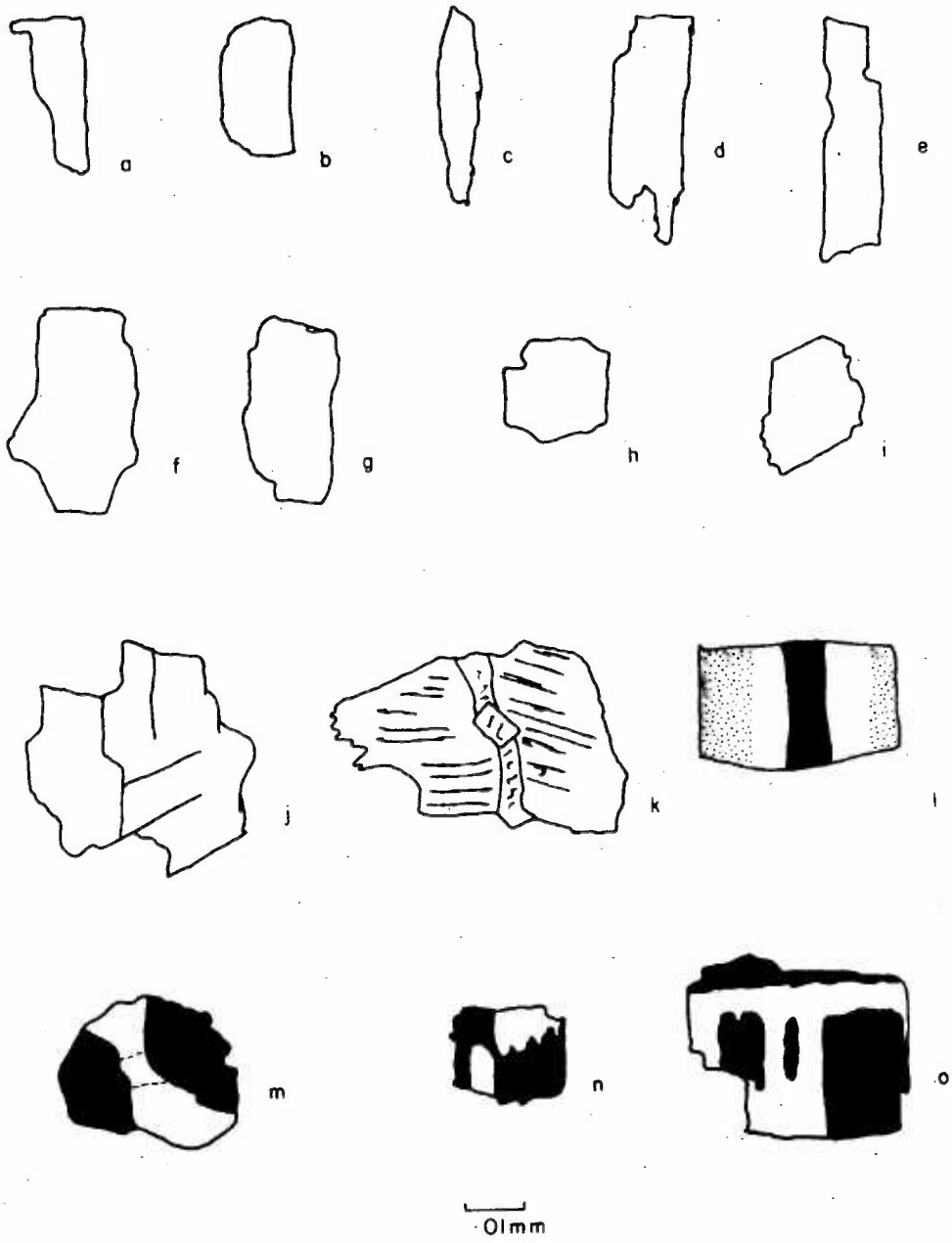

Fig. II - Sketches of microcline grains in gypsiferous dolomite from interval 280' - 285' (85·34m - 86·86m)

Sphene

Sphene is present as tiny greyish-brown equant subhedral to anhedral grains.

Plagioclase

One small angular detrital grain of plagioclase was noted, showing lamellar twinning transverse to its length.

Ilmenite

One rounded detrital grain of an opaque mineral was observed, and is interpreted as ilmenite because of its outgrowths of euhedral rutile.

ROCK DESCRIPTIONS

Dolomite-Gypsum Breccia

(T.S.'s 71110001, -002, -004, -006, -007, -008, -013, -014, -015, -288, -289, -292, -294, -295, -296, -297, -298, -299).

The dolomite-gypsum breccia is the most abundant rock-type in the Ringwood core, and comprises clasts and broken and contorted laminae of gypsiferous dolomite rock forming up to 50 percent of the total in a matrix of white crystalline gypsum. The clasts are composed of pale grey laminated dolomite diffusely speckled and mottled with white gypsum. They range in size up to 10 cm across, are angular to subrounded, equant to tabular, and are commonly arranged in a subparallel orientation, so that the rock has both a partly bedded and a partly brecciated appearance (Fig. 12). A few clasts are composed of dark grey soft friable dolutite.

In thin section, the breccia appears as a mixture of medium to coarse-grained granular gypsum and abundant rather ragged fragments of fine-grained gypsiferous dolomite rock, plus many partly dismembered laminae of dolomite, and isolated rhombs of recrystallized dolomite (Fig. 13). The dolomite laminae commonly extend without interruption through several gypsum crystals (Fig. 14). In many places, the gypsum forms granular masses of fine-grained subhedral crystals, and in places these grade into laminae and small cross-cutting veins and veinlets of acicular gypsum (Fig.

14). Inclusions of other minerals are common in the gypsum, and, apart from the dolomite already mentioned, include anhydrite (Fig. 15), quartz, tourmaline, celestite, and pyrite; the anhydrite inclusions increase in size and abundance down the core, and many display a common optical orientation. Below 465 feet (141.71 m), anhydrite is sufficiently abundant in the rock to form monomineralic laminae of pure crystalline anhydrite; in every case, these laminae are separated from the rest of the dolomite-gypsum breccia by layers (or selvedges) of clear prismatic gypsum. Rare laminae of felted anhydrite plus granular dolomite are present below about 700 feet (200 m).

The clasts of gypsiferous dolomite are composed of a mass of very small anhedral grains of dolomite set in a subordinate patchy matrix of poikilitic gypsum. Small euhedra of quartz are the most abundant accessory, but there are also aggregates of anhedral angular silt-sized quartz grains (Fig. 21), and these aggregates grade into distinct silty laminae of dolomite, quartz, and gypsum. Other accessory minerals include irregular patches of chalcedonic silica, euhedra of pyrite, tourmaline, and rutile, anhedral grains of sphene, ragged porphyroblasts of chlorite (Fig. 7), and organic matter staining. Between 280 and 285 feet (85.34 m to 86.86 m), the silty laminae contain abundant grains of microcline, plus increased amounts of tourmaline, rutile, and chlorite.

Tables 1 and 2 list the results of X-ray diffraction analyses of core and cuttings samples of the gypsiferous dolomite-gypsum breccia. Chemical analyses of three bulk samples of the breccia are listed in Table 7.

Bituminous Dolomite

(T.S.'s 71110010, -012, -016, -017, -018, -304, -305)

Bituminous dolomite is the characteristic rock-type of the lower part of the core (Fig. 2), and is dark grey, grey-brown, or black, very fine-grained, tough, commonly colour-laminated, and almost everywhere brecciated. The clasts are sharp-edged and blocky, and generally range, up to 2 cm across; a few are up to 5 cm across. They are set in a cement of white, grey-blue, or blue anhydrite which in many places is partly replaced by gypsum along the margins of the clasts. In some parts of the core, e.g., at 584 feet (178 m), the anhydrite cement forms a single large skeletal crystal up to 10 cm across, poikilitically enclosing the dolomite fragments.

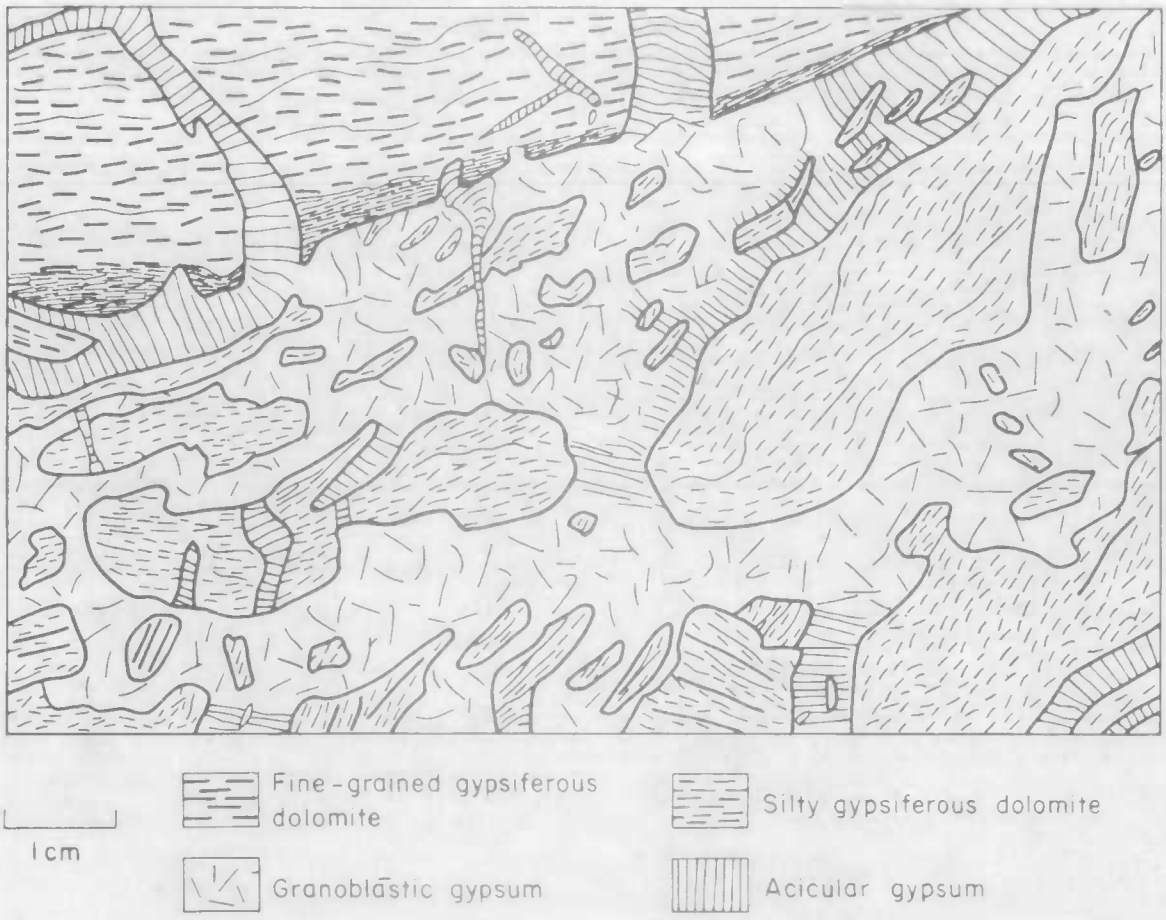

Fig.12 Sketch (from slabbed core) of dolomite-gypsum breccia, from about 275' (84 m) showing partly bedded and partly brecciated appearance.

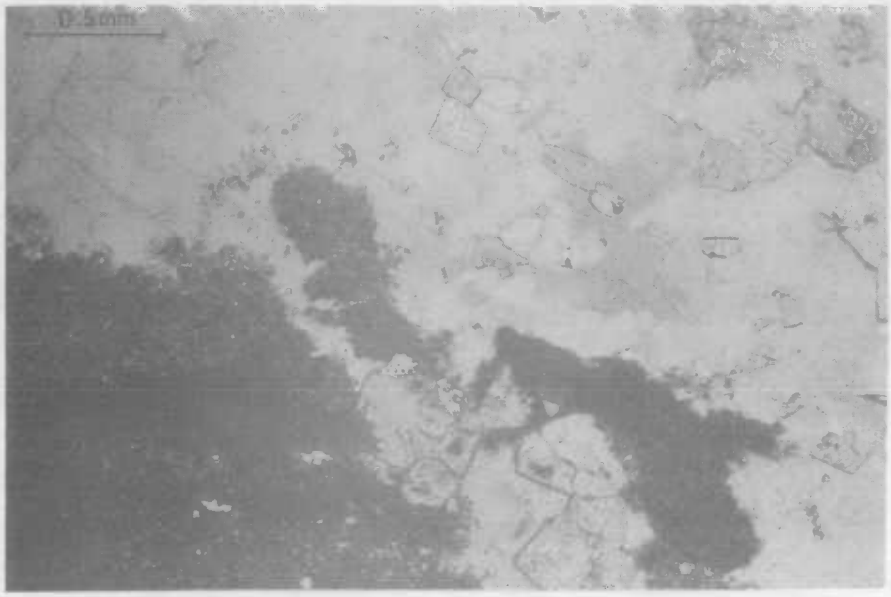

Fig. 13 - Photomicrograph of dolomite-gypsum breccia, showing ragged clasts of fine-grained gypsiferous dolomite and euhedral rhombs of recrystallized dolomite in coarse-grained granular gypsum. TS 71110001 from 116'10" (35.61 m). Plain light.

Fig. 14 - Photomicrograph of dolomite-gypsum breccia, showing contorted and broken laminae of gypsiferous dolomite rock in matrix of coarse poikilitic gypsum. Veins of prismatic to acicular gypsum may represent former solution channels, and grade into granular aggregates of stubby gypsum grains. g = gypsum poikiliths, in extinction position. TS 71110007 from 354'1" (107.92 m). Crossed nicols.

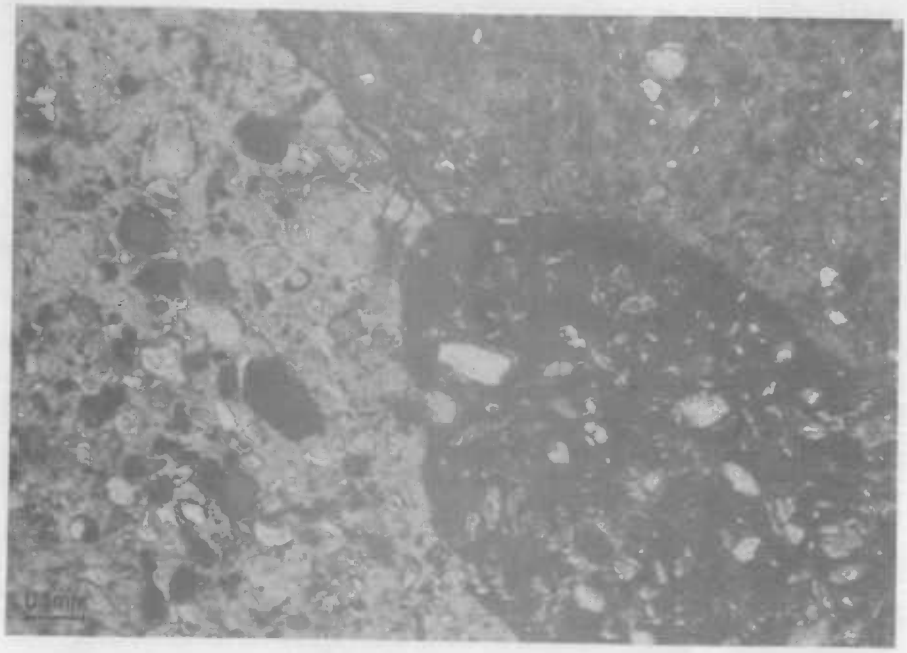

Fig. 15 - Photomicrograph of gypsum poikiliths (one in extinction position) containing inclusions of anhydrite. TS 71110015 from 740'11" (225.87 m). Crossed nicols.

Table 1: Results of X-ray diffraction analyses of core samples of dolomite-gypsum breccia.

Sample No*	Depth Feet & inches	Depth Metres	Minerals Identified+
044	230'0" - 230'2"	70.10 - 70.15	Gyp, dol, qtz, chl
045	230'6" - 230'8"	70.26 - 70.31	Gyp, qtz (tr), dol (tr)
046	231'0" - 231'2"	70.41 - 70.46	Gyp, dol, qtz (tr), chl (tr)
047	231'6" - 231'8"	70.56 - 70.61	Gyp, dol, chl, qtz
048	232'0" - 232'2"	70.71 - 70.76	Gyp, dol, qtz (tr), chl (tr)
049	232'6" - 232'8"	70.87 - 70.92	Gyp, dol, qtz (tr), chl (tr)
050	233'0" - 233'2"	71.02 - 71.07	Gyp, qtz, dol (tr), chl (tr)
051	233'6" - 233'8"	71.17 - 71.22	Gyp, qtz (tr), chl (tr), dol (tr)
052	234'0" - 234'2"	71.32 - 71.37	Gyp, dol, qtz, chl
053	234'6" - 234'8"	71.48 - 71.53	Gyp, dol, qtz, chl
054	235'0" - 235'2"	71.63 - 71.68	Gyp, dol, qtz, chl
055	235'6" - 235'8"	71.78 - 71.83	Gyp, dol, qtz, chl
056	236'0" - 236'2"	71.93 - 71.98	Gyp, dol, chl, qtz (tr)
057	236'6" - 236'8"	72.09 - 72.14	Gyp, dol, chl (tr), qtz (tr)
058	237'0" - 237'2"	72.24 - 72.29	Gyp, dol, qtz, chl (tr)
059	237'6" - 237'8"	72.39 - 72.44	Gyp, dol, qtz (tr)
060	238'0" - 238'2"	72.54 - 72.59	Gyp, dol, chl (tr), qtz (tr)
061	238'6" - 238'8"	72.69 - 72.75	Gyp, dol, qtz (tr)
062	239'0" - 239'2"	72.85 - 72.90	Gyp, dol, qtz (tr)
063	239'6" - 239'8"	73.00 - 73.05	Gyp, dol, qtz, chl, musc
064	240'0" - 240'2"	73.15 - 73.20	Gyp, qtz, dol, chl (tr)

From: BMR Laboratory Report No. 38, 24 February 1971
Analyst: G.H. Berryman

+For each sample, the minerals are listed in order of decreasing abundance, as indicated by their relative intensities. Abbreviations: gyp = gypsum, dol = dolomite, qtz = quartz, chl = chlorite, musc = muscovite, feld = feldspar, tr = trace.

*All sample numbers are prefixed by 71110.

Table 2: Results of X-ray diffraction analyses of cuttings samples of dolomite-gypsum breccia, plus minor amounts of other rock-types as indicated

Sample No.*	Depth Feet	Depth Metres	Rock-types in core+	Minerals Identified+
35	107 - 112	32.61 - 34.14	DGB + Dlt	Gyp, dol, qtz, chl, musc, feld
118	240 - 245	73.15 - 74.68	DGB + Dlt	Gyp, dol, qtz, chl, musc,
119	245 - 250	74.68 - 76.20	DGB	Gyp, dol, qtz, chl, musc, feld
120	250 - 255	76.20 - 77.72	DGB + Dlt	Gyp, dol, qtz, chl, musc
121	255 - 260	77.72 - 79.25	DGB	Gyp, dol, qtz, chl, musc, feld
122	260 - 265	79.25 - 80.77	DGB	Gyp, dol, qtz, chl, feld, musc
037	265 - 270	80.77 - 82.30	DGB	Gyp, dol, qtz, chl, musc
124	270 - 275	82.30 - 83.82	DGB + AG	Gyp, dol, qtz, chl, musc, feld
125	275 - 280	83.82 - 85.34	DGB	Gyp, dol, qtz, chl, feld, musc
126	280 - 285	85.34 - 86.87	DGB + AG	Gyp, dol, qtz, chl, feld, musc
127	285 - 290	86.87 - 88.39	DGB	Gyp, dol, qtz, chl, feld, musc
128	290 - 295	88.39 - 89.92	DGB + AG	Gyp, dol, qtz, chl, musc, feld
130	295 - 300	89.92 - 91.44	DGB + Dlt	Gyp, dol, qtz, chl, musc, feld
131	300 - 305	91.44 - 92.96	DGB + Dlt	Gyp, dol, qtz, chl, musc, feld

From: BMR Laboratory Report No. 165, 16 December 1971
Analyst: G.H. Berryman

+For each sample, minerals are listed in order of decreasing abundance. Mineral abbreviations as in Table 1. Rock abbreviations: DGB = dolomite-gypsum breccia, Dlt = dolutite, AG = acicular gypsum.

*All sample numbers are prefixed by 71110.

In thin section, the bituminous dolomite is seen to be composed of a mass of very small irregular dolomite grains tightly cemented together (Fig. 16); thin, linear, intersecting zones of coarser euhedral dolomite are present in places, and probably represent healed cracks in the rock. The colour lamination is found to be an effect of grainsize, the dark laminae being finer-grained than the pale laminae. Minor constituents in the dolomite clasts include isolated euhedra of quartz, small masses of chalcedonic silica, disseminated pyrite, dark brown organic matter, and tiny rounded grains of detrital material.

The cement between the dolomite fragments consists of medium to coarse-grained colourless anhydrite, generally accompanied by gypsum (Fig. 16); in a few places, the cement is composed solely of anhydrite or gypsum. The anhydrite forms elongate prismatic crystals which generally have a random orientation, but in some places are parallel or subparallel to the margins of the dolomite clasts. The gypsum (or where gypsum is absent, the anhydrite) forms large, skeletal, single crystals which enclose several dolomite clasts. Included anhydrite grains are abundant in the gypsum, and generally have a common optical orientation, indicating that they are remnants of larger anhydrite crystals which have been partly replaced by the gypsum. Dolomite along the margins of the clasts next to the gypsum is in places recrystallized to much coarser grains. In a few places, the cement between the dolomite fragments consists of subhedral to euhedral dolomite which is much coarser-grained than that of the fragments. In these areas, pyrite is also coarser-grained than normal (Fig. 17), and organic matter is concentrated at the junction of fine and coarse-grained dolomite (Fig. 18).

Impure varieties of the bituminous dolomite contain masses and laminae of pale brown very fine-grained chalcedonic silica (Fig. 6), forming up to 50 percent of the rock in a few places. Under high power, blebs of bituminous organic matter are visible in the silica (Fig. 8). In thin section 71110012, the silica forms oolites rimmed with grains of dolomite.

Table 3 shows the results of X-ray diffraction analyses of three core samples of the bituminous dolomite. Table 7 lists chemical analyses of three composite samples of bituminous dolomite.

The single bed of bituminous dolomite in the upper part of the core, between 220'10" and 223'11" (67.31 m to 68.25 m) (T.S. 71110005), is massive and non-brecciated, and

has a finely spotted appearance. Each spot consists of a single anhedral gypsum crystal, which is generally accompanied by a single euhedral quartz crystal crowded with minute dusty inclusions; a dark ring of organic matter surrounds each gypsum spot.

Table 3: Results of X-ray diffraction analyses of core samples of bituminous dolomite.

Sample No	Depth Feet & Inches	Metres	Minerals Identified+
69110003	560'0"	170.69	Qtz, dol
69110007	759'3"	231.46	Qtz, dol, gyp, anh (tr)
69110008	763'0"	232.60	Dol, gyp, qtz

From: BMR Laboratory Report No. 22, 19 March 1969

Analyst: G.H. Berryman

+Minerals are listed in order of decreasing abundance. Abbreviations as in Table 1, plus anh = anhydrite.

Dolutite

(T.S.'s 71110003, -009, -300, -301, -302, -303)

The dolutite in the Ringwood core is a pale to dark grey, soft and friable, very fine-grained, massive to poorly bedded rock which is easily crumbled by the fingers; it was originally identified as 'claystone' at the drill site (Stewart, 1969). It forms discrete beds which are up to 1.3 m thick, and are generally cut by an anastomosing network of gypsum veins; rough, uneven masses of concretionary gypsum are also common in some beds. In thin section, the rock appears as a very fine-grained, faintly laminated, uncemented mass of tiny round grains of dolomite, many of which do not touch each other (Fig. 19); they range in diameter from 0.0016 mm to 0.008 mm, and thus include both silt and clay-sized fractions. The rock is cut by a network of linear zones of coarse-grained dolomite, which, as in the bituminous dolomite, represent healed cracks, because streaky aggregates of pyrite are slightly offset where intersected by the coarser zones. Accessory minerals include abundant pyrite as isolated euhedra and in elongate streaky aggregates, irregular streaks and regular veins of chalcedonic silica, rare needles of tourmaline, detrital grains of sphene, and dark laminar stains of

Fig. 16 - Photomicrograph of brecciated bituminous dolomite, showing angular clasts of fine-grained dolomite rock cemented by coarse prismatic anhydrite (a) with single skeletal crystal of gypsum (g) between anhydrite and dolomite. White streaks in sypsum at contact with dolomite clasts are bassanite (b). TS 71110012 from 559'11" (170.66 m). Crossed nicols.

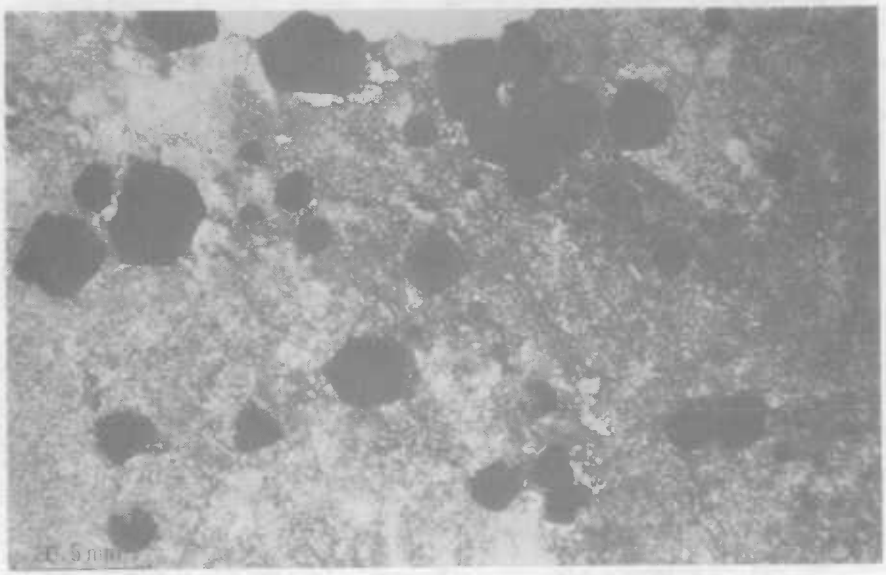

Fig. 17 - Photomicrograph of recrystallized bituminous dolomite, showing coarsened subhedral dolomite and enlarged euhedral pyrite crystals. TS 71110018 from 826'6" (251.88 m). Plain light.

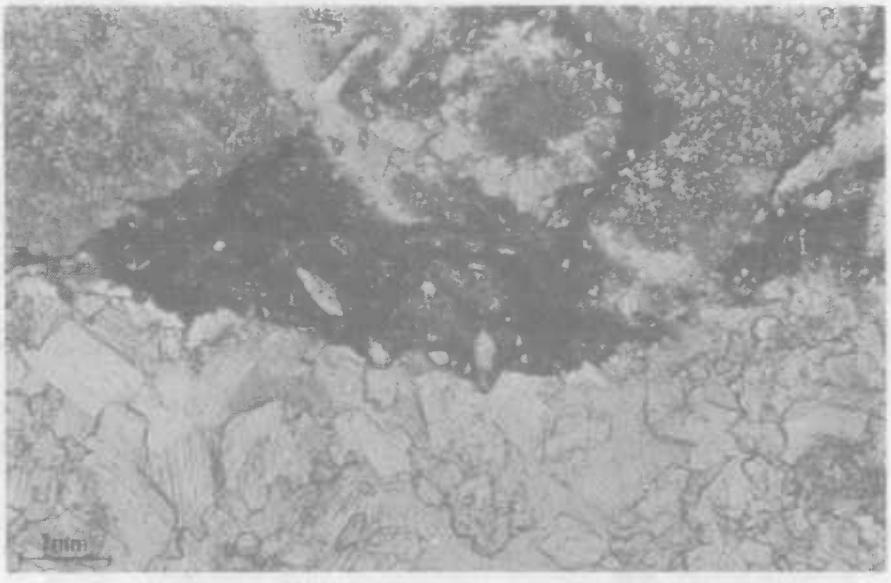

Fig. 18 - Photomicrograph of recrystallized bituminous dolomite, showing coarsened subhedral to euhedral dolomite and concentrations of opaque organic matter around clasts of fine-grained unrecrystallized dolomite. TS 71110010 from 528'11" (161.21 m). Plain light.

Fig. 19 - Photomicrograph of poorly cemented friable dolutite, showing round grains of dolomite and opaque pyrite grains. TS 71110301 from 440'6" (134.24 m). Plain light.

organic matter, which is commonly concentrated in layers on each side of the veins of chalcedonic silica. Anhydrite is totally lacking in the thin sections of the dolutite, but some appears as a normative mineral in one of the three analysed samples of the rock (Table 8). The veins and masses of gypsum rock consist of coarse prismatic to equant anhedral gypsum accompanied by much coarse recrystallized dolomite at their margins. X-ray diffraction analysis of eight samples of dolutite indicates the presence of chlorite and muscovite in the rock (Tables 4 and 5), but these minerals were not observed in thin section; however, chlorite is abundant as a normative mineral (Table 8). Table 7 lists chemical analyses of three composite samples of dolutite.

Table 4: Results of X-ray diffraction analyses of core samples of dolutite[+].

Sample No.*	Depth Feet	Depth Metres	Minerals Identified[+]
065	143	43.58	Dol, qtz, chl, gyp (tr), musc (tr)
066	326	99.37	Dol, qtz, gyp, chl, musc (tr)
067	329	100.28	Dol, gyp, qtz, chl, musc (tr)
068	480	146.28	Gyp, dol, qtz, chl, musc (tr)

From: BMR Laboratory Report No 38, 24 February 1971

Analyst: G.H. Berryman

[+]Minerals listed in order of decreasing abundance.

Abbreviations as in Table 1.

*All sample numbers prefixed by 71110.

Anhydrite

(T.S.'s 71110011, -033)

Anhydrite rock is present only in the lower part of the core, below 465 feet (141.71 m), and occurs as three varieties. The first is a speckled bluish-grey crystalline rock, medium-grained and lineated, forming discrete masses up to 2'3" (0.69 m) thick in the core; in places, the anhydrite is interlaminated with bituminous dolomite, and with disruption of the bedding this grades into the bitumin-

Table 5: Results of X-ray diffraction analyses of cuttings samples of dolutite plus minor amounts of other rock-types as indicated[+].

Sample No.*	Depth Feet	Depth Metres	Rock-types in core	Minerals Identified
096	145 - 150	44.20 - 45.72	Dlt + DGB	Dol, gyp, qtz, chl, musc
164	440 - 445	134.11 - 135.64	Dlt + BD	Dol, qtz, gyp, chl, musc
165	445 - 450	135.64 - 137.16	No core recovered	Dol, qtz, gyp, chl, musc
166	450 - 455	137.16 - 138.68	Dlt	Dol, qtz, gyp, chl, musc

From: BMR Laboratory Report No. 165, 16 December 1971

Analyst: G.H. Berryman

[+]Minerals listed in order of decreasing abundance. Abbreviations as in Tables 1 and 2, plus BD = bituminous dolomite.

*All sample numbers prefixed by 71110.

ous dolomite breccia with subordinate anhydrite matrix (described above). Crystalline anhydrite also forms contorted laminae in the dolomite-gypsum breccia in the lower part of the core. In thin section, the crystalline anhydrite is seen to consist of coarse colourless equant to prismatic anhedral crystals of anhydrite, which show the cleavage traces and polysynthetic twinning characteristic of the mineral (Fig. 20). Accessory minerals in the rock include numerous small euhedra of quartz (some of them broken), rare pyrite, and dark brown uneven laminae of organic matter; the anhydrite associated with the organic matter is very fine-grained and very anhedral.

The second variety of anhydrite occurs only between 611'6" and 612'00" (186.41 m to 186.56 m), where it forms a dark grey to black fine-grained rock which contains anhedral crystals of black dolomite up to 12 mm across; the rock has a prominent parting across the core. In thin section, the rock consists of disturbed laminae of fine-grained granular anhydrite with abundant organic matter alternating with laminae of coarse-grained anhydrite, with a little euhedral dolomite but without organic matter. The dolomite megacrysts comprise single crystals of dolomite crowded with anhedral inclusions of anhydrite and organic matter arranged in rows parallel to the lamination outside the megacryst. Surrounding the dolomite megacryst is a nearly complete shell of clear, coarse, poikilitic gypsum with included grains of anhydrite. Accessory minerals in the rock include euhedra of quartz, dark brown needles of rutile, colourless needles of tourmaline, and tiny euhedra of pyrite.

The third variety of anhydrite is a clear pale blue mineral which fills cross-cutting veins in the bituminous dolomite in the lower part of the core; the most prominent veins are situated between 612 and 615 feet (186.56 m to 187.47 m) and between 760'0" and 763'6" (231.69 m to 232.91 m). As elsewhere, a layer of coarse gypsum separates the anhydrite from the dolomite wall-rock. The anhydrite is pure and coarse-grained and forms anhedral elongate prisms with a decussate arrangement.

Table 6 lists the results of X-ray diffraction analyses of five core samples representing the first and third varieties of anhydrite.

Table 6: Results of X-ray diffraction analyses of core samples of anhydrite rock.

Sample No	Depth Feet & inches	Metres	Rock-type present	Minerals Identified+
69110002	556'6"	169.62	Speckled anhydrite rock	Anh
69110004	560'0"	170.69	Bituminous dolomite breccia + anhydrite-gypsum matrix	Anh, qtz, dol, gyp
69110006	658'11"	200.86	Speckled anhydrite rock	Anh, dol, qtz
69110009	763'0"	232.60	Clear blue vein anhydrite + gypsum selvedge	Anh, gyp
69110010	814'9"	248.30	Speckled anhydrite rock	Anh, dol, qtz (tr)

From: BMR Laboratory Report No 22, 19 March 1969

Analyst: G.H. Berryman

+Minerals listed in order of decreasing abundance. Abbreviations as in Tables 1 and 3.

Fig. 20 - Photomicrograph of medium to coarse-grained anhydrite rock, showing polysynthetic twinning and cleavage traces. Quartz euhedra (q) also visible. TS 71110011 from 556'6" (169.62 m). Crossed nicols.

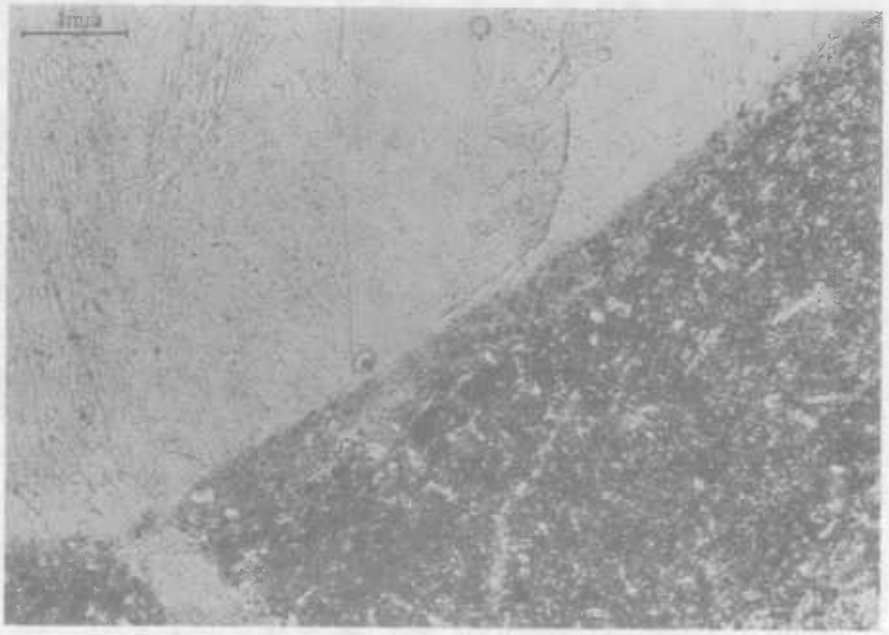

Fig. 21 - Photomicrograph of acicular gypsum and silty gypsiferous dolomite with selvedge of chalcedonic silica situated between the two rock-types. TS 71110002 from 136'10" (41.63 m). Plain light.

Acicular Gypsum

(T.S.'s 71110002, -006, -008, -293)

Acicular gypsum (or satin-spar) most commonly forms cross-cutting, parallel-sided veins up to 10 cm wide, but in places it also forms thin beds in the dolomite-gypsum breccia. It is more abundant in the upper part of the core, where 23 cross-cutting veins were noted, than in the lower part (12). The needles of gypsum are oriented perpendicularly to the walls of the veins, or nearly so. The margins of some veins are marked by thin laminar concentrations of other minerals, including friable uncemented dolomite (the most common), disseminated pyrite, chalcedonic silica (Fig. 21), and organic matter. In thin section, the gypsum appears as long and narrow prismatic to acicular crystals, some slightly tapering (Fig. 21). Inside the vein, parallel to its margins but not generally at or even near its centre, is a narrow zone of randomly arranged stubby crystals of gypsum, and this presumably marks the junction where the encrusting needles met as they grew from the walls of the vein. Compositionally, the cross-cutting veins are almost pure gypsum, but the laminae and thin beds commonly contain small amounts of recrystallized dolomite and celestite, and small xenoliths of fine-grained dolomite rock.

DISCUSSION

Origin of Gypsum and Anhydrite

The petrographic textures visible in the Ringwood evaporites indicate that the gypsum originated by hydration of anhydrite; the evidence includes the selvedges of gypsum at the margins of anhydrite masses in the lower part of the core, and the numerous inclusions of anhydrite in the gypsum of the gypsiferous dolomite, many of them with a common optical orientation. Moreover, the gypsum is accompanied by celestite, which is consistent with the known ability of anhydrite to take up strontium in solid solution (up to 42% according to Grahmann, 1920), in contrast to gypsum, which can take up very little strontium (Noll, 1934; analyses in Deer et al., 1962); when the anhydrite hydrated to gypsum, the strontium was unable to enter the gypsum lattices, and so precipitated as a separate mineral. If this is so, the high content of strontium in the parent anhydrite implies that it was primary anhydrite, not secondary anhydrite that had formed by dehydration of pre-existing gypsum. Other evidence for the existence of primary anhydrite is given on pp.42-43.

Much of the gypsum in the Ringwood rocks occurs in gypsiferous dolomite, which was presumably anhydritic dolomite before it was hydrated, and the rare laminae of felted anhydrite plus granular dolomite below 700 feet (200 m) may be the remnants of the original evaporite rock.

The hydration of anhydrite to gypsum involves a volume increase by about half (Goldman, 1952; Pettijohn, 1957), and the consequent swelling of the whole rock mass probably caused the brecciation of the dolomite, the gaps between the clasts furnishing some of the extra space required by the new gypsum. The laminae and cross-cutting veins of acicular gypsum that are without marginal concentrations of dolomite, pyrite, silica, and organic matter are probably infilled joints and channels through which water of hydration flowed into the anhydrite-bearing rocks, and out through which flowed solutions carrying excess calcium sulphate that was unable to precipitate in the body of the rock when the available space had been filled. In contrast, the laminae and veins of gypsum that do have marginal concentrations of the minerals presumably formed by recrystallization of the rock along tight joint surfaces, allowing outward migration of the impurities until they came up against the adjoining unrecrystallized rock.

The almost complete absence of anhydrite from the friable dolutite is notable, and it is possible that the marked permeability of this rock facilitated the entry of water, and thus enabled hydration of anhydrite to go to completion. The permeability probably allowed the gypsum to aggregate into the anastomosing veins and concretions, rather than remaining dispersed through the rock.

Origin of Dolomite, Chalcedonic Silica, and Quartz

The dolomite rocks in the Ringwood evaporites consist of a very fine-grained aggregate of tiny anhedral dolomite grains generally cemented together except in the beds of friable dolutite. The dolomite shows no evidence of a late diagenetic origin, such as replacement textures or relict biogenic structures, and, except where it forms a recrystallized cement between breccia clasts or next to gypsum veins, there are no lateral variations in grainsize or clusters of euhedral or subhedral crystals in an allotriomorphic groundmass. However, separate laminae are commonly of different grainsize, and there are rare instances of graded bedding. Thus it is very probable that the dolomite is a primary or early diagenetic mineral.

Friedman (1972) has shown that the bituminous calcilutite at the bottom of the Red Sea has probably formed by anaerobic bacterial oxidation of organic matter to carbonate, which then precipitates as calcium carbonate, concomitant with reduction of sulphate to sulphide, which precipitates as iron sulphide. The calcilutite is interbedded with layers of aragonite, which, by analogy with observed 'whitenings' in the Dead Sea, does appear to have formed by inorganic precipitation of carbonate ions from solution (Friedman, op. cit.). The dolomite in the Ringwood core could be an early diagenetic mineral, and hence it may have started as a basinal calcilutite of the Red Sea type which then underwent early dolomitization. However, an origin of limestone by bacterial activity means that all the carbon in the limestone is derived from organic matter, not from carbonate ions dissolved in seawater. Would there have been enough organic matter in Proterozoic time to form a dolomite in this way? Also, the lack of celestite in association with the Ringwood dolomite militates against the possibility that aragonite, which holds considerably more strontium in solid solution than does calcite (Deer et al., 1962), was the inorganic carbonate in the basinal deposit before dolomitization. Moreover, Friedman's suggestion ignores the experimental fact that inorganic carbonate forms the first precipitate in the experimental evaporation of seawater. Thus it appears to me that the evidence in the Ringwood rocks indicates that the dolomite originated by precipitation of inorganic carbonate, either as calcite that was dolomitized shortly afterwards, or as primary dolomite.

A similar evaporitic origin is also possible for the masses of chalcedonic silica in the dolomite rocks; their laminar or shred-like form and nearly isotropic character suggest that the silica precipitated as an opaline deposit simultaneously with the deposition of the dolomite, as is happening at the present time in the lakes associated with the Coorong Lagoon in South Australia (Peterson & von der Borch, 1965). With burial and the passage of time, the opal became more or less recrystallized to chalcedonic quartz. The small euhedra of quartz present in all the evaporite rocks are probably recrystallized detrital grains.

Origin of Chlorite

The occurrence of high-magnesium chlorite in the dolomitic rocks of the Ringwood core was unexpected, as neither Stewart (1963) nor Borchert & Muir (1964) include chlorite in their lists of evaporite rock constituents. Stewart (1949) recorded talc in the halite rocks (but not in the anhydrite-carbonate rocks) of the Magnesian Limestone of northern England, and its occurrence along cleavage cracks

and grain boundaries of the halite led him to suggest that it had been precipitated from solution as a late secondary mineral. The porphyroblastic nature of the Ringwood chlorite indicates that it is likewise of secondary origin. As described later (p. 30), normative chlorite in the Ringwood evaporites is most abundant in dolutite. Changes in the amounts of several other normative minerals in the dolutite are consistent with the rock's having contained a significant amount of clay, and if this were the case the chlorite may have formed by the following reaction (suggested by Zen, 1959, p. 36):

$$4.1CaMg(CO_3)_2 + 1.15Al_2Si_2O_5(OH)_4 + 0.6SiO_2 + 1.7H_2O + 0.1Ca^{++} + 0.6O^{=} + 0.5Fe^{++}$$

dolomite; kaolinite; quartz; water

$$\longrightarrow 4.1CaCO_3 + Mg_{4.1}Fe_{.5}Al_{1.2}Ca_{.1}Si_{2.9}Al_{1.1}O_{10}(OH)_8 + 4.1CO_2$$

calcite; chlorite (as analysed); carbon dioxide

A similar reaction involving ankerite as well as dolomite was postulated by Muffler & White (1969) to account for the disappearance, with increasing depth, of dolomite, kaolinite, and ankerite and the simultaneous appearance of chlorite (containing slightly more iron than the Ringwood chlorite) observed in the cuttings from wells in the Salton Sea geothermal field. The temperature in the wells where the transition occurs is about 200°C. The assemblage in the chlorite-bearing rocks at Ringwood - dolomite-chlorite-quartz - places them in the lowest subfacies, the muscovite-chlorite-dolomite-quartz subfacies proposed by McNamara (1965) as a three-fold subdivision of the greenschist facies, with a hypothetical temperature of about 200°C corresponding to a depth of about 2 kb (bottom of the Amadeus Basin).

Calcite has not been recognized in the Ringwood rocks, but this may be because it is petrographically similar to dolomite, and also because the two strongest peaks in its X-ray diffraction pattern very nearly coincide with prominent peaks in the patterns of gypsum and quartz.

Origin of Pyrite and Organic Matter

Pyrite and organic matter are common in the lower parts of evaporite sequences. The pyrite is generally attributed to the action of sulphate-reducing bacteria, which oxidize the remains of organisms that sink down to the bottom of the evaporating basin after death (Friedman, 1972). Simultaneous reduction of sulphate during the bacterial decay produces hydrogen sulphide, which then reacts

with dissolved iron and forms pyrite. Excess organic matter not decomposed by the bacteria is incorporated directly into the sediments.

Origin of Microcline

The small angular grains of microcline (Fig. 9) show evidence of both detrital and authigenic origin. The elongate shapes of some grains (which suggests that they are cleavage fragments), the existence of such optical phenomena as undulatory extinction, rare lamellar twinning, and cross-hatched twinning, the absence of inclusions, and the association with increased amounts of quartz, tourmaline, and rutile, all indicate a detrital origin, whereas the highly angular shapes (including re-entrant angles), the general absence of twinning, and, when twins are found, their 'fourling' appearance indicate an authigenic origin (Kastner, 1971). The microcline is probably of detrital origin, and has been somewhat recrystallized during diagenesis or burial metamorphism.

Origin of Detrital Minerals

The Ringwood evaporites contain numerous tiny grains of quartz, tourmaline, rutile, sphene, and a few other minerals. These grains may have been brought into the basin by surface runoff from a nearby landmass, but their very small size and ubiquitous occurrence throughout the core rather suggest that the grains were blown into the basin as wind-borne dust, which was possibly a fairly common phenomenon during the Proterozoic, in a landscape devoid of vegetation. The increased amounts and larger size of these grains in the interval 280 to 285 feet (85.34 m to 86.86 m), plus the presence of silt-sized grains of microcline, does suggest a local influx of water-borne terrigenous detritus.

Recrystallization

There is abundant textural evidence for recrystallization in the Ringwood evaporite rocks. The evidence includes:

1. The large skeletal crystals of anhydrite and gypsum which form the cement in the bituminous dolomite breccia;

2. The crusts of coarse dolomite and laminar concentrations of chalcedonic silica and pyrite at the margins of some veins and laminae of acicular gypsum;

3. The existence of anastomosing veins and concretionary masses of gypsum in dolutite;

4. The coarse grain and lineated texture of the anhydrite, with euhedral rhombs of dolomite in places;

5. The coarse grain of the dolomite which forms the cement in parts of the bituminous dolomite breccia, with concentrations of organic matter at the margins of the coarse-grained masses; also, the coarse-grained dolomite in the intersecting cracks;

6. The euhedral shapes of quartz crystals, tourmaline over-growths, and rutile needles;

7. The enlargement of pyrite in some laminae, and the occurrence of large interpenetration twins of pyrite;

8. The angular shapes, with re-entrant angles, of microcline grains.

The three major rock-forming minerals of the Ringwood evaporites show different degrees of recrystallization, and different grainsizes, thus:

1. Gypsum is everywhere recrystallized, and forms the coarsest-grained rocks.

2. Anhydrite is almost everywhere recrystallized to medium-sized grains, the only probable exception being the very fine-grained laminae of felted anhydrite laths and dolomite granules at 740'11" (225.87 m).

3. Dolomite is in general not recrystallized: recrystallization is very local and occurs mostly where dolomite is associated with gypsum.

Thus the three minerals can be arranged in the following order of decreasing ease of recrystallization: gypsum, anhydrite, dolomite.

Much of the recrystallization in the Ringwood rocks probably took place during diagenesis and burial metamorphism, e.g., the coarsening of anhydrite, the formation of euhedral quartz, tourmaline, and rutile, the enlargement of pyrite, the 'resculpturing' of microcline, and, after brecciation of the rocks, the local coarsening of dolomite and formation of large skeletal crystals of anhydrite as cement around the breccia clasts. The recrystallization of gypsum into concretions and some of the laminae and cross-cutting veins occurred much later, after uplift of the rocks and hydration of the anhydrite to gypsum.

GEOCHEMICAL STUDY OF EVAPORITES

MAJOR ELEMENTS - FULL ANALYSES

Introduction

Twelve samples of evaporite rocks from the Ringwood core were analysed for major and minor elements by the Australian Mineral Development Laboratories, Adelaide. The set of samples comprised a bulk sample (306) from the whole of 'Cuttings Samples Set 2', two bulk samples (307 and 308) from the upper and lower parts (respectively) of 'Cuttings Samples Set 2', and three samples from each of the three major rock-types of the core: the dolomite-gypsum breccia (Samples 309, 310, 311; cuttings), friable dolutite (Samples 312, 313, 314; core), and bituminous dolomite (Samples 315, 316, 317; core). The positions down the core of the nine rock-type samples are plotted in Figure 2. Details of the sampling and analytical procedures are set out in Appendix 1.

Results

General

The results of the full analyses are set out in Table 7. These data were then used to calculate a set of total rock norms in order to facilitate comparison of the major rock-types with each other; the results are set out in Table 8. Details of the method of calculation and assumptions made are set out in Appendix 1. The five normative minerals marked with an asterisk in Table 8 are not known to occur in thin section, and were used to account for certain elements present in small amounts. Also, because of the positive correlation shown by potassium, fluorine, and dolomite in the lower part of the core (Fig. 25), potassium fluoride (KF) was used to account for all K_2O for samples below 133 m. This is not meant to suggest that such a mineral exists in the rocks; the potassium and fluorine are probably held in some form of isomorphous replacement in the dolomite. Likewise, microcline was used only for samples from above 133 m. Finally, several different varieties of chlorite were used, as noted in Table 8; the formulae of the different chlorites were based on the analysis of the chlorite described in the section on 'Petrographic Description of

Table 7: Results in percent of full analyses of Ringwood evaporites

Sample No.*	306	307	308	309	310	311	312	313	314	315	316	317
Lithology		Bulk samples		Dolomite-gypsum breccia				Dolutite		Bituminous dolomite		
Depth	0-260	0-133	133-260	45.72 -47.24	120.39 -121.92	225.59 -227.11	43.80	155.11	250.20	171.35 &171.71	207.03 &207.16	244.33 &245.65
Sample type	Cuttings	Cuttings	Cuttings	Cuttings	Cuttings	Cuttings	Core	Core	Core	Core	Core	Core
SiO_2	11.6	9.75	13.3	6.20	7.20	9.00	33.2	32.3	30.4	34.3	5.35	43.4
Al_2O_3	1.53	1.26	1.75	0.81	1.06	1.50	5.25	5.70	6.15	0.11	0.67	0.10
Fe_2O_3**	0.51	0.38	0.63	0.46	0.24	0.29	1.35	1.25	1.50	0.30	0.58	0.33
CaO	26.9	28.1	26.3	33.0	31.1	28.0	14.5	14.1	15.1	20.6	28.0	17.5
MgO	7.40	5.25	9.25	3.00	4.60	4.40	17.4	17.6	16.0	10.2	19.3	10.2
Na_2O	0.10	0.03	0.16	0.03	0.05	0.09	0.07	0.34	0.47	0.04	0.07	0.05
K_2O	0.17	0.19	0.14	0.16	0.12	0.09	0.38	0.34	0.36	0.02	0.06	0.02
MnO	0.01	0.01	0.01	0.01	0.01	0.01	0.01	0.01	0.01	0.01	0.02	0.01
H_2O^+	2.30	3.30	2.75	5.80	1.30	1.65	3.55	3.50	4.35	1.89	1.15	0.40
H_2O^-	9.75	11.0	6.45	11.2	6.95	8.9	0.49	0.40	0.75	1.31	0.60	1.01
P_2O_5	0.03	0.02	0.03	0.01	0.02	0.03	0.06	0.07	0.07	0.01	0.03	0.01
TiO_2	0.10	0.08	0.14	0.04	0.05	0.07	0.27	0.30	0.34	0.01	0.09	0.01
SrO	0.05	0.06	0.04	0.05	0.08	0.06	0.01	0.06	0.02	0.02	0.01	0.01
Cl	0.10	0.03	0.17	0.02	0.05	0.08	0.04	0.30	0.32	0.04	0.06	0.04
F	0.09	0.05	0.10	0.07	0.03	0.06	0.28	0.33	0.35	0.02	0.04	0.02
S***	0.1	0.1	0.6	1.0	0.1	0.1	1.2	1.5	1.5	0.1	0.1	0.1
SO_3	27.9	31.9	23.4	33.5	43.0	38.2	0.61	0.40	6.60	8.55	2.75	4.65
CO_2	11.8	8.7	14.8	5.3	4.70	7.00	21.4	21.3	15.8	22.6	40.4	22.3
Total	100.44	100.21	100.02	100.66	100.66	99.53	100.07	99.80	100.09	100.11	99.28	100.16
FeO****	0.46	0.34	0.56	0.42	0.22	0.26	1.22	1.12	1.34	0.26	0.52	0.30

Analyst: AMDL, Report AN3249/73, 16 February 1973

* Preceded by 71110 ** And total iron *** Sulphide plus elemental sulphur **** Calculated from Fe_2O_3

Table 8: Total rock norms for Ringwood evaporites

Sample No.#	306	307	308	309	310	311	312	313	314	315	316	317
Lithology		Bulk samples		Dolomite-gypsum breccia				Dolutite		Bituminous dolomite		
Depth	0-260	0-133	133-260	45.72 -47.24	120.39 -121.92	225.59 -227.11	48.80	155.11	250.20	171.35 &171.71	207.03 &207.16	244.33 &245.65
Sample type	Cuttings	Cuttings	Cuttings	Cuttings	Cuttings	Cuttings	Core	Core	Core	Core	Core	Core
Gypsum	53.43	65.68	43.49	72.05	34.79	48.06	1.31	0.60	7.50	15.30	5.92	6.75
Anhydrite	4.55	2.31	5.40	-	40.46	18.95	-	-	5.40	2.41	-	2.57
Dolomite	24.72	18.23	31.01	11.12	9.84	14.67	44.85	44.63	33.11	46.71	84.65	46.66
Quartz	9.10	7.68	10.88	5.05	4.85	7.80	25.79	24.65	21.86	34.30	4.37	43.40
Chlorite	6.971	4.451	8.442	1.933	8.354	4.125	25.842	26.692	29.822	-	2.926	-
Pyrite	0.19	0.19	0.94	0.71	0.19	0.19	2.04	1.87	2.24	0.19	0.19	0.19
Microcline	0.61	1.11	-	0.95	-	-	-	-	-	-	-	-
Celestite	0.09	-	-	-	0.15	0.11	-	0.11	0.04	0.04	-	-
Rutile	0.10	0.08	0.14	0.04	0.05	0.07	0.27	0.30	0.34	0.01	0.09	0.01
*Apatite	0.24	0.19	0.24	0.05	0.19	0.24	0.47	0.50	0.50	0.05	0.24	0.05
*Halite	0.16	0.06	0.28	0.04	0.08	0.14	0.07	0.50	0.53	0.07	0.11	0.07
*Fluorite	-	0.05	0.09	0.14	-	-	0.16	-	-	-	0.03	0.01
*KF	0.08	-	0.17	-	0.15	0.12	0.46	0.42	0.44	0.02	0.07	0.02
*Calcite	-	-	-	-	-	-	-	-	-	0.70	-	0.07
Total	100.26	100.03	101.08	92.08	99.10	94.47	101.26	100.27	101.78	99.79	98.59	99.82

1. Analysed chlorite 2. Iron-free, aluminium-rich chlorite 3. Iron-free chlorite
4. Iron-poor chlorite 5. Moderate-iron chlorite 6. Iron-rich chlorite

Preceded by 71110 * Not known in thin section

quartz, chlorite, and dolomite; there was no trace of $Ca(OH)_2$, nor of any of the rare hydrated calcium silicates such as those of the tobermorite group. The later are high-temperature minerals, and occur in drusy cavities in basalt (Heddle, 1880; Currie, 1905), in thermally metamorphosed limestone (McConnell, 1954), and in building materials such as sand-lime bricks and steam-cured portland cement (Heller & Taylor, 1956). They are not likely to be present in evaporites, and the excesses of CaO and H_2O in sample 309 are probably caused by inaccuracies in the chemical analysis.

Dolutite

The calculated norms for the three dolutite samples (312, 313, 314) are markedly consistent with each other, indicating that the dolutite has a fairly uniform composition throughout the core. The large amounts of normative quartz (plus chalcedonic silica) and chlorite are notable, and these two minerals constitute approximately half the rock, whereas normative dolomite forms somewhat less than half. The chlorite is free of iron and rich in aluminium, and this is again presumably related to the high content of normative pyrite in the rock. Normative gypsum and anhydrite are present only in very small amounts (except in sample 314), agreeing with the petrographic findings. Normative chlorite, and the minor normative minerals, rutile, apatite, and halite, show systematic decreases up the core.

Bituminous Dolomite

The calculated norms for the three bituminous dolomite samples (315, 316, 317) show marked and unsystematic variations, especially in the amounts of normative dolomite and quartz (plus chalcedonic silica). Chlorite is absent in two of the norms, and pyrite is low in all three. A small amount of calcite appears in two of the norms; it probably reflects substitution of calcium for magnesium in the dolomite.

Comparison of Three Major Rock-Types

Comparison between the calculated norms of the three major evaporite rock-types reveals the following differences:

1. Normative gypsum and anhydrite are concentrated in the dolomite-gypsum breccia (as expected), and, concomitantly, normative dolomite is concentrated in the dolutite and bituminous dolomite rocks.

2. Normative quartz (plus chalcedonic silica) is concentrated in dolutite (up to 25 percent of the rock) and in bituminous dolomite (up to 43 percent of the rock).

3. Normative chlorite and pyrite are markedly concentrated in dolutite, in amounts which are up to ten times greater than those in the other two major rock-types.

4. Normative rutile, apatite, and halite are similarly concentrated in dolutite.

5. The content of normative halite decreases up the core in both dolutite and dolomite-gypsum breccia.

Discussion

The changes in the amounts of the major normative minerals in the Ringwood evaporites are more or less as anticipated from lithologic examination of the core. Both modal and normative dolomite, anhydrite, and pyrite are most abundant in the lower part of the core, and modal and normative gypsum in the upper part. More unexpected are the relative concentrations of normative pyrite, quartz (plus chalcedonic silica), chlorite, rutile, apatite, and halite in the dolutite rock, and the upward decreases in the normative amounts of the last four of these minerals.

The concentration of normative pyrite in the dolutite indicates that the dolutite formed when the evaporating basin was most stagnant, and the concentration of normative quartz (plus chalcedonic silica) in the same rock-type is also consistent with stagnation; the opaline silica forming at the present time in the ephemeral lakes associated with the Coorong lagoon of South Australia precipitates during stagnation and drying of the lakes (Peterson & von der Borch, 1965).

Rutile in the evaporites is probably of wind-borne detrital origin, and its concentration in the dolutite is also consistent with stagnation, as this implies drought conditions, a reduced water level and the basin isolated from the ocean, accompanied by drying of the surrounding plant-free terrain leading to an increase in the amount of wind-borne detritus entering the basin during dust storms. This would also explain the concentration of normative apatite in the dolutite, as, according to Stewart (1963), phosphorus in evaporites is concentrated chiefly in clay, again presumably brought in by wind. The systematic upward

decrease in the normative amounts of rutile and apatite indicates a lessening in the amount of incoming wind-borne detritus.

The concentration of normative chlorite in the dolutite follows from the concentration of clay, if the chlorite formed by the reaction of dolomite and kaolinite, as suggested on p.22 .

Why normative halite is concentrated in the dolutite, and why its distribution is similar to that of rutile and apatite, are not known; by analogy with these last two minerals, the halite would appear to have come down during times of clay deposition. If the halite were of evaporitic origin, it should show an upward increase in the norms.

MAJOR ELEMENTS - PARTIAL ANALYSES

Introduction

Twenty-five samples chosen randomly from 'Cuttings Samples Set 2' were forwarded to the Australian Mineral Development Laboratories, Adelaide, for analysis for calcium, magnesium, sulphate, carbonate, and water.

Details of sampling, analytical procedures, and limits of precision are set out in Appendix 1.

Results

The results of the analyses are set out in Table 9, and plotted as bar graphs in Figure 22; the percentage of residue in each sample was calculated by difference.

Discussion

The bar graphs show clear differences between the lower and upper parts of the hole, corresponding to the upper limit, at 436 feet (132.87 m), of dark bituminous dolomite in the core. Magnesium and carbonate are more abundant in the lower part of the hole, and calcium, sulphate, and water in the upper part. In addition, calcium and sulphate show a slight decrease, and magnesium and carbonate a slight increase upwards in the upper part of the

Table 9: Results in percent of partial analyses of Ringwood evaporites

Sample No.*	Depth Interval Feet	Depth Interval Metres	Ca (AMDL)	Mg (AMDL)	SO_4 (AMDL)	CO_3 (AMDL)	H_2O (AMDL)	Residue (calculated)
259	45 - 50	13.72 - 15.24	20.4	2.90	39.2	12.0	14.6	10.9
260	70 - 75	21.34 - 22.86	19.2	3.60	34.7	14.8	12.8	14.9
261	107 - 112	32.61 - 34.14	19.9	2.80	39.0	10.6	14.3	13.4
262	122 - 129	37.19 - 39.32	20.6	2.50	41.5	8.6	15.5	11.3
263	200 - 205	60.96 - 62.48	21.6	2.05	46.1	8.05	16.5	5.7
264	230 - 235	70.10 - 71.63	21.8	1.66	47.0	6.75	17.4	5.39
265	245 - 250	74.68 - 76.20	19.4	3.35	37.8	10.8	13.9	14.75
284	245 - 250	74.68 - 76.20	19.3	3.30	38.1	11.5	13.9	13.9
	Average of 265 and 284		19.35	3.325	37.95	11.15	13.9	14.325
266	260 - 265	79.25 - 80.77	20.4	2.50	41.3	9.85	15.1	10.85
267	310 - 315	94.49 - 96.01	22.9	1.76	46.7	7.0	16.8	4.84
268	330 - 335	100.58 - 102.11	20.6	2.25	42.4	8.8	15.5	10.45
269	360 - 365	109.73 - 111.25	21.1	1.98	44.7	7.85	16.4	7.97
270	380 - 385	115.82 - 117.35	23.7	1.51	52.4	6.15	10.1	6.14
271	470 - 475	143.26 - 144.78	17.3	7.00	22.5	25.7	7.75	19.75
272	490 - 495	149.35 - 150.88	16.5	6.95	19.1	27.1	7.15	23.2
285	490 - 495	149.35 - 150.88	16.8	6.70	20.7	25.1	7.25	23.45
	Average of 272 and 285		16.65	6.825	19.9	26.1	7.20	23.325
273	520 - 525	158.50 - 160.02	20.4	2.95	41.1	10.1	14.6	10.85
274	560 - 565	170.69 - 172.21	17.5	4.90	26.8	20.6	8.70	21.5
275	580 - 585	176.78 - 178.31	18.1	5.45	28.4	20.1	9.95	18.0
276	595 - 600	181.36 - 182.88	22.1	2.50	**44.8	***8.95	9.65	12.0
277	630 - 635	192.02 - 193.55	19.2	4.20	36.4	13.4	9.50	17.3
278	680 - 685	207.26 - 208.79	19.0	6.50	25.6	27.3	8.40	13.2
279	700 - 705	213.36 - 214.88	18.8	4.35	34.2	14.3	10.8	17.55
286	700 - 705	213.36 - 214.88	18.7	4.30	34.5	13.4	10.8	18.3
	Average of 279 and 286		18.75	4.325	34.35	13.85	10.8	17.925
280	730 - 735	222.50 - 224.03	21.8	2.90	45.5	10.1	6.40	13.3
281	800 - 805	243.84 - 245.36	19.1	4.65	32.7	17.4	9.90	16.25
282	825 - 830	251.46 - 252.98	18.8	6.50	25.3	26.7	8.15	14.55
283	845 - 850	257.56 - 259.08	21.9	3.35	44.8	12.1	4.40	13.45

Analysts: R.J. Buckley, AMDL Report AN3870/71, 13 May 1971.
G. Collinge, AMDL Report AN 3249/73, 12 February 1973 (CO_3 only).

* All sample numbers are prefixed by the figures 71110.
** AMDL Report AN2373/74, 13 December 1973; supersedes erroneous result of 23.5 in report AN3870/71.
***Average of 8.65 (report AN3249/73) and 9.25 (report AN2373/74).

decrease in the normative amounts of rutile and apatite indicates a lessening in the amount of incoming wind-borne detritus.

The concentration of normative chlorite in the dolutite follows from the concentration of clay, if the chlorite formed by the reaction of dolomite and kaolinite, as suggested on p.22 .

Why normative halite is concentrated in the dolutite, and why its distribution is similar to that of rutile and apatite, are not known; by analogy with these last two minerals, the halite would appear to have come down during times of clay deposition. If the halite were of evaporitic origin, it should show an upward increase in the norms.

MAJOR ELEMENTS - PARTIAL ANALYSES

Introduction

Twenty-five samples chosen randomly from 'Cuttings Samples Set 2' were forwarded to the Australian Mineral Development Laboratories, Adelaide, for analysis for calcium, magnesium, sulphate, carbonate, and water.

Details of sampling, analytical procedures, and limits of precision are set out in Appendix 1.

Results

The results of the analyses are set out in Table 9, and plotted as bar graphs in Figure 22; the percentage of residue in each sample was calculated by difference.

Discussion

The bar graphs show clear differences between the lower and upper parts of the hole, corresponding to the upper limit, at 436 feet (132.87 m), of dark bituminous dolomite in the core. Magnesium and carbonate are more abundant in the lower part of the hole, and calcium, sulphate, and water in the upper part. In addition, calcium and sulphate show a slight decrease, and magnesium and carbonate a slight increase upwards in the upper part of the

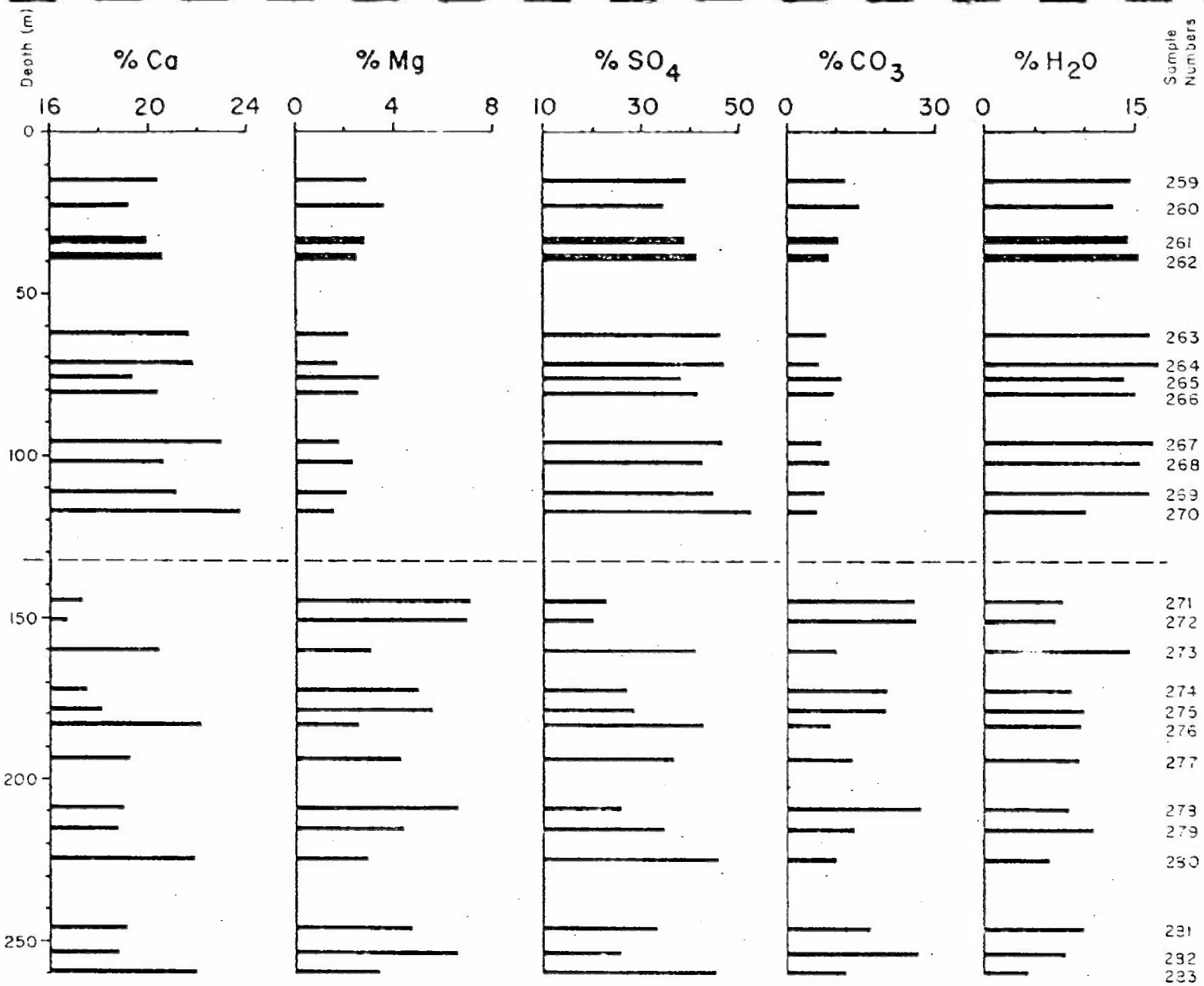

Fig 22 Bar chart showing results in percent of partial rock analyses (calcium, magnesium, sulphate, carbonate, and water) of Ringwood evaporites plotted against depth in metres. Dashed line indicates division into lower and upper parts of rock. Sample numbers preceded by TRIO.

hole. This suggests that the sedimentary sequence was nearing the end of calcium sulphate deposition, either by a gradual return to dolomite deposition, or by the approach to halite deposition: the latter, however, seems less likely, as one would then expect carbonate to decrease upwards, rather than increase.

Using certain simplifying assumptions (set out in Appendix 1), partial rock norms expressed as percentages of gypsum, anhydrite, dolomite, chlorite, celestite, and a residue calculated as quartz were calculated for each sample, and the results are set out in Table 10 and plotted as bar graphs in Figure 23.

As found in the bulk total rock norms, normative dolomite is more abundant in the lower part of the core, and normative gypsum in the upper part. The calculated quartz residue also shows a marked decrease at about 133 m, suggesting that much of it is of non-detrital origin. The residue comprises mostly chalcedonic silica, and the geochemical evidence for a non-detrital origin agrees with the petrographic evidence that it formed as a primary precipitate.

The normative amounts of gypsum and anhydrite were used to calculate the gypsum:anhydrite ratio for each analysed sample, and the results are shown in Figure 24. The ratio shows an irregular but roughly exponential increase upwards, indicating that the gypsum originated by the hydration of anhydrite by meteoric water. It might be thought that the curve is also consistent with the dehydration of gypsum to anhydrite with increasing depth, or even with a primary origin for both minerals, the changing proportions of the two arising from changing conditions during deposition. However, the principal factor affecting a hydration-dehydration reaction is temperature, which at the shallow depths with which this study is concerned increases linearly with depth, and so the gypsum:anhydrite depth curve should also be linear if dehydration were the principal cause of the change. The bar graphs for the major elements (Fig. 22) indicate that depositional changes during formation of the primary minerals were non-exponential. Thus, all the evidence indicates that the gypsum originated by hydration of anhydrite by meteoric water.

Table 10: Partial rock norms for Ringwood evaporites[+]

Sample No*	Depth Feet	Depth Metres	Gyp	Anh	Dol	Chl	Qtz	Cel
			Normative Mineral Content (%)					
259	45 - 50	13.72 - 15.24	68.14	1.67	18.44	2.73	9.12	-
260	70 - 75	21.34 - 22.86	59.09	1.59	22.75	3.48	12.77	0.15
261	107 - 112	32.61 - 34.14	66.08	3.04	16.28	3.77	10.98	-
262	122 - 129	37.19 - 39.32	71.46	2.31	13.22	4.36	11.00	-
263	200 - 205	60.96 - 62.48	77.40	2.97	12.37	2.44	4.26	0.11
264	230 - 235	70.10 - 71.63	82.15	1.37	10.38	1.67	4.31	0.13
265**	245 - 250	74.68 - 76.20	62.75	3.28	17.14	6.15	10.54	0.11
266	260 - 265	79.25 - 80.77	70.43	2.34	15.14	2.90	9.05	0.11
267	310 - 315	94.49 - 96.01	79.09	3.65	10.75	2.00	3.12	-
268	330 - 335	100.58 - 102.11	72.45	2.63	13.51	2.72	8.70	0.17
269	360 - 365	109.73 - 111.25	77.04	1.77	12.07	2.24	6.57	0.13
270	380 - 385	115.82 - 117.35	47.37	35.98	9.46	1.51	5.20	0.17
271	470 - 475	143.26 - 144.78	30.86	4.93	39.51	10.35	13.56	0.09
272**	490 - 495	149.35 - 150.88	29.11	3.70	40.11	8.88	17.81	0.11
273	520 - 525	158.50 - 160.02	66.66	4.98	15.52	5.22	7.59	0.15
274	560 - 565	170.69 - 172.21	39.09	5.04	31.67	4.18	19.09	0.09
275	580 - 585	176.78 - 178.31	42.81	4.61	30.90	7.95	13.23	0.07
276	595 - 600	181.36 - 182.88	43.75	28.91	13.75	3.96	9.32	-
277	630 - 635	192.02 - 193.55	40.29	17.91	20.61	8.57	12.13	0.09
278	680 - 685	207.26 - 208.79	36.80	4.31	41.96	5.62	9.99	0.09
279**	700 - 705	213.36 - 214.88	46.37	11.08	21.29	8.79	12.53	0.09
280	730 - 735	222.50 - 224.03	27.64	40.59	15.54	4.94	10.31	0.13
281	800 - 805	243.84 - 245.36	43.43	10.63	26.75	6.50	12.31	0.09
282	825 - 830	251.46 - 252.98	35.18	5.58	41.04	6.32	10.87	0.07
283	845 - 850	257.56 - 259.08	17.93	46.36	20.06	5.20	10.52	0.09

[+]Abbreviations as in Table 3, plus cel = celestite.
* Preceded by 71110
** Average results of samples 265 and 284, 272 and 285, 279 and 286

hole. This suggests that the sedimentary sequence was nearing the end of calcium sulphate deposition, either by a gradual return to dolomite deposition, or by the approach to halite deposition: the latter, however, seems less likely, as one would then expect carbonate to decrease upwards, rather than increase.

Using certain simplifying assumptions (set out in Appendix 1), partial rock norms expressed as percentages of gypsum, anhydrite, dolomite, chlorite, celestite, and a residue calculated as quartz were calculated for each sample, and the results are set out in Table 10 and plotted as bar graphs in Figure 23.

As found in the bulk total rock norms, normative dolomite is more abundant in the lower part of the core, and normative gypsum in the upper part. The calculated quartz residue also shows a marked decrease at about 133 m, suggesting that much of it is of non-detrital origin. The residue comprises mostly chalcedonic silica, and the geochemical evidence for a non-detrital origin agrees with the petrographic evidence that it formed as a primary precipitate.

The normative amounts of gypsum and anhydrite were used to calculate the gypsum:anhydrite ratio for each analysed sample, and the results are shown in Figure 24. The ratio shows an irregular but roughly exponential increase upwards, indicating that the gypsum originated by the hydration of anhydrite by meteoric water. It might be thought that the curve is also consistent with the dehydration of gypsum to anhydrite with increasing depth, or even with a primary origin for both minerals, the changing proportions of the two arising from changing conditions during deposition. However, the principal factor affecting a hydration-dehydration reaction is temperature, which at the shallow depths with which this study is concerned increases linearly with depth, and so the gypsum:anhydrite depth curve should also be linear if dehydration were the principal cause of the change. The bar graphs for the major elements (Fig. 22) indicate that depositional changes during formation of the primary minerals were non-exponential. Thus, all the evidence indicates that the gypsum originated by hydration of anhydrite by meteoric water.

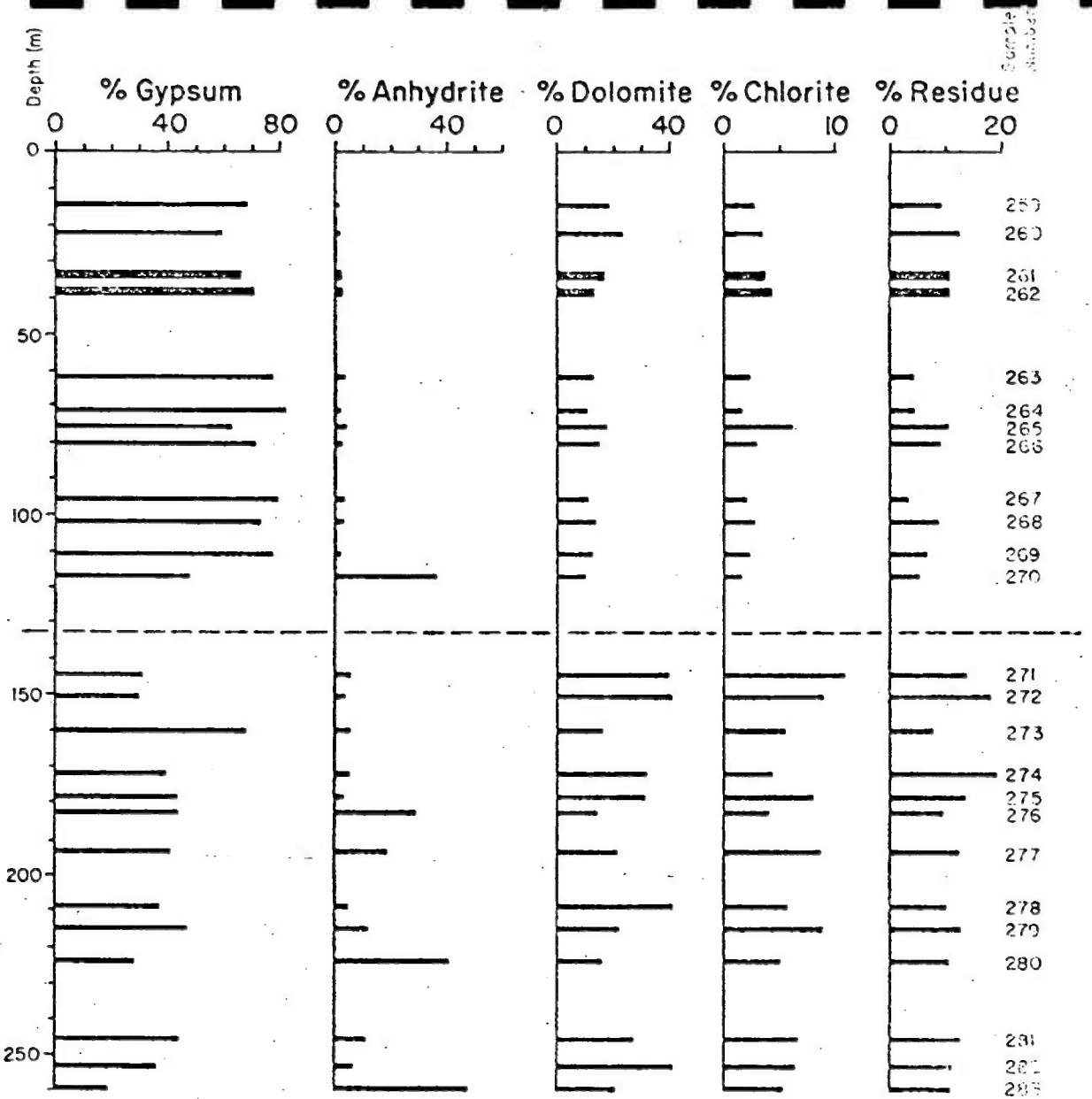

Fig. 23 Bar chart showing results in percent of partial rock norms (gypsum, anhydrite, dolomite, chlorite, and [illegible] analyses of Ringwood evaporites, plotted against depth (in metres). Dashed line marks [illegible] hole. Sample numbers preceded by 7111O.

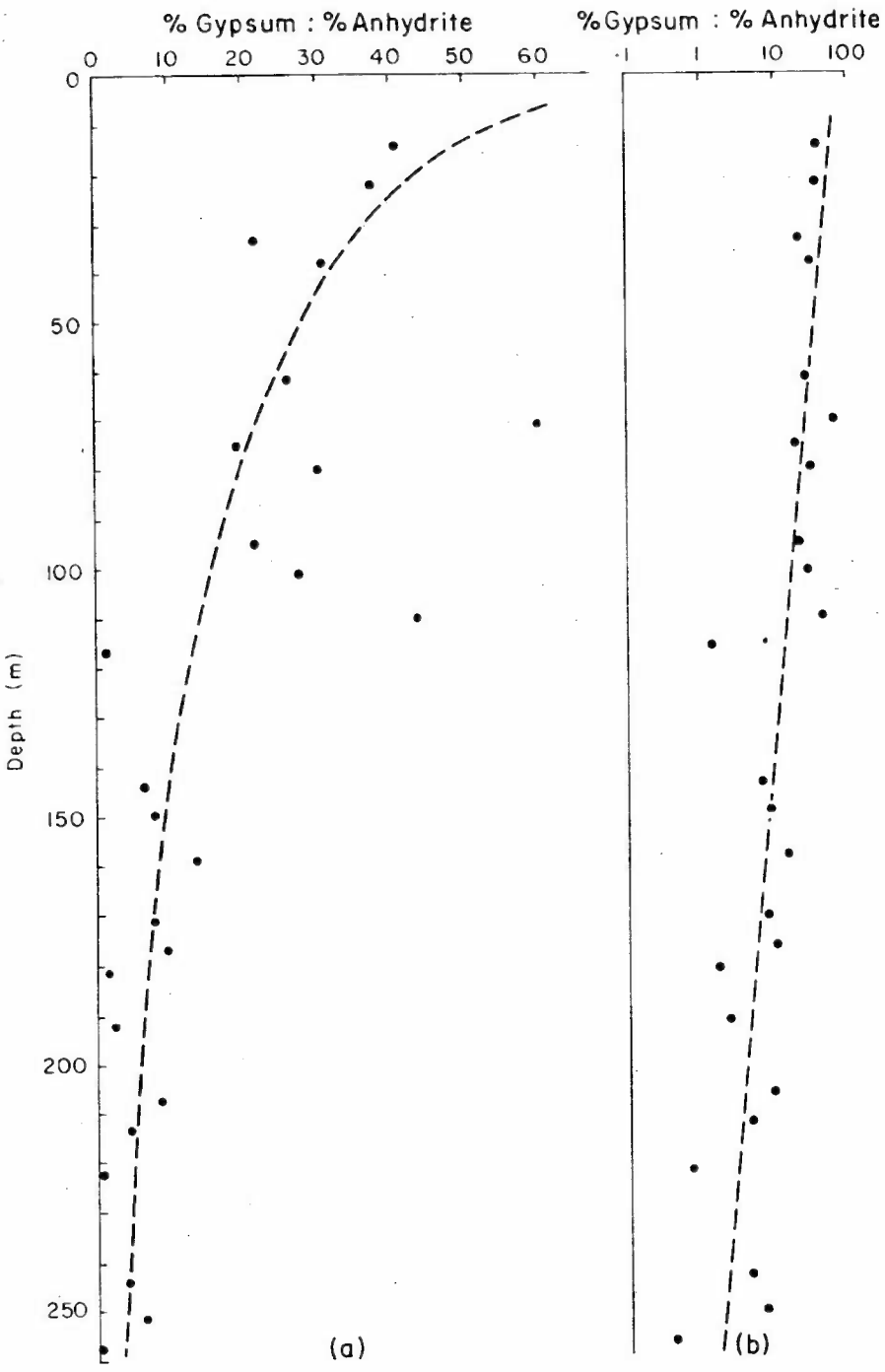

Fig. 24 Graphs showing normative gypsum : normative anhydrite ratio calculated from partial rock norms plotted against depth in metres; (a) arithmethic abscissa (b) logarithmic abscissa

Record 1974/145

F 53/A14/194

MINOR ELEMENTS

Introduction

One of the objectives of the Ringwood drilling was to look for potash, and so the whole of 'Cuttings Samples Set 2' was analysed for potassium by atomic absorption spectrophotometry. (An earlier set of results from spectrographic analyses of the core set out in the completion report (Stewart, 1969) is of unacceptable quality, for reasons given in Appendix 1, and should be disregarded.) The cuttings were also analysed for fluorine, strontium, and manganese, as these three elements (among others) show specific patterns of behaviour during the deposition of marine evaporites; fluorine and strontium are concentrated in the earlier products of deposition, particularly in the sulphate zone (Stewart, 1963), and strontium and manganese show significant differences in concentration in gypsum and anhydrite. Details of sampling, analytical procedures, and limits of precision for the minor elements are set out in Appendix 1.

Results

The results of the analyses are set out in Table 11 and plotted as bar graphs in Figure 25. Like those for the major elements, all the results show an appreciable change at 436 feet (132.87 m). The average contents of the four elements determined are set out in Table 12.

Potassium

Potassium does not occur in economic quantities in the Ringwood cuttings, and the maximum value found was 0.603 percent between 280 and 285 feet (85.34 m to 86.87 m). The content of potassium shows a slight and irregular increase up the hole, interrupted by a sudden increase and decrease on each side of the maximum value (Fig. 25). The maximum value appears anomalous when compared with the potassium analyses over the rest of the hole, and so 13 thin sections were cut from samples taken every few centimetres along the section of core between 85.34 m and 86.87 m. Microcline occurs in abundance in several of the thin sections, and its absence from elsewhere in the core indicates that it is the repository of the extra potassium. Whether the microcline is detrital or authigenic is discussed on p. 23 .

Table 11: Results in percent of analyses for minor elements in Ringwood evaporites

Sample No.*	Depth Interval Feet	Depth Interval Metres	K AMDL	K Corrected	F AMDL	Sr AMDL	Mn AMDL	Mn Corrected
070	0 - 5	0 - 1.52	.13	.115	.04	.07	.008	.00625
071	5 - 10	1.52 - 3.05	.13	.115	.02	.05	.005	.00390
072	10 - 15	3.05 - 4.57	.18	.159	.02	.08	.007	.00547
073	15 - 20	4.57 - 6.10	.22	.194	.03	.08	.008	.00625
074	20 - 25	6.10 - 7.62	.20	.177	.06	.03	.015	.0118
075	25 - 30	7.62 - 9.14	.13	.115	.02	.06	.009	.00703
076	30 - 35	9.14 - 10.67	.11	.098	.02	.065	.008	.00625
077	35 - 40	10.67 - 12.19	.14	.123	.02	.065	.006	.00469
078	40 - 45	12.19 - 13.72	.035	.0308	.02	.03	.016	.0126
090	40 - 45	12.19 - 13.72	.045	.0395	.02	.03	.016	.0126
	Average of 078 and 090		.040	.0351	.02	.03	.016	.0126
079	45 - 50	13.72 - 15.24	.16	.141	.03	.065	.008	.00625
No sample	50 - 55	15.24 - 16.76	-	-	-	-	-	-
080	55 - 60	16.76 - 18.29	.03	.0264	.02	.025	.009	.00703
081	60 - 65	18.29 - 19.81	.10	.089	.03	.045	.009	.00703
082	65 - 70	19.81 - 21.34	.075	.0657	.02	.04	.006	.00469
083	70 - 75	21.34 - 22.86	.10	.089	.04	.065	.009	.00703
084	75 - 80	22.86 - 24.38	.26	.229	.04	.045	.011	.0087
085	80 - 85	24.38 - 25.91	.21	.185	.03	.065	.008	.00625
086	85 - 95	25.91 - 28.96	.22	.194	.06	.14	.015	.0118
111	85 - 95	25.91 - 28.96	.19	.168	.05	.13	.014	.0111
	Average of 086 and 111		.205	.181	.055	.135	.0145	.0115
087	95 - 107	28.96 - 32.61	.22	.194	.04	.095	.009	.00703
035	107 - 112	32.61 - 34.14	.30	.264	.05	.055	.012	.0094
089	112 - 117	34.14 - 35.66	.16	.141	.04	.06	.006	.00469
091	117 - 122	35.66 - 37.19	.15	.132	.05	.08	.005	.0039
092	122 - 129	37.19 - 39.32	.15	.132	.06	.055	.006	.00469
093	129 - 135	39.32 - 41.15	.15	.132	.03	.06	.006	.00469
094	135 - 140	41.15 - 42.67	.14	.124	.04	.065	.009	.00703
095	140 - 145	42.67 - 44.20	.13	.115	.12	.015	.024	.0188
112	140 - 145	42.67 - 44.20	.13	.115	.12	.015	.025	.0196
	Average of 095 and 112		.13	.115	.12	.015	.0245	.0192
096	145 - 150	44.20 - 45.72	.30	.264	.19	.015	.018	.0141
097	150 - 155	45.72 - 47.24	.13	.115	.07	.05	.006	.00469
098	155 - 160	47.24 - 48.77	.24	.211	.17	.03	.018	.0141
099	160 - 164	48.77 - 49.99	.19	.168	.09	.05	.012	.0094
100	164 - 170	49.99 - 51.82	.045	.0395	.03	.05	.005	.00390
101	170 - 175	51.82 - 53.34	.035	.0308	.03	.10	.004	.00313
102	175 - 180	53.34 - 54.86	.15	.132	.09	.04	.011	.0087
036	180 - 185	54.86 - 56.39	.16	.141	.12	.035	.014	.0111

Table 11. (cont.)

Sample No.*	Depth Interval Feet	Depth Interval Metres	AMDL	K Corrected	F AMDL	Sr AMDL	Mn AMDL	Mn Corrected
104	185 - 190	56.39 - 57.91	.09	.0789	.08	.04	.009	.00703
113	185 - 190	56.39 - 57.91	.09	.0789	.11	.045	.009	.00703
	Average of 104 and 113		.09	.0789	.095	.0425	.009	.00703
105	190 - 195	57.91 - 59.44	.05	.0438	.06	.06	.005	.00390
106	195 - 200	59.44 - 60.96	.16	.141	.11	.04	.013	.0102
107	200 - 205	60.96 - 62.48	.04	.0351	.02	.055	.005	.00390
108	205 - 210	62.48 - 64.01	.04	.0351	.03	.07	.005	.00390
109	210 - 215	64.01 - 65.53	.13	.115	.09	.07	.009	.00703
110	215 - 220	65.53 - 67.06	.065	.057	.04	.06	.005	.00390
114	220 - 225	67.06 - 68.58	.10	.0875	.07	.035	.009	.00703
115	225 - 230	68.58 - 70.10	.12	.106	.06	.05	.005	.00390
116	230 - 235	70.10 - 71.63	.045	.0395	.03	.06	.003	.00236
117	235 - 240	71.63 - 73.15	.055	.0481	.05	.055	.003	.00236
135	235 - 240	71.63 - 73.15	.07	.0612	.04	.05	.003	.00236
	Average of 117 and 135		.0625	.0547	.045	.0525	.003	.00236
118	240 - 245	73.15 - 74.68	.22	.194	.08	.04	.003	.00236
119	245 - 250	74.68 - 76.20	.15	.132	.06	.05	.008	.00625
120	250 - 255	76.20 - 77.72	.19	.168	.05	.05	.009	.00703
121	255 - 260	77.72 - 79.25	.29	.255	.05	.06	.009	.00703
122	260 - 265	79.25 - 80.77	.16	.141	.04	.05	.007	.00547
037	265 - 270	80.77 - 82.30	.45	.395	.05	.05	.011	.0087
124	270 - 275	82.30 - 83.82	.15	.132	.03	.085	.005	.00390
125	275 - 280	83.82 - 85.34	.44	.385	.04	.05	.008	.00625
138	275 - 280	83.82 - 85.34	.42	.369	.04	.05	.008	.00625
	Average of 125 and 138		.43	.377	.04	.05	.008	.00625
126	280 - 285	85.34 - 86.87	.69	.603	.06	.05	.012	.0094
127	285 - 290	86.87 - 88.39	.30	.264	.05	.05	.008	.00625
128	290 - 295	88.39 - 89.92	.48	.420	.06	.035	.011	.0087
130	295 - 300	89.92 - 91.44	.40	.351	.06	.045	.009	.00703
131	300 - 305	91.44 - 92.96	.46	.403	.05	.055	.008	.00625
132	305 - 310	92.96 - 94.49	.13	.115	.03	.055	.003	.00236
133	310 - 315	94.49 - 96.01	.13	.115	.03	.06	.004	.00313
134	315 - 320	96.01 - 97.54	.13	.115	.03	.04	.004	.00313
136	320 - 325	97.54 - 99.06	.40	.351	.06	.04	.008	.00625
151	320 - 325	97.54 - 99.06	.42	.369	.06	.035	.008	.00625
	Average of 136 and 151		.41	.360	.06	.0375	.008	.00625
137	325 - 330	99.06 - 100.58	.20	.177	.07	.065	.008	.00625
139	330 - 335	100.58 - 102.11	.14	.123	.03	.075	.009	.00703
140	335 - 340	102.11 - 103.63	.11	.098	.03	.075	.006	.00469
141	340 - 345	103.63 - 105.16	.12	.106	.03	.065	.007	.00547
038	345 - 350	105.16 - 106.68	.11	.098	.02	.07	.006	.00469
143	350 - 355	106.68 - 108.20	.12	.106	.03	.07	.005	.00390
144	355 - 360	108.20 - 109.73	.09	.0789	.02	.07	.005	.00390
145	360 - 365	109.73 - 111.25	.11	.098	.03	.065	.005	.00390

Table 11. (cont.)

Sample No.*	Depth Interval Feet	Metres	AMDL	K Corrected	F AMDL	Sr AMDL	Mn AMDL	Mn Corrected
152	360 - 365	109.73 - 111.25	.11	.098	.03	.06	.005	.00390
	Average of 145 and 152		.11	.098	.03	.0625	.005	.00390
146	365 - 370	111.25 - 112.78	.085	.0745	.03	.06	.005	.00390
147	370 - 375	112.78 - 114.30	.11	.098	.04	.06	.007	.00547
148	375 - 380	114.30 - 115.82	.12	.106	.04	.07	.006	.00469
149	380 - 385	115.82 - 117.35	.07	.0612	.02	.075	.004	.00313
150	385 - 390	117.35 - 118.87	.11	.098	.03	.065	.006	.00469
153	390 - 395	118.87 - 120.40	.095	.0832	.02	.08	.006	.00469
154	395 - 400	120.40 - 121.92	.09	.0789	.02	.075	.005	.00390
155	400 - 405	121.92 - 123.44	.10	.0875	.03	.06	.007	.00547
157	405 - 410	123.44 - 124.97	.13	.115	.03	.055	.008	.00625
179	405 - 410	123.44 - 124.97	.12	.106	.04	.055	.006	.00469
	Average of 157 and 179		.125	.110	.035	.055	.007	.00547
158	410 - 415	124.97 - 126.49	.11	.098	.03	.065	.006	.00469
159	415 - 420	126.49 - 128.02	.15	.132	.04	.06	.008	.00625
160	420 - 425	128.02 - 129.54	.11	.098	.03	.08	.006	.00469
161	425 - 430	129.54 - 131.06	.11	.098	.04	.065	.008	.00625
162	430 - 435	131.06 - 132.59	.07	.0612	.02	.07	.005	.00390
039	435 - 440	132.59 - 134.11	.065	.057	.04	.04	.012	.0094
164	440 - 445	134.11 - 135.64	.30	.264	.33	.04	.017	.0134
165	445 - 450	135.64 - 137.16	.30	.264	.37	.02	.018	.0141
166	450 - 455	137.16 - 138.68	.28	.246	.27	.03	.019	.0149
167	455 - 460	138.68 - 140.21	.11	.098	.12	.05	.008	.00625
168	460 - 465	140.21 - 141.73	.08	.070	.10	.045	.006	.00469
180	460 - 465	140.21 - 141.73	.085	.0745	.10	.045	.008	.00625
	Average of 168 and 180		.0825	.0723	.10	.045	.007	.00547
169	465 - 470	141.73 - 143.26	.10	.089	.08	.065	.010	.0079
170	470 - 475	143.26 - 144.78	.13	.115	.13	.04	.012	.0094
040	475 - 480	144.78 - 146.30	.16	.141	.14	.03	.014	.0111
172	480 - 485	146.30 - 147.83	.22	.194	.23	.04	.014	.0111
173	485 - 490	147.83 - 149.35	.13	.115	.09	.065	.012	.0094
174	490 - 495	149.35 - 150.88	.14	.123	.12	.05	.014	.0111
175	495 - 500	150.88 - 152.40	.14	.123	.11	.04	.015	.0118
176	500 - 505	152.40 - 153.92	.13	.115	.12	.03	.014	.0111
177	505 - 510	153.92 - 155.45	.12	.106	.10	.03	.014	.0111
178	510 - 515	155.45 - 156.97	.22	.194	.21	.035	.014	.0111
201	510 - 515	155.45 - 156.97	.19	.168	.21	.03	.012	.0094
	Average of 178 and 201		.205	.180	.21	.0325	.013	.0102
181	515 - 520	156.97 - 158.50	.12	.106	.10	.045	.008	.00625
182	520 - 525	158.50 - 160.02	.07	.0612	.07	.065	.005	.00390
184	525 - 530	160.02 - 161.54	.09	.0789	.08	.045	.007	.00547
185	530 - 535	161.54 - 163.07	.055	.0481	.05	.035	.012	.0094
186	535 - 540	163.07 - 164.59	.065	.057	.07	.03	.008	.00625

Table 11. (cont.)

Sample No.*	Depth Interval Feet	Depth Interval Metres	AMDL	K Corrected	F AMDL	Sr AMDL	AMDL	Mn Corrected
187	540 - 545	164.59 - 166.12	.065	.057	.06	.055	.005	.00390
188	545 - 550	166.12 - 167.64	.06	.0525	.05	.065	.004	.00313
189	550 - 555	167.64 - 169.16	.07	.0612	.07	.05	.005	.00390
202	550 - 555	167.64 - 169.16	.075	.0657	.07	.05	.005	.00390
	Average of 189 and 202		.0725	.0635	.07	.05	.005	.00390
190	555 - 560	169.16 - 170.69	.12	.106	.08	.05	.006	.00469
191	560 - 565	170.69 - 172.21	.08	.070	.07	.04	.008	.00625
192	565 - 570	172.21 - 173.74	.14	.123	.07	.045	.009	.00703
193	570 - 575	173.74 - 175.26	.10	.089	.07	.055	.006	.00469
041	575 - 580	175.26 - 176.78	.08	.070	.09	.05	.006	.00469
195	580 - 585	176.78 - 178.31	.14	.123	.08	.035	.012	.0094
196	585 - 590	178.31 - 179.83	.13	.115	.07	.035	.008	.00625
197	590 - 595	179.83 - 181.36	.11	.098	.08	.035	.008	.00625
198	595 - 600	181.36 - 182.88	.075	.0657	.05	.06	.004	.00313
203	595 - 600	181.36 - 182.88	.07	.0612	.06	.06	.004	.00313
	Average of 198 and 203		.0725	.0635	.055	.06	.004	.00313
No Sample	600 - 605	182.88 - 184.40	-	-	-	-	-	-
199	605 - 610	184.40 - 185.93	.065	.0569	.09	.06	.004	.00313
200	610 - 615	185.93 - 187.45	.07	.0612	.08	.06	.005	.00390
204	615 - 620	187.45 - 188.98	.11	.098	.10	.04	.009	.00703
205	620 - 625	188.98 - 190.50	.22	.194	.28	.025	.011	.0087
206	625 - 630	190.50 - 192.02	.14	.123	.11	.04	.008	.00625
207	630 - 635	192.02 - 193.55	.12	.106	.06	.04	.006	.00469
208	635 - 640	193.55 - 195.07	.10	.089	.12	.035	.005	.00390
209	640 - 645	195.07 - 196.60	.075	.0657	.07	.04	.004	.00313
210	645 - 650	196.60 - 198.12	.09	.0789	.10	.025	.011	.0087
231	645 - 650	196.60 - 198.12	.12	.106	.12	.025	.010	.0079
	Average of 210 and 231		.105	.0925	.11	.025	.0105	.0083
211	650 - 655	198.12 - 199.64	.075	.0657	.09	.045	.008	.00625
213	655 - 660	199.64 - 201.17	.06	.0525	.05	.075	.005	.00390
214	660 - 665	201.17 - 202.69	.06	.0525	.06	.055	.005	.00390
042	665 - 670	202.69 - 204.22	.06	.0525	.06	.05	.005	.00390
216	670 - 675	204.22 - 205.74	.065	.057	.06	.04	.007	.00547
217	675 - 680	205.74 - 207.26	.09	.0789	.06	.035	.011	.0087
218	680 - 685	207.26 - 208.79	.095	.0832	.09	.04	.009	.00703
219	685 - 690	208.79 - 210.31	.075	.0657	.07	.045	.005	.00390
220	690 - 695	210.31 - 211.84	.20	.177	.21	.03	.011	.0087
221	695 - 700	211.84 - 213.36	.17	.150	.20	.03	.011	.0087
222	700 - 705	213.36 - 214.88	.14	.123	.11	.04	.007	.00547
232	700 - 705	213.36 - 214.88	.13	.115	.09	.04	.007	.00547
	Average of 222 and 232		.135	.120	.10	.04	.007	.00547

Table 11. (cont.)

Sample No.*	Depth Interval Feet	Depth Interval Metres	K AMDL	K Corrected	F AMDL	Sr AMDL	Mn AMDL	Mn Corrected
223	705 - 710	214.88 - 216.41	.14	.123	.12	.05	.007	.00547
224	710 - 715	216.41 - 217.93	.12	.106	.11	.025	.009	.00703
225	715 - 720	217.93 - 219.46	.11	.098	.12	.03	.010	.0079
226	720 - 725	219.46 - 220.98	.23	.202	.08	.035	.006	.00469
227	725 - 730	220.98 - 222.50	.12	.106	.06	.065	.004	.00313
228	730 - 735	222.50 - 224.03	.12	.106	.06	.06	.004	.00313
229	735 - 740	224.03 - 225.55	.075	.0657	.05	.05	.004	.00313
230	740 - 745	225.55 - 227.08	.07	.0657	.06	.06	.004	.00313
247	740 - 745	225.55 - 227.08	.065	.057	.05	.06	.004	.00313
	Average of 230 and 247		.0675	.0634	.055	.06	.004	.00313
233	745 - 750	227.08 - 228.60	.12	.106	.14	.045	.006	.00469
234	750 - 755	228.60 - 230.12	.10	.089	.08	.025	.009	.00703
235	755 - 760	230.12 - 231.65	.095	.0832	.08	.02	.012	.0094
236	760 - 765	231.65 - 233.17	.10	.089	.07	.03	.009	.00703
237	765 - 770	233.17 - 234.70	.11	.098	.07	.05	.008	.00625
238	770 - 775	234.70 - 236.22	.10	.089	.07	.06	.004	.00313
239	775 - 780	236.22 - 237.74	.075	.0657	.06	.055	.005	.00390
240	780 - 785	237.74 - 239.27	.13	.115	.06	.06	.004	.00313
241	785 - 790	239.27 - 240.79	.10	.089	.09	.055	.007	.00547
248	785 - 790	239.27 - 240.79	.095	.0832	.10	.055	.006	.00469
	Average of 241 and 248		.0975	.0863	.095	.055	.0065	.00508
242	790 - 795	240.79 - 242.32	.14	.123	.14	.02	.011	.0087
243	795 - 800	242.32 - 243.84	.12	.106	.07	.035	.014	.0111
287	795 - 800	242.32 - 243.84	.11	.098	.07	.03	(.035,	Discarded)
	Average of 243 and 287		.115	.102	.07	.0325	.014	.0111
244	800 - 805	243.84 - 245.36	.11	.098	.06	.045	.008	.00625
043	805 - 810	245.36 - 246.89	.065	.057	.09	.03	.009	.00703
246	810 - 815	246.89 - 248.41	.10	.089	.06	.05	.006	.00469
249	815 - 820	248.41 - 249.94	.18	.159	.21	.03	.009	.00703
250	820 - 825	249.94 - 251.46	.15	.132	.14	.045	.009	.00703
251	825 - 830	251.46 - 252.98	.13	.115	.08	.03	.009	.00703
252	830 - 835	252.98 - 254.51	.11	.098	.10	.02	.012	.0094
257	830 - 835	252.98 - 254.51	.13	.115	.11	.02	.012	.0094
	Average of 252 and 257		.12	.106	.105	.02	.012	.0094
253	835 - 840	254.51 - 256.03	.065	.057	.05	.02	.012	.0094
254	840 - 845	256.03 - 257.56	.065	.057	.05	.02	.013	.0102
255	845 - 850	257.56 - 259.08	.07	.0612	.07	.045	.005	.00390
256	850 - 852	259.08 - 259.69	.07	.0612	.07	.025	.009	.00703

All sample numbers are prefixed by the figures 71110.

Analyst: B. Hopton, AMDL Report AN4846/71, 30 June 1971

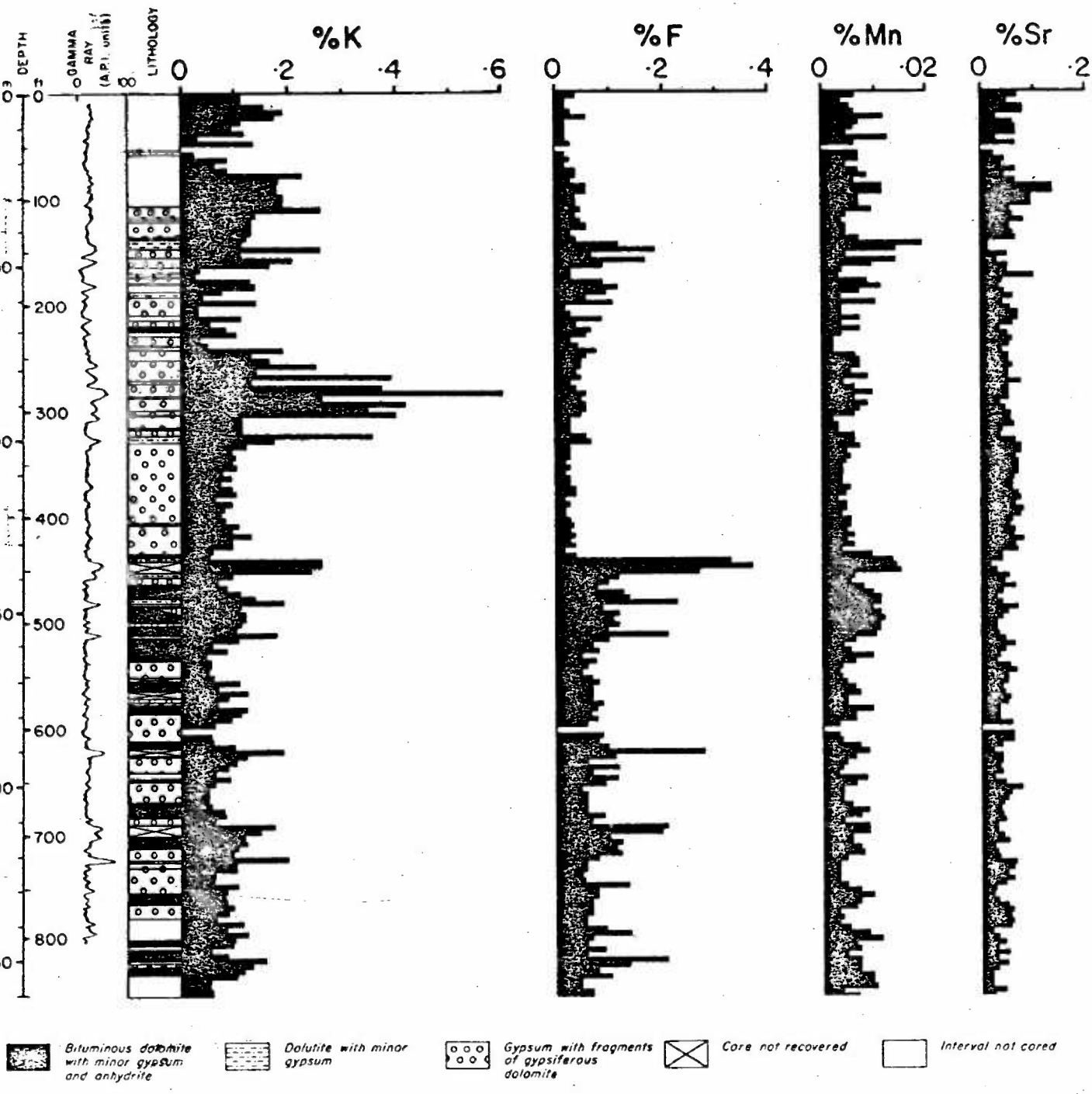

Fig 25 — Bar chart showing results in percent of analysis for minor elements (potassium, fluorine, manganese, and strontium) in Ringwood evaporites plotted against depth in metres. Lithologic log (generalized from Stewart, 1960) and γ-ray log also shown

Table 12: Average contents in percent of minor elements in Ringwood evaporites

Element	Average below 133 m	Average above 133 m	Average over entire hole
K	0.102	0.138	0.123
F	0.10	0.05	0.07
Sr	0.04	0.06	0.05
Mn	0.0066	0.0064	0.0065

Inspection of the potassium bar graph (Fig. 25) reveals that the high peaks are opposite dolomite or dolutite beds in the core (or opposite intervals of no recovery which presumably correspond to dolutite beds), and the low peaks are opposite gypsum.

Fluorine

The distribution of fluorine in the Ringwood rocks is somewhat similar to that of potassium, especially in the lower part of the hole. Like potassium, fluorine is concentrated in dolomite as opposed to gypsum, particularly the dark bituminous dolomite in the lower part of the hole, and when deposition of this rock ceased the concentration of fluorine in the rocks fell by half (Table 12). The maximum concentration of fluorine is 0.37 percent from 445 to 450 feet (135.64 m to 137.61 m), i.e., at the top of the lower part of the hole. No specific fluorine-bearing mineral was identified in thin sections of the core.

The close match between the behaviour of fluorine and potassium in the lower part of the hole is shown in Figure 26. The match is poor in the upper part of the hole (Fig. 26), particularly in the case of the maximum potassium value, which has no corresponding fluorine peak at all (Fig. 25).

Strontium

Unlike the other three elements determined, strontium is concentrated in the gypsum beds; Figure 27 illustrates the antipathetic relations of strontium and fluorine and of strontium and manganese. The maximum concentration recorded is 0.135 percent at 85 to 95 feet

(25.91 m to 28.96 m). The bar graph (Fig. 25) shows a perceptible change in strontium content at 436 feet (132.87 m), and this is reflected in the averages for the lower and upper parts of the hole (Table 12).

Manganese

The concentration of manganese is very low in the Ringwood evaporites, and is only about one-tenth or less of those of the other elements determined. The maximum concentration recorded is 0.019 percent at 140 to 145 feet (42.67 m to 44.20 m). The manganese is concentrated in dolomite, where it presumably substitutes for magnesium, and shows a reasonable match with potassium and fluorine in the lower part of the hole, but less so in the upper part (Fig. 25).

Discussion

The abundances and changes in concentration with depth of the four minor elements determined in the Ringwood cuttings are typical of marine evaporites; potassium and strontium show slight increases in concentration upwards (though in different rock-types), whereas fluorine and, to a lesser extent, manganese decrease in concentration upwards. The increase in potassium content reflects the increase in the concentration of potassium in the evaporating marine brine, whereas strontium follows calcium and reflects the greater content of this element in the upper part of the deposit.

The strontium and manganese analyses also provide evidence on the origin of the gypsum and anhydrite in the Ringwood evaporites, as these two elements show significant differences in concentration in the two sulphates. Kropachev (1960) found that manganese is low in anhydrite (0.012 percent Mn) and higher in gypsum (0.037 percent Mn), and so the low concentration (0.0065 percent Mn) in the Ringwood rocks is consistent with the deposition of primary anhydrite. With regard to strontium, analyses published in Deer et al. (1962) show up to 0.60 percent Sr in anhydrite but only 0.0008 percent Sr in gypsum, and Noll (1934) found up to 0.58 percent Sr in anhydrite rock but only 0.11 percent Sr in gypsum rock. (However, Kropachev (1960) found the opposite situation in sulphates from the Perm Basin, viz., 0.06 percent Sr in anhydrite and 0.14 percent Sr in gypsum.) Grahmann (1920) found that anhydrite can take up to 42 percent of $SrSO_4$ in solid solution at room temperature.

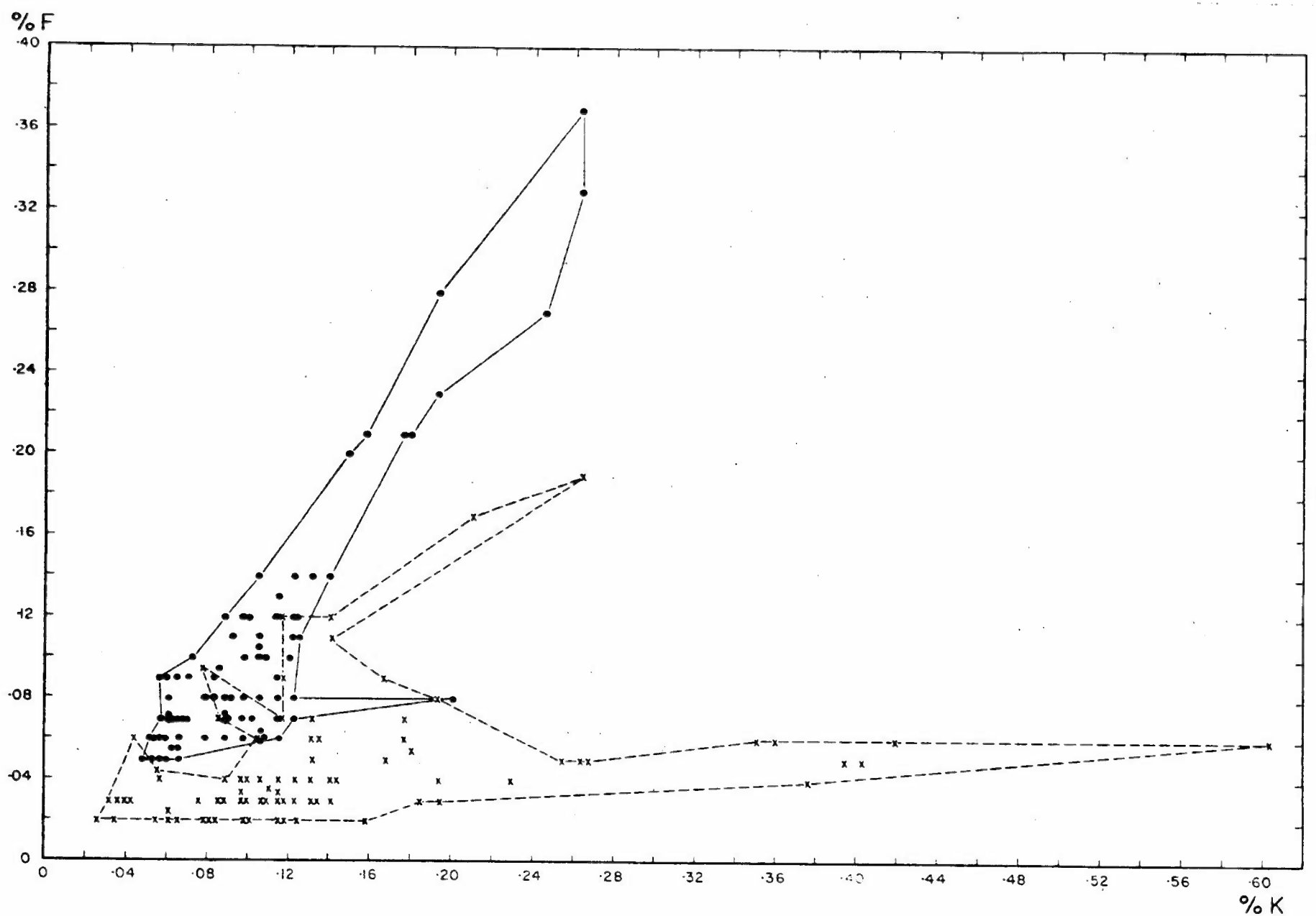

Fig 26 – Graph showing fluorine and potassium content (in percent) for each analysed sample from Ringwood evaporites. Solid circles are results from lower part of hole below 436'(132·87m), crosses are results from upper part of hole.

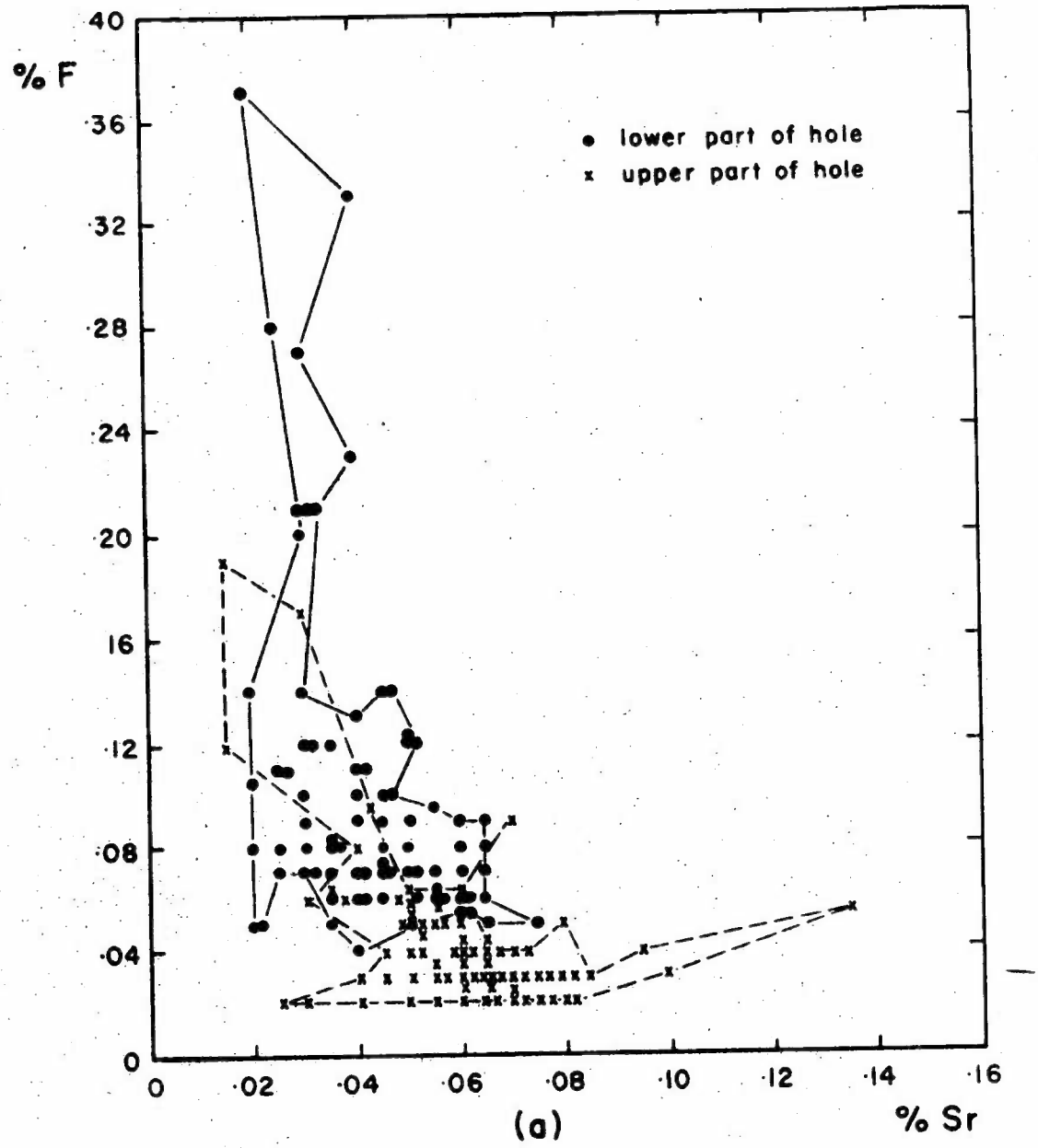

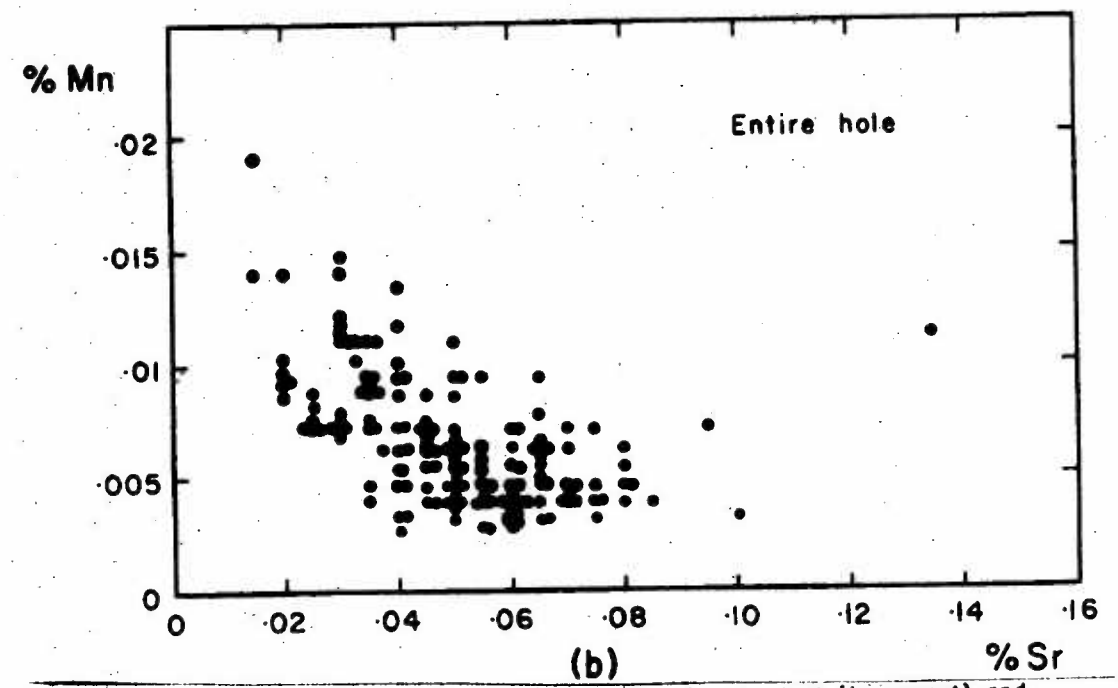

Fig 27 Graphs showing (a) fluorine and strontium content (in percent) and (b) manganese and strontium content for each analysed sample from Ringwood evaporites

The proportion of gypsum increases up the hole (Fig. 24), and if it were primary then the analyses in Deer et al. (1962) and Noll (1934) would lead one to expect that the concentration of strontium would correspondingly decrease, and that of manganese increase, upwards. However, the opposite is the case, indicating that the gypsum is not primary; and this agrees with the petrographic evidence. But, as the strontium is in fact concentrated in the gypsum beds, it was presumably deposited during precipitation of the calcium sulphate as anhydrite. The occurrence of celestite in the gypsum beds confirms the secondary origin of the gypsum, the celestite having formed from the strontium released from solid solution during hydration of anhydrite to gypsum.

The possibility remains that the anhydrite was of secondary origin, and formed by dehydration of primary evaporative gypsum during burial; but again the comparatively high content of strontium in the sulphate indicates that this was not the case.

Base Metals

Two samples of the dark bituminous dolomite from the lower part of the core were analysed for base metals by atomic absorption spectrophotometry and the results are set out in Table 13. No metal enrichment is apparent.

Boron

Fourteen core samples were analysed for boron by semi-quantitative methods; the samples were chosen from the two intervals, both of friable dolutite, that had given the highest values for boron, viz., 0.21 percent at 480'3" (146.36 m) and 0.24 percent at 820'0" (249.90 m), during earlier analyses of the core by the Australian Mineral Development Laboratories, Adelaide, the results of which are set out in the completion report (Stewart, 1969; for reasons given in Appendix 1, these results should be disregarded). The new results are set out in Table 14.

Table 13: Results (in percent) of analyses for base-metal content in bituminous dolomite

Sample No.	Depth	Fe	Mn	Cu	Pb	Zn
71110016	760'3" (231.72 m)	0.75	0.0117	0.0015	0.0039	0.00075
71110018	826'6" (251.92 m)	1.99	0.0182	0.0016	0.0034	0.00127

Analyst: C. Robison (BMR), 30 November 1971

Table 14: Results in percent of semi-quantitative analyses for boron in Ringwood evaporites

Sample No.*	Depth Feet and Inches	Depth Metres	%B
19	478'3" - 478'9"	145.75 - 145.91	0.005
20	478'9" - 479'3"	145.91 - 146.06	0.01
21	479'3" - 479'9"	146.06 - 146.21	0.016
22	479'9" - 480'3"	146.21 - 146.36	0.016
23	480'3" - 480'9"	146.36 - 146.52	0.016
24	480'9" - 481'2"	146.52 - 146.64	0.016
25	481'2" - 481'7"	146.64 - 146.77	0.016
26	481'7" - 482'0"	146.77 - 146.89	0.016
27	819'6" - 820'0"	249.74 - 249.90	0.01
28	820'0" - 820'6"	249.90 - 250.05	0.016
29	820'6" - 821'0"	250.05 - 250.20	0.02
30	821'0" - 821'6"	250.20 - 250.35	0.02
31	821'6" - 822'0"	250.35 - 250.51	0.016
32	822'0" - 822'6"	250.51 - 250.66	0.016

*All sample numbers are prefixed by 711100.

From: BMR Laboratory Report No. 25, 8 February 1971

Analysts: C.W. Claxton and J. Weekes

Claxton and Weekes also reported that 'A scan of the spectrograms revealed calcium, magnesium, aluminium, silica (sic) and sodium as major constituents with traces of iron and manganese. Very faint traces of lead, nickel, cobalt, copper and titanium were also observed'.

CONCLUSIONS

Introduction

The origin of marine evaporites has been debated for at least the last hundred years. At the present time several sedimentary models explain many but not all the phenomena observed in evaporites, and the possibility that evaporites are of volcanic origin has recently been proposed (Sozansky, 1973), reviving the old controversy between neptunist and vulcanist.

The oldest and still the most popular hypothesis of evaporite formation involves the evaporation of a body of seawater which is partly cut off from the ocean, such as in a shallow lagoon behind barrier bars or reefs (Miller, 1847, pp. 183, 214; Bischof, 1855; Ochsenius, 1877), or in deep barred basins like fjords (Schmalz, 1969) or the Red Sea (Friedman, 1972). Modifications to the bar theory were introduced by Branson (1915), King (1947), Scruton (1953), and Adams & Rhodes (1960) to explain the considerable departures of natural evaporite successions from the succession obtained by the experimental evaporation of seawater; the modifications proposed various mechanisms for removal of chloride-rich brines from regions of sulphate deposition in order to build up thick monomineralic deposits. A second hypothesis of evaporite formation was put forward by Richter-Bernburg (1955), who suggested that evaporites could be deposited on the gently sloping shelves of epeiric seas without a barrier restriction, provided the solubility product of each evaporite mineral were exceeded. The disadvantages of the bar and epeiric sea theories are that they are largely hypothetical, and that modern analogues are either lacking or are too small to explain the great thickness and wide extent of many ancient evaporite deposits (e.g., those in Germany, western Canada, eastern USA, and the Mediterranean region).

Recent hypotheses of ancient evaporite formation are the sabkha and the desiccating deep basin models. Both are represented by present-day examples, and are thus more easily examined and tested. The sabkha hypothesis (Kinsman, 1966; 1969) has arisen out of work in the Persian Gulf, where the very arid climate results in the formation of gypsum, anhydrite, aragonite, dolomite, and celestite at the present time. The evaporite minerals precipitate in the interstices of near-shore marine carbonate sediments in the supratidal environment, where brines derived from seawater are concentrated by evaporation to salinities ten times that of normal seawater. As depositional off-lap proceeds, the evaporite belt moves progressively seaward and its area increases considerably. The textures of these evaporites are distinctive, and several ancient evaporites have been interpreted as sabkha deposits (Schenk, 1967; Holliday, 1968, 1969; Fuller & Porter, 1969; other references in Friedman, 1972, p. 1073).

The desiccating deep basin model (Hsu, 1972) is the most startling and yet in some ways the simplest of the hypotheses of evaporite formation. The hypothesis suggests that the widespread evaporites in the floor and coastal regions of the Mediterranean Sea were deposited simply by

closing of the Strait of Gibraltar and wholesale drying up of the entire Mediterranean Sea, so that a giant basin floored with salt lakes and playas came into existence thousands of metres below sea-level. The hypothesis explains the great thickness and extent of many evaporite deposits, and also the concentric arrangement of the outcrops of the successive evaporite minerals in the large deposits, where the early products of evaporation crop-out around the periphery of the basin and the later products occupy smaller concentric areas towards the centre of the basin.

Origin of the Ringwood Evaporite Deposit

The Ringwood deposit is only one of many evaporite outcrops in the Bitter Springs Formation of the Amadeus Basin, but it is not known whether they represent a single large sheet of evaporite or many small lenticular beds; the absence of evaporites from many outcrops of the Bitter Springs Formation suggests that the latter is the case.

Considering the four main hypotheses in turn, the desiccated deep basin model does not appear to be applicable, because the Bitter Springs Formation and the sediments below (Heavitree Quartzite) are shallow marine, and above (tillite and coarse periglacial conglomerate of the Areyonga Formation) are continental. One could also point to the non-concentric pattern of gypsum and halite distribution in the Bitter Springs Formation (Fig. 1). However, it must be remembered that the present margins of the Amadeus Basin are not the depositional limits of the basin, but are structural margins; at the end of sedimentation the basin was considerably more extensive than it is now, especially to thee north, and so the present distribution of evaporites in the basin cannot be representative of the original depositional limits. Nevertheless, the absence of deep-water sediments associated with the evaporites and of conglomerate-filled canyons in the basement rocks around the basin render the desiccated deep basin model inapplicable.

The principal criteria for a sabkha origin are (from Kinsman, 1969): abundant nodules of anhydrite with felted lath texture, or 'chickenwire' texture in anhydrite rock; stromatolites indicative of algal mats; desiccation cracks and flat-pebble conglomerate; interbeds of cross-laminated aeolian silt and sand; evidence of oxidizing conditions, such as red-beds; and association of celestite with dolomite (the strontium set free by the dolomitization of aragonite). The Ringwood deposit shows none of these features, although it must be admitted that deformation, recrystallization, and low-grade metamorphism must have

obliterated some of the original depositional characteristics, such as nodular and 'chickenwire' anhydrite textures, and desiccation cracks. However, other features such as interbeds of terrigenous sand and silt and the association of celestite with dolomite could be expected to survive tectonism, and other characteristics such as red beds and stromatolites are common elsewhere in the Bitter Springs Formation, and so should have survived at Ringwood if they were ever present. It thus appears that the sabkha model does not apply to Ringwood either.

The evaporating epeiric sea hypothesis implies evaporation in an open ocean, with unrestricted circulation and oxidizing conditions. However, the Ringwood deposit begins with a black pyritic bituminous carbonate, pyrite is abundant at numerous other places higher in the deposit, and the entire core is coloured in shades of grey, not red, all indicative of restricted circulation and euxenic conditions. Thus the epeiric sea hypothesis is not applicable to the Ringwood deposit.

We are left with the classical barred basin hypothesis for the origin of the Ringwood evaporites, and the rocks show all the criteria for this origin, namely, a dark grey to black bituminous pyritic siliceous carbonate at the base, overlain by gypsum with inclusions of anhydrite, overlain in turn by limestone breccia and then by massive algal limestone. The evidence is consistent with diachronous deposition of carbonate and sulphate in a restricted basin behind a fringing algal reef. Celestite is not associated with dolomite, but it is associated with gypsum, and hence probably represents the strontium taken up in solid solution by primary anhydrite and then released during hydration to gypsum. The only terrigenous materials in the evaporite sequence are an influx of arkosic silt near the middle of the upper part of the core, and possible wind-blown clay in the dolutite interbeds.

Geological History of Ringwood Evaporite Deposit

The geological history of the Ringwood evaporite can be summarized thus:

1. Growth of an off-shore barrier reef, forming a lagoon with restricted access to the open ocean outside the reef. Stagnancy ensues, followed by concentration of lagoon water by evaporation.

2. Deposition in lagoon of primary dolomite, primary opaline silica, organic matter, and pyrite.

3. Further concentration of lagoon water, leading to deposition of calcium sulphate, probably as primary anhydrite as discussed above. The interbeds within the lower part of the deposit indicate that conditions fluctuated between those of dolomite deposition and those necessary for sulphate deposition, but eventually conditions stabilized and sulphate became the dominant precipitate, forming the upper part of the deposit.

4. Dolutite formed at various times during the life of the lagoon, and represents additions of very fine-grained terrigenous material to the chemical deposits of the lagoon either as wind-borne dust or pluvial run-off. The presence of abundant silt-sized particles of quartz and microcline in the upper part of the deposit represents an influx of alluvium.

5. After the main period of sulphate deposition, conditions began a fluctuating return to those of the early part of the lagoon's history; carbonate formed an increasing proportion of the deposit, and at one stage bituminous pyritic dolomite precipitated. Evaporation was eventually terminated by a return to normal marine conditions, implying burial or collapse of the algal reef, or general subsidence of the entire area, or both.

6. The remainder of the Bitter Springs Formation was then deposited, followed by the succeeding formations of the Amadeus Basin sequence, burying the Ringwood evaporite to a depth of about 7000 m.

7. Diagenesis, recrystallization, and burial metamorphism affected the evaporite rocks, and resulted in such phenomena as: (1) growth of chlorite porphyroblasts; (2) crystallization of opaline silica to chalcedonic silica and chert; (3) growth of euhedral quartz crystals; (4) formation of interpenetrating growth twins of pyrite; (5) sculpturing of microcline grains; (6) overgrowths of colourless tourmaline around detrital cores; (7) conversion of any pre-existing gypsum to anhydrite.

8. The deposit was moved tectonically during the Carboniferous, when the evaporites were folded and brecciated, and tourmaline needles and quartz euhedra broken. Anhydrite was mobilized and formed the cement between breccia clasts, recrystallizing to a blocky or bladed texture; anhydrite also formed contorted lenses and laminae where interbedded with anhydritic (now gypsiferous) dolomite. At this time dolomite also underwent local recrystallization, mainly at the margins of breccia clasts, forming crusts of euhedral dolomite and concentrations of organic matter.

9. Erosion of landscape to present day; eventually the land surface was lowered sufficiently for meteoric water percolating down joints to reach the evaporites, and hydration of the anhydrite to gypsum ensued, accompanied by swelling and brecciation of the sulphate-bearing dolomite beds, resulting in the partly bedded, partly brecciated appearance of the dolomite-gypsum breccia. Strontium held in solid solution in the anhydrite was set free and precipitated as celestite. Joints in the evaporites were eventually filled with acicular gypsum.

Epilogue

The Ringwood evaporite lagoon must have been a silent lonely place. We can imagine a hot windless day at the edge of the Bitter Springs sea, where a smelly saline stagnant lagoon lies inside a low or partly submerged offshore algal reef. The sun burns relentlessly overhead. Behind stretches a low subdued landscape, hot, dry, dusty, and devoid of vegetation. No living thing disturbs the stillness; the only movement is the slow sway to and fro of masses of algae in the swell. On other days the wind blows unhindered and the air is filled with dust. On the rare occasions when rain falls, the lagoon is clouded with silt and clay washed in from the adjoining land. As the years go by both the shoreline and the off-shore reef transgress shoreward, leaving the evaporite sediments as a diachronous lens beneath the limestone breccia and stromatolitic skeletons of the reef. Ultimately, epeirogenic movement lowers the entire area, drowning the lagoon and its surrounding reef, and leading to a new episode of sedimentation, this time of the normal marine environment, and resulting in the burial of the evaporite body beneath the clastic sediments now exposed on the southern flank of the Ringwood Dome.

ACKNOWLEDGEMENT

My wife Dr Aimorn Chaicharn Stewart assisted in the collection and preparation of core and cuttings samples at the Ringwood drill site in 1968.

REFERENCES

ADAMS, J.E., & RHODES, M.L., 1960 - Dolomitization by seepage refluxion. Bull. Am. Assoc. Petrol. Geol., 44, 1912-20.

BISCHOF, G., 1855 - LEHRBUCH DER CHEMISCHEN UND PHYSIKALISCHEN GEOLOGIE, Vol. 2, pt 3, 1667-2512. Bonn, Adolph Marcus.

BORCHERT, H., & MUIR, R.O., 1964 - SALT DEPOSITS: THE ORIGIN, METAMORPHISM, AND DEFORMATION OF EVAPORITES. London, Van Nostrand.

BRANSON, E.B., 1915 - Origin of thick gypsum and salt deposits. Bull. geol. Soc. Am., 26, 231-42.

CURRIE, J., 1905 - Note on some new localities for gyrolite and tobermorite. Miner. Mag., 14, 93-5.

DEER, W.A., HOWIE, R.A., & ZUSSMAN, J., 1962 - ROCK-FORMING MINERALS, 5, NON-SILICATES. London, Longmans.

DEER, W.A., HOWIE, R.A., & ZUSSMAN, J., 1963 - ROCK-FORMING MINERALS, 4, FRAMEWORK SILICATES. London, Longmans.

FRIEDMAN, G.M., 1972 - Significance of Red Sea in problem of evaporites and basinal limestones. Bull Am. Assoc. Petrol. Geol., 56, 1072-86.

FULLER, J.G.C.M., & PORTER, J.W., 1969 - Evaporites and carbonates; two Devonian basins of western Canada. Bull. Canad. Petrol. Geol., 17, 182-93.

GOLDMAN, M.I., 1952 - Deformation, metamorphism, and mineralization in gypsum-anhydrite cap rock, Sulphur Salt Dome, Louisiana. Mem. geol. Soc. Am., 50.

GRAHMANN, W., 1920 - Uber Barytocolestin und das Verhaltnis von Anhydrit zu Colestin and Baryt. N. Jb. Miner. Geol. Palaeont., 1, 1-23.

HEDDLE, M.F., 1880 - Preliminary notice of substances which may prove to be new minerals. Miner. Mag., 4, 117-23.

HELLER, L., & TAYLOR, H.F.W., 1956 - CRYSTALLOGRAPHIC DATA FOR THE CALCIUM SILICATES. London, HMSO.

HEY, M.H., 1954 - A new review of the chlorites. Miner. Mag., 30, 277-92.

HOLLIDAY, D.W., 1968 - Early diagenesis in Middle Carboniferous nodular anhydrite of Spitsbergen. Proc. York. geol. Soc., 36, 277-92.

HOLLIDAY, D.W., 1969 - The origin of penemosaic texture in evaporites of the Detroit River Formation (Middle Devonian) in northern Indiana: discussion of a paper by L.F. Rooney and R.R. French. J. sediment. Petrol., 39, 1256-8.

HOLMES, A., 1930 - PETROGRAPHIC METHODS AND CALCULATIONS. London, Murby.

HSU, K.J., 1972 - Origin of saline giants: a critical review after the discovery of the Mediterranean Evaporite. Earth-Sci. Rev., 8, 371-96.

KASTNER, MIRIAM, 1971 - Authigenic feldspars in carbonate rocks. Am. Miner. 56, 1403-42.

KING, R.H., 1947 - Sedimentation in Permian Castile sea. Bull. Am. Assoc. Petrol. Geol., 31, 470-7.

KINSMAN, D.J.J., 1966 - Gypsum and anhydrite of Recent age, Trucial Coast, Persian Gulf. In RAU, J.L. (ed.), SECOND SYMPOSIUM ON SALT, 1, 302-26. N. Ohio geol. Soc., Cleveland.

KINSMAN, D.J.J., 1969 - Modes of formation, sedimentary associations, and diagnostic features of shallow-water and supra-tidal evaporites. Bull. Am. Assoc. Petrol. Geol., 58, 830-40.

KROPACHEV, A.M., 1960 - Malye elementy v angidritakh i epigeneticheskikh gypsakh permskogo preduralya (Minor elements in anhydrites and epigenetic gypsums of the Permian of the fore-Urals). Vseo. miner. Obshch. Zapiski, 89, 598-602.

McCONNELL, J.D.C., 1954 - The hydrated calcium silicates riversideite, tobermorite, and plombierite. Miner. Mag., 30, 293-305.

McNAMARA, M., 1965 - The lower greenschist facies in the Scottish Highlands. Geol. Foren. Forh., 87, 347-89.

MILLER, H., 1847 - FIRST IMPRESSIONS OF ENGLAND AND ITS PEOPLE. London.

MUFFLER, L.J.P., & WHITE, D.E., 1969 - Active metamorphism of Upper Cenozoic sediments in the Salton Sea geothermal field and the Salton Trough, southeastern California. Bull. geol. Soc. Am., 80, 157-82.

NOLL, W., 1934 - Geochemie des Strontiums; mit Bemerkungen zur Geochemie des Bariums. Chemie der Erde, 8, 507-600.

OCHSENIUS, C., 1877 - DIE BILDUNG DER STEINSALZLAGER UND IHRER MUTTERLAUGENSALZE. Halle, Pfeffer.

PETERSON, M.N.A., & VON DER BORCH, C.C., 1965 - Chert: modern inorganic deposition in a carbonate-precipitating locality. Science, 149, 1501-3.

PETTIJOHN, F.J., 1957 - SEDIMENTARY ROCKS. N.Y., Harper & Row.

RICHTER-BERNBURG, G., 1955 - Ueber salinare sedimentation. Z. dtsch. geol. Ges., 105, 593-645.

ROGERS, A.F., & KERR, P.F., 1942 - OPTICAL MINERALOGY. N.Y., McGraw-Hill.

SCHENK, P.E., 1967 - The Macumber Formation of the Maritime Provinces, Canada - Mississippian analogue to recent strand-line carbonates of the Persian Gulf. J. sediment. Petrol., 37, 365-76.

SCHMALZ, R.F., 1969 - Deep-water evaporite deposition: a genetic model. Bull. Am. Assoc. Petrol. Geol., 53, 798-823.

SCRUTON, P.C., 1953 - Deposition of evaporites. Bull. Am. Assoc. Petrol. Geol., 37, 2498-512.

SOZANSKY, V.I., 1973 - Origin of salt deposits in deep-water basins of Atlantic Ocean. Bull. Am. Assoc. Petrol. Geol., 57, 589-90.

STEWART, A.J., 1969 - Completion report, BMR Alice Springs No. 3 (Ringwood) Bur. Miner. Resour. Aust. Rec. 1969/7 (unpubl.).

STEWART, A.J., 1974 - Amendments to Record 1969/7, 'Completion report, BMR Alice Springs No. 3 (Ringwood)'. Bur. Miner. Resour. Aust. Rec. 1969/7 (Supplement).

STEWART, F.H., 1949 - The petrology of the evaporites of the Eskdale No. 2 boring, east Yorkshire. Part 1. The lower evaporite bed. Miner. Mag., 28, 621-75.

STEWART, F.H., 1963 - Marine evaporites. In FLEISCHER, M. (ed.), Data of Geochemistry, Sixth Edition, Chapter Y. U.S. geol. Surv. prof. Pap. 440-Y.

WELLS, A.T., FORMAN, D.J., RANFORD, L.C., & COOK, P.J., 1970 - Geology of the Amadeus Basin, central Australia. Bur. Miner. Resour. Aust. Bull. 100.

WELLS, A.T., & KENNEWELL, P.J., 1972 - Evaporite drilling in the Amadeus Basin: Goyder Pass, Gardiner Range, and Lake Amadeus, Northern Territory. Bur. Miner. Resour. Aust. Rec. 1972/36 (unpubl.).

WELLS, A.T., RANFORD, L.C., STEWART, A.J., COOK, P.J., & SHAW, R.D., 1967 - Geology of the north-eastern part of the Amadeus Basin, Northern Territory. Bur. Miner. Resour. Aust. Rep. 113.

ZEN, E-AN, 1959 - Clay mineral-carbonate relations in sedimentary rocks. Am. J. Sci., 257, 29-43.

APPENDIX I - SAMPLING AND ANALYTICAL PROCEDURES, COMPUTATIONS, AND ESTIMATES OF PRECISION AND ACCURACY OF RESULTS

INTRODUCTION

The completion report on the Ringwood drilling (Stewart, 1969), included, without the author's knowledge, semi-quantitative spectrographic analyses for potassium and boron on chip samples of the drill core, and maximum values of 1 percent potassium and 0.24 percent boron were recorded. However, several incorrect steps in the sampling procedure and presentation of results rendered much of the work useless. Samples from above 465 feet (141.73 m) were analysed by BMR, and here 'only the evaporitic part of the core was selected and analysed', whereas samples below this depth were submitted to the Australian Mineral Development Laboratories in Adelaide, who crushed and analysed the whole core sample. Further, the lower limit of detection for the potassium analyses by BMR was 0.5 percent (and all but one of the BMR results was listed as less than 0.5 percent), whereas the lower limit of the AMDL analyses was 0.0005 percent; thus, the average potassium content of the core below 141.73 m was 0.06 percent based on AMDL's results, whereas all that could be said about the part of the core above this depth was that its potassium content was less than 0.5 percent. Two sets of analyses, one by AMDL and the other by BMR, were on samples taken from overlapping depth intervals, but the results are very different (Table 15), probably because of the difference in sampling methods.

TABLE 15

Comparison of analyses by BMR and AMDL

Sample No.	Depth	%K	%B	Analysis by:
68090176	230'2"/235'3"/240'3"	1.0 - 0.5	0.16	BMR
69660500	230'2" - 230'4"	0.03	<0.005	AMDL

Further, many of the results were tabulated as referring to composite samples from a range of depths (e.g., No. 68090176 in Table 15), but no reason was given why this was done. For these reasons, it was decided at the beginning of the present study to re-analyse the Ringwood rocks, and the analyses set out in the completion report should be disregarded.

SAMPLING PROCEDURES AT WELL SITE

A continuous sample of the dust produced by the drilling was collected in a dry bucket placed beneath the rotary table directly beside the hole. Every 5 feet (1.52 m), the contents of the bucket were emptied on to a sheet of clean dry polythene and thoroughly mixed by stirring; duplicate samples were placed in standard plastic cuttings bags and forwarded to BMR Canberra, where they are stored in the Core and Cuttings Laboratory (registered well no. 1002). After ocoring started at 107 feet (32.61 m), considerable difficulty was experienced in washing the cuttings, and it was decided not to wash the bulk of the samples, as follows:

Cuttings Samples Set 1				Cuttings Samples Set 2 (Duplicate set)			
0' (0 m)	- 150' (45.7 m)	washed		0' (0 m)	- 107' (32.61 m)	washed	
150' (45.7 m)	- 830' (252.98 m)	unwashed		107' (32.61 m)	- 852' (269.69 m)	unwashed	
830' (252.98 m)	- 852' (259.69 m)	washed					

Coring of the Ringwood evaporite rocks was slow (1.32 feet (0.4 m) per hour) so as to minimize damage to the core and maximize core recovery. Standard 15-foot (4.57 m) cores were cut and placed in order on corrugated sheets of galvanized iron after removal from the core barrel. The cores were washed with petrol to remove grease and dust, labelled, and lithologically logged. The dolomite-gypsum breccia and bituminous dolomite formed good strong core, but the dolutite was recovered as broken fragments, and was bagged up in 6-inch (15 cm) lengths of polythene core tubing. The entire core is stored in the BMR Core and Cuttings Laboratory.

PROCEDURES AND COMPUTATIONS IN LABORATORY

Full Analyses

Twelve samples of evaporite rocks were taken for full chemical analysis. Cuttings were chosen for the three composite analyses (samples 306, 307, 308) because they already represented composite samples of each 5-foot (1.52 m) interval down the core. The slow rate of penetration

throughout the drilling (1.32 feet (.4 m) per hour) ensured that the cuttings arriving at the surface were in fact those coming from the depth being drilled at the same time; the close match between the potassium content of the cuttings and the γ-ray log of the hole confirms this (Fig. 25). Approximately 10 g was taken from each of the 166 bags of cuttings, brought together and thoroughly mixed on a sheet of polythene, and about 25 g was removed for analysis as sample 306 (composite sample of entire core). A similar procedure was followed for the composite samples (307, 308) of the upper and lower parts of the core.

Cuttings were also chosen for the dolomite-gypsum breccia samples (309, 310, 311) because this particular rock forms lengths of core considerably longer than 5 feet (1.52 m), and so the cuttings provide an excellent bulk sample of the rock. Core samples were chosen for the dolutite (samples 312, 313, 314) and bituminous dolomite (315, 316, 317) because these rocks form lengths of core shorter than 5 feet (1.52 m). For the dolutite, one fragment was removed from each of the 6 inch (15 cm) bags corresponding to the three selected dolutite intervals, and then combined into three composite samples for crushing and analysis. For the bituminous dolomite, two chips a few centimetres apart were sawn from each of the three selected intervals, and then combined into three composite samples.

The twelve samples were analysed for eighteen elements by the Australian Mineral Development Laboratories, using atomic absorption spectrophotometry: the results are set out in Table 7.

Calculation of Total Rock Norms

The results of the full analyses were used to calculate total rock norms, and the following minerals known from petrographic examination to be present in the evaporites were used as normative minerals: Gypsum, Anhydrite, Dolomite, Quartz, Chlorite, Pyrite, Microcline, Celestite, and Rutile. In addition, the following five minerals not known in thin section were used where necessary to account for elements present in small amounts: Apatite, Halite, Fluorite, Potassium Fluoride, and Calcite. As a general rule, all but one of the normative minerals used have reasonably pure natural compositions and so ideal end-member formulae were used in the calculations. The exception to this rule is chlorite, which undergoes so much ionic substitution that no formula can be assumed for it. Hence, one crystal of the chlorite in question was analysed with the electron probe microanalyser, and a structural formula

calculated from the results and used in the norm calculations, which were done by the method set out in Holmes (1930), as follows:

1. Fe_2O_3 was converted to FeO, because there is no evidence of any ferric iron in the core; the rocks are grey, not red.

2. MnO was added to MgO.

3. H_2O^+ was added to H_2O^- and treated as H_2O.

4. The percentage of each oxide was converted to the corresponding molecular proportion, and allotted to the normative minerals as follows:

5. S and FeO were allotted to pyrite, in ratio of 2 : 1. Any remaining S was left as excess; any remaining FeO was allotted to chlorite (step 8 below).

6. P_2O_5, CaO, and F were allotted to apatite in ratio of 3 : 10 : 1; this used up all P_2O_5 in all cases, and left excess CaO and F.

7. CO_2, MgO, and CaO were allotted to dolomite in ratio of 2:1:1.

8. MgO, FeO, CaO, Al_2O_3, SiO_2, and H_2O were allotted to chlorite in various ratios depending on the amounts of FeO and Al_2O_3 available. The various chlorite formulae used are set out in Table 16.

In samples 306 and 307, the analysed chlorite was used, and the oxides were allotted in ratio of

$$\text{MgO: FeO: CaO: } Al_2O_3\text{: } SiO_2\text{: } H_2O$$

$$= 4.1\text{: } 0.5\text{: } 0.1\text{: } \frac{2.3}{2} = 1.15\text{:}2.9\text{: } 4$$

In samples 308, 312, 313, 314, there was no FeO remaining from step 5, and the amount of Al_2O_3 in the analysis necessitated the use of the iron-free aluminium-rich chlorite listed in Table 16. The oxides were allotted in the ratio of

$$\text{MgO: FeO: CaO: } Al_2O_3\text{: } SiO_2\text{: } H_2O)$$

$$= 4.44\text{: } 0 \text{ : } 0.1\text{: } \frac{2.46}{2} \text{ : } 2.9 \text{ : } 4$$

Table 16: Chlorite formulae used in total rock norm calculations

Mg	Fe	Al^{vi}	Ca	Si	Al^{iv}	O	$(OH)_8$	Molecular weight used*	Used in total rock sample no.
Iron-rich chlorite									
3.6	1.0	1.2	0.1	2.9	1.1	10	8	144.735	316
Analysed chlorite									
4.1	0.5	1.2	0.1	2.9	1.1	10	8	140.793	306, 307
Moderate-iron chlorite									
4.3	0.3	1.2	0.1	2.9	1.1	10	8	139.216	311
Iron-poor chlorite									
4.5	0.1	1.2	0.1	2.9	1.1	10	8	137.639	310
Iron-free chlorite									
4.6	0.0	1.2	0.1	2.9	1.1	10	8	136.851	309
Iron-free, aluminium-rich chlorite									
4.44	0.0	1.36	0.1	2.9	1.1	10	8	136.958	308, 312, 313, 314

* The molecular weight used in the norm calculations is one quarter of the formula weight, because there are approximately four magnesium ions in one formula unit.

In sample 309, there was no FeO available from step 5, and the Al_2O_3 in the analysis satisfied the requirement of the analysed chlorite, and so the iron-free chlorite of Table 16 was used, and oxides allotted in the ratio of

$$MgO : FeO : CaO : Al_2O_3 : SiO_2 : H_2O$$

$$= 4.6 : 0 : 0.1 : 1.15 : 2.9 : 4$$

In sample 310, only a very small amount of FeO was available from step 5, and so the iron-poor chlorite of Table 16 was used, and the oxides allotted in the ratio of

$$MgO : FeO : CaO : Al_2O_3 : SiO_2 : H_2O$$

$$= 4.5 : 0.1 : 0.1 : 1.15 : 2.9 : 4$$

In sample 311, a moderate amount of FeO was left from step 5, though not enough to satisfy the analysed chlorite, and so the moderate-iron chlorite of Table 16 was used, and the oxides allotted in the ratio of

$$MgO : FeO : CaO : Al_2O_3 : SiO_2 : H_2O$$

$$= 4.3 : 0.3 : 0.1 : 1.15 : 2.9 : 4$$

In sample 316, a considerable amount of FeO remained from step 5, twice that required by the analysed chlorite, and so the iron-rich chlorite of Table 16 was used, and the oxides allotted in the ratio of

$$MgO : FeO : CaO : Al_2O_3 : SiO_2 : H_2O$$

$$= 3.6 : 1.0 : 0.1 : 1.15 : 2.9 : 4$$

9. H_2O, SO_3, and CaO were allotted to gypsum in the ratio of 2 : 1 : 1; in all cases this step used up all the H_2O remaining from step 8.

10. SO_3 and CaO were allotted to anhydrite in ratio of 1 : 1.

11. Any remaining SO_3 and SrO were allotted to celestite in ratio of 1 : 1.

12. In samples 306, 307, 309, 310, i.e. the composite samples and dolomite-gypsum breccia samples from above 133 m, K_2O, Al_2O_3, and SiO_2 were allotted to microcline in ratio of 1 : 1 : 6, providing some Al_2O_3 remained from step 8.

13. SiO_2 remaining from steps 8 and 12 was allotted to quartz.

14. K_2O remaining from step 12 and F remaining from step 6 were allotted to KF in ratio of 1 : 2.

15. Na_2O and Cl were allotted to halite in ratio of 1 : 2.

16. TiO_2 was allotted to rutile.

17. CaO remaining from steps 9 and 10 and F remaining from step 14 were allotted to fluorite in ratio of 1 : 2.

18. CaO remaining from step 16 and CO_2 remaining from step 7 were allotted to calcite in ratio of 1 : 1.

19. The molecular proportion of the cation in each mineral (Mg for chlorite) was multiplied by the molecular weight of the mineral to give the weight percent of the mineral, and the results tabulated in Table 8.

20. In each norm calculation, very small amounts of some oxides remained, and were left as 'residue'.

Partial Analyses

Twenty-five samples chosen randomly from 'Cuttings Samples Set 2' were analysed for calcium, magnesium, sulphate, carbonate, and water by the Australian Mineral Development Laboratories, Adelaide, using atomic absorption spectrophotometry. Three of the samples were analysed in duplicate, and the following estimates of precision were calculated:

Element	Precision (%) (σ)
Ca	0.75
Mg	3
SO_4	2
CO_3	4
H_2O	0.5

The results of the analyses are set out in Table 9, and plotted as bar graphs in Figure 22.

Calculation of Partial Rock Norms

The data of Table 9 were then used to calculate partial rock norms by the same method used for the total rock norms. The partial normative minerals used were: Gypsum, Anhydrite, Dolomite, Chlorite, Celestite, and Residue (calculated as Quartz). Only the analysed chlorite of Table 16 was used for the chlorite calculation. The molecular proportions of each oxide (CaO, MgO, SrO, SO_3, CO_2, H_2O) were calculated first: at this stage the residue consists of SiO_2 and Al_2O_3 in unknown proportion.

The steps then were:

1. CO_2, MgO, and CaO were allotted to dolomite; this used up all CO_2.

2. MgO remaining from step 1, CaO, H_2O, SiO_2 and Al_2O_3 were allotted to chlorite (as analysed); this used up the remainder of the MgO, and enabled the weights in percent of SiO_2 and Al_2O_3 required for the chlorite to be calculated.

3. H_2O remaining from step 2, CaO, and SO_3 were allotted to gypsum; this used up all the H_2O.

4. CaO remaining from steps 2 and 3 and SO_3 remaining from step 3 were allotted to anhydrite.

5. Any SO_3 remaining from step 4, and SrO were allotted to celestite.

6. The weight percent of SiO_2 required to make up the total weights in percent to 100 after step 2 was calculated, and its equivalent molecular proportion calculated and allotted to quartz.

The weights in percent of each mineral were calculated as for the total rock norms, and tabulated in Table 10 and plotted as bar graphs in Figure 23.

Minor Elements

The whole of 'Cuttings Samples Set 2' (166 samples) was forwarded to the Australian Mineral Development Laboratories, Adelaide, for analysis for potassium, fluorine, strontium, and manganese. Potassium, strontium, and manganese were determined by atomic absorption spectrophotometry, and fluorine was determined by a wet

chemical method. Eighteen of the samples were analysed in duplicate, and enabled the following 'analytical errors' to be calculated:

Element	Analytical Error	Precision (%) (σ)
K	$\pm$ 0.006	4
F	$\pm$ 0.005	7
Sr	$\pm$ 0.005	10
Mn	$\pm$ 0.0005	8

Accuracy of Results of Minor Element Analyses

In order to provide a check on the accuracy of the results of the analyses for minor elements, six spiked samples were inserted randomly into the set of cuttings. The spiked samples were prepared in the following manner:

Two initial spikes, A and B, were formulated by A.D. Haldane and prepared by J. Weekes (both of BMR), and consisted of known amounts of the following bench reagents (AR grade):

Spike A	Spike B
1.144 gm of KCl	0.229 gm of H_3BO_4
0.009128 gm of $SrCl_2.6H_2O$	0.007124 gm of $BaCl_2.2H_2O$
0.2436 gm of $MnSO_4.4H_2O$	0.236124 gm total
2.10 gm of $(Fe(NH_4))_2 (SO_4)_3.7H_2O$	
3.496728 gm total	

The amounts of the bench reagents were chosen so as to give each initial spike the following contents (Table 17) of the elements to be analysed:

Table 17

Initial spike compositions (in percent)

Spike	K	B	Sr	Ba	Mn	Fe
A	2	-	.01	-	.2	1
B	-	.1	-	.01	-	-

Each initial spike was then added to a known amount of one of the cuttings samples, No. 71110253 from 835 to 840 feet (254.51 m to 256.03 m), as follows:

Mixture X	Mixture Y
3.496728 gm of spike A	0.236124 gm of spike B
26.51 gm (S_A) of sample 71110253	39.80 gm (S_B) of sample 71110253
30.006728 gm total weight (W_A)	40.036124 gm total weight (W_B)

Mixtures X and Y were then mixed in the following proportions (Table 18) to form the six spiked samples:

Table 18

Mixing proportions (in percent) of mixtures X and Y

Spiked Sample No.	Proportion (P) of X	Proportion (100-P) of Y
1	90	10
2	1	99
3	50	50
4	20	80
5	80	20
6	10	90

From this procedure, the six final spikes in the six spiked samples have the compositions listed in Table 19. (Subsequent to the preparation of the spiked samples, fluorine was added to the analytical programme, and boron, barium, and iron were deleted).

Table 19: Final spike compositions (M)

Spiked Sample No.	K	Sr	Mn
1	1.8	0.009	0.18
2	0.02	0.0001	0.002
3	1.0	0.005	0.1
4	0.4	0.002	0.04
5	1.6	0.008	0.16
6	0.2	0.001	0.02

The small amounts (denoted by N_K, N_{Sr}, and N_{Mn} respectively) of potassium, strontium, and manganese in sample 71110253 in the two mixtures X and Y must be added to the values listed in Table 19 in order to arrive at the overall composition of the spiked samples. The results of the analysis of sample 71110253 were as follows (in percent):

K = 0.065 F = 0.05 Sr = 0.02 Mn = 0.012

The amounts of potassium, strontium, and manganese to be added to the spike compositions (M) are calculated as follows:

Let M = content (in percent) of an element in spike (Table 19), and M_K, M_{Sr}, and M_{Mn} represent the content of potassium, strontium, and manganese, respectively.

N = content (in percent) of an element in sample 71110253.

So, $N_K = 0.065$ $N_{Sr} = 0.02$ $N_{Mn} = 0.012$

P = fraction (in percent) of mixture X in spiked sample (Table 17), and (100-P) = fraction (in percent) of mixture Y in spiked sample (as above)

S_A, S_B = weight of sample 71110253 in mixtures X and Y, respectively (as above).

W_A, W_B = total weight of mixtures X and Y, respectively (as above)

Then, calculated total content (T) of an element is given by

$$T = M + \frac{PNS_A}{100W_A} + \frac{(100-P)NS_B}{100W_B}$$

The calculated compositions of the six spiked samples are listed in Table 20, together with the results of the analyses by AMDL on the spiked samples, and the calculated percentage difference between the two figures for each sample.

Table 20: Calculated and measured contents of elements inspiked samples, and percentage differences

Spiked Sample No.	Registration No.*	Calculated content (%)	Measured content by AMDL** (%)	Calculated content + analytical error	Measured content - analytical error	Percentage difference
Potassium (analytical error = 0.006)						
1	088	1.858	2.2	1.864	2.194	17.8
2	103	0.085	0.09	0.091	0.084	-
3	123	1.061	1.23	1.067	1.224	14.8
4	142	0.464	0.53	0.470	0.524	11.6
5	163	1.662	1.83	1.668	1.824	9.4
6	171	0.264	0.3	0.270	0.294	9.1
Strontium (analytical error = 0.005)						
1	088	0.027	0.03	0.032	0.025	-
2	103	0.020	0.025	0.025	0.020	-
3	123	0.024	0.025	0.029	0.020	-
4	142	0.021	0.02	0.026	0.015	-
5	163	0.026	0.03	0.031	0.025	-
6	171	0.021	0.02	0.026	0.015	-
Manganese (analytical error = 0.0005)						
1	088	0.191	0.24	0.1915	0.2395	25.1
2	103	0.014	0.016	0.0145	0.0155	7.14
3	123	0.111	0.14	0.1115	0.1395	25.2
4	142	0.052	0.065	0.0525	0.0645	23.1
5	163	0.171	0.15	0.1715	0.1505	-12.3
6	171	0.032	0.043	0.0325	0.0425	31.25

* All sample registration numbers are prefixed by 71110

**Analyst: B. Hopton, AMDL Report AN4846/71, 30 June 1971

From these data, the content of potassium measured by AMDL was, on the average, 12.5 percent too high, the content of strontium measured by AMDL agreed with the calculated value (within experimental error), and the content of manganese measured by AMDL was, on the average, 22 percent too high.

The results of the analyses by AMDL for minor elements in the whole cuttings set are set out in Table 11, together with the corrected values for potassium and manganese. The values are also plotted as bar graphs in Figure 25.